

STRUCTURAL BIOLOGY OF PRION PROTEIN USING NMR SPECTROSCOPY

Dissertation
zur Erlangung des Doktorgrades
der Naturwissenschaften

vorgelegt beim Fachbereich Biochemie, Chemie und Pharmazie
der Goethe-Universität
in Frankfurt am Main

von
Jitendra Kumar
aus
Aligarh, Indien

Frankfurt am Main
2010
D30

Dem Fachbereich Biochemie, Chemie und Pharmazie der
Goethe-Universität als Dissertation vorgelegt.

Dekan: Prof. Dr. Dieter Steinhilber

1. Gutachter: Prof. Dr. Harald Schwalbe
2. Gutachter: Prof. Dr. Clemens Glaubitz

Datum der Disputation: 2010

This thesis was prepared under the supervision of Prof. Dr. Harald Schwalbe between February 2003 and September 2010 at the Institute for Organic Chemistry and Chemical Biology of the Goethe-University, Frankfurt.

Dedicated to my teachers,
among whom, my mother is first...

विद्या ददाति विनयं विनयाद्याति पात्रताम् ।
पात्रत्वाद्धनमाप्नोति धनाद्धर्मं ततः सुखम् ॥

Education gives Humility,
Humility gives Character,
From character one gets wealth,
From wealth one gets righteousness, in righteousness there is joy.

न चौर हार्यम न च राज हार्यम ।
न भ्रात्रभाज्यम न च भारकारी ॥
व्यये कृते वर्धते नित्यं ।
विद्या धनं सर्वे धनं प्रधानम् ॥

No one can steal it, no authority can snatch,
Not divided in brothers, not heavy to carry,
As you consume or spend, it increases; as you share, it expands,
Education is the best wealth among all the wealth anyone can have.

TABLE OF CONTENTS

<i>Table of Contents</i>	<i>i</i>
<i>List of Figures</i>	<i>iv</i>
<i>List of Abbreviations</i>	<i>x</i>
Abstract	- 1 -
Chapter 1	- 3 -
Protein Misfolding, Amyloid and Prion Diseases	- 3 -
Protein folding, misfolding and aggregation	- 4 -
Amyloidosis: a protein conformational disease.....	- 11 -
Amyloid	- 13 -
Prion diseases	- 15 -
Protein-only hypothesis.....	- 17 -
Development of prion concept.....	- 17 -
“Protein-only” hypothesis	- 19 -
Evidences supporting the protein-only hypothesis	- 20 -
Prion strains and species barriers:	- 22 -
PrP ^C	- 23 -
The structure of PrP ^C	- 23 -
The cellular function of PrP ^C	- 25 -
Mutations associated with the PRNP gene	- 26 -
The rouge conformations: PrP ^{Sc}	- 28 -
Prion Conversion Models.....	- 28 -
Nucleation dependent polymerization model	- 28 -
Heterodimer (template assisted) model	- 30 -
Current knowledge about PrP^{Sc} structure.	- 31 -
in-vitro conversion studies	- 32 -
Toxicity of in-vitro generated prions	- 34 -
Current structural models for PrP^{Sc}	- 36 -
Fungal prions	- 38 -
Methods to study protein aggregation and amyloid structure	- 38 -
Direct non-morphological techniques.....	- 39 -
Indirect Non-morphological techniques	- 41 -
Morphological methods	- 41 -
Electron microscopy.....	- 45 -
NMR methods	- 47 -
Diffusion ordered spectroscopy	- 48 -
H/D exchange methods	- 49 -
Aim of the thesis.....	- 51 -
Chapter 2	- 52 -
Material and methods	- 52 -
Materials	- 52 -

Plasmids.....	- 52 -
pJCTEV	- 52 -
pRSET A	- 52 -
pKM263.....	- 52 -
Software.....	- 53 -
Buffers and solutions.....	- 54 -
Lysis buffer:.....	- 54 -
Inclusion Body wash buffer	- 54 -
Refolding and proteolytic cleavage buffer.....	- 54 -
Purification buffers.....	- 54 -
Prion Protein Protocols.....	- 55 -
Safety considerations.....	- 55 -
Constructs	- 56 -
Recombinant human PrP ₉₀₋₂₃₀	- 56 -
Recombinant human PrP ₁₂₁₋₂₃₀	- 56 -
Recombinant human PrP ₁₆₆₋₂₃₀	- 57 -
Expression of prion protein for NMR.....	- 58 -
Expression of isotope labeled protein	- 58 -
Procedure 1	- 58 -
Procedure 2.....	- 58 -
Purification of prion protein:.....	- 59 -
Purification of His-tag free protein	- 59 -
Procedure 1:.....	- 59 -
Procedure 2:.....	- 60 -
Fast purification of his-tag protein	- 60 -
Procedure 3:.....	- 60 -
Procedure 4:.....	- 61 -
Fibril formation	- 61 -
AFM:.....	- 63 -
EM:	- 63 -
NMR spectroscopy	- 63 -
Backbone resonance assignment.....	- 64 -
MUSIC based HSQCs.....	- 66 -
Diffusion ordered NMR spectroscopy	- 72 -
Deuterium exchange.....	- 73 -
Chapter 3.....	- 74 -
Results.....	- 74 -
Assignments of recombinant prion fragments.....	- 75 -
Amyloidal core residues in prion fibrils	- 87 -
Polymorphism in prion fibrils	- 100 -
Electron microscopic images	- 101 -
Atomic force microscopy.....	- 108 -
Solid state NMR of PrP fibrils	- 114 -
Hydrogen/Deuterium exchange of fibril core.....	- 117 -
Chapter 4.....	- 120 -
Outlook	- 120 -

Appendix	- 128 -
Chemical shift values for recombinant prion protein ₉₀₋₂₃₀	- 128 -
Literature	- 132 -
Ausführliche Deutschsprachige Zusammenfassung	- 149 -
Einleitung.....	- 149 -
Ziel der Arbeit	- 150 -
Ergebnisse.....	- 151 -
Zuordnung	- 151 -
Aminosäuren des Fibrillenkerens	- 152 -
Polymorphismus	- 153 -
Adaptierung	- 154 -
Ausblick.....	- 155 -
Acknowledgements	- 157 -
Curriculum vitae	- 160 -

LIST OF FIGURES

<i>Number</i>	<i>Page</i>
Figure 1.1: Schematic representation of central dogma of molecular biology: the flow of biological information.	3 -
Figure 1.2: Schematic representation of folding energy landscapes. (a) Smooth funnel model: An idealized funnel landscape. As the chain forms increasing numbers of intrachain contacts, and lowers its internal free energy, its conformational freedom is also reduced (b) Bumpy bowl model which display that native structure N is achieved through intermediate stages with kinetic traps, energy barriers, and some narrow throughway paths (c) a cross-sectional view of funnel. (adapted from (Dill and Chan, 1997)).	6 -
Figure 1.3: Folding of β -Hairpin Peptide routing through nonnative structures. (Adapted from (Thukral et al., 2009)).....	8 -
Figure 1.4: Outline of protein folding, misfolding and aggregation in living cell: in the normal path (green arrows), molecular chaperones regulate the folding and proteasomal degradation pathway prevents protein misfolding. In abnormal conditions (red arrows), failure in these mechanisms results in increased protein aggregation by self-association of partially folded ensembles which lead to formation of small oligomers, protofibrils and mature fibril deposits (adapted from (Jahn and Radford, 2005))......	10 -
Figure 1.5: extension of protein funnel with addition of aggregation funnel in magenta, when extended ensembles trap to form aggregates or amyloids. adapted from (Jahn and Radford, 2005).	14 -
Figure 1.6: Prion cycle in cell. Prion proteins are synthesized and processed in ER and Golgi and transported to cell membrane (green) while, when they come in contact with rouge conformer (red), conversion of normal PrP to rouge conformation happened at cell surface and cell intake misfolded protein by endocytosis. These misfolded prions pile up in lysosome and where they grow in volume leading to cell death.	19 -
Figure 1.7: NMR structure of human prion protein (PDB:1QM0), C-ter 23 to 125 are unstructured while N-ter 126 -228 have well-defined structure having three α -helices and two β -strands forming an anti-parallel sheet. The N-ter unstructured part consist of five octapeptide repeats followed by charge cluster (CC), hydrophobic cluster (HC), while structured part is having two β -strand (S1 & S2) and three α -helices (H1, H2 & H3)	25 -
Figure 1.8: The pathogenic point mutations associated with hereditary prion diseases in PrP 27-30 region. (Prusiner, 1998, van der Kamp and Daggett, 2009)......	27 -
Figure 1.9: Nucleation dependent polymerization model of prion propagation, early conversion to β -rich structure is reversible and slow, therefore rate-limiting step.	28 -

Figure 1.10: Template assisted model of prion propagation; first external misfolded conformer act as seed, which drive native PrP to misfold.....	30 -
Figure 1.11: Two different biochemical protocols yield recombinant PrP with different level of infectivity. The amyloid fibrils, which are formed by incubating recombinant PrP with chemical denaturants were less infectious (left) while mixing recombinant PrP with phospholipid and RNA produces highly infectious prions (right). Adapted from (Supattapone, 2010).	35 -
Figure 1.12: The left handed β -helical model adapted from (Govaerts et al., 2004).....	36 -
Figure 1.13: spiral model of prion fibrils, adapted from (DeMarco and Daggett, 2004).....	37 -
Figure 1.14: schematic diagram of atomic force microscopy (AFM) setup, showing cantilever & tip. (Adopted from wikipedia).....	44 -
Figure 1.15: Time scales of molecular motions for the prion (PrP) protein and linked NMR-techniques.....	47 -
Figure 2.1: Model for <i>in vitro</i> prion fibrillation in denaturing environment. The native-like conformer (a) of recombinant hPrP ₉₀₋₂₃₀ compass three α -helices and two β -strand forming anti-parallel sheet (PDB:1QMO) (Zahn et al., 2000). Addition of 8M Urea and acidic pH changes the equilibrium between unfolded extended confirmation (b) and β -sheet rich conformation (c)(Baskakov, 2004). These β -sheet rich monomers lead to either amorphous aggregate (f) or fibril formation (g) when agitated at 600 rpm at 37°C; probably through formation of intermediate oligomer (d) and protofibrils (e).	62 -
Figure 2.2: Two dimensional landscapes of C_{β} and C_{α} chemical shifts with characteristics areas for different amino acid types. The circle shows approximate areas with standard deviations of the chemical shift values found in Biological Magnetic Resonance Bank database (www.Bmrb.wisc.edu)	67 -
Figure 2.3: The distribution of MUSIC based selective HSQCs for all amino acids	68 -
Figure 3.1: ^1H ^{15}N HSQC spectra for various urea concentrations recorded with recombinant human prion protein 121-230, the spectra for 4 M urea concentrations display line broadening and disappearance of signals, indicating molten globule state of protein, while spectra in 8 M urea, shows characteristics low dispersion of signals.....	77 -
Figure 3.2: ^1H ^{15}N HSQC spectra in 8 M urea, pH 2 for recombinant human prion protein (90-230) with assignments.	79 -
Figure 3.3: ^1H ^{15}N MUSIC based HSQC spectra in 8 M urea, pH 2 for recombinant human prion protein (90-230) for $i+1$ residues for Alanine (left) and either Leucine or Alanine (right).....	80 -
Figure 3.4: ^1H ^{15}N MUSIC based HSQC spectra in 8 M urea, pH 2 for recombinant human prion protein (90-230) for $i+1$ residues for Valine, Isoleucine or Alanine (left) and either aromatic Phenylalanine, Tyrosine or Histidine (right).	81 -

Figure 3.5: ^1H ^{15}N MUSIC based HSQC spectra in 8 M urea, pH 2 for recombinant human prion protein (90-230) for i+1 residues for Glutamate, Glutamine and Glycine.	82 -
Figure 3.6: Strip plots for three dimensional HNN experiments for 10 residues long sequence (111-120) including palindrome sequence AGAAAAGA . (next page).....	83 -
Figure 3.7: Strip plots for three dimensional HNCACB, and CBCA(CO)NH experiments for 10 residues long sequence (111-120) including palindrome sequence AGAAAAGA.	84 -
Figure 3.8: Chemical shift deviation plots for recombinant human prion protein 90-230 (previous page). The cumulative (Kumar et al., 2008) shift indicates random coil structure for whole sequence with slight preference for β -sheets.....	85 -
Figure 3.9: Chemical shift Index (CSI) (Berjanskii and Wishart, 2005) plots for recombinant human prion protein 90-230. The CSI values shows β -sheet preferences for residues 182-83 and 189-193, primarily consist of theronine residues.	86 -
Figure 3.10: TALOS+ analysis; S^2 and β -sheet propensity (Shen et al., 2009) plots for recombinant human prion protein 90-230. The RCI values shows β -sheet preferences for residues 208-210 and 213-214, rest of chain shows random coil preferences.	86 -
Figure 3.11: Electron micrograph of the hPrP ₉₀₋₂₃₀ sample showing long straight fibrils. Scale bar: 500 nm.	87 -
Figure 3.12: Solution NMR of human prion fibrils. (a) ^1H , ^{15}N -HSQC spectra of hPrP ₉₀₋₂₃₀ at 298K in 8M urea, pH 2 at a concentration of 200 μM in 10% D ₂ O. Spectrum acquired 30 minutes after dissolving hPrP ₉₀₋₂₃₀ . The spectrum is well resolved and 135 out of 136 cross peaks are assigned (Figure 3.2). Spectra acquired (b) 4 days and (c) 7 days after dissolving hPrP ₉₀₋₂₃₀ under constant agitation.	88 -
Figure 3.13: Disappearing signals include the region comprising the residues 166-230 of hPrP sequence. (a) ^1H , ^{15}N -HSQC spectrum of hPrP ₉₀₋₂₃₀ acquired immediately after dissolving the protein in the denaturing conditions (8 M urea, pH 2.0, 25°C). (b) Overlay of the spectra in (a) acquired on the 4 th day (blue) and the construct hPrP ₁₆₆₋₂₃₀ (8 M urea, pH 2.0, 25°C) acquired immediately after sample preparation. The disappearing signals in the hPrP ₉₀₋₂₃₀ include region 166-230, * represents signals for the palindrome sequence AGAAAAGA (113-120).	89 -
Figure 3.14: Integrated PFGSE profiles for prion protein in fibril state as a function of field strength. Data is plotted for a range of Δ .(in grey) with a lysozyme monomer (black). These values are in accordance with earlier reported values for SH3 fibrils (Baldwin et al., 2008) supporting the presence of large molecular structures like the fibrils, in solution.	90 -
Figure 3.15: Bar diagram showing decrease in NMR peak intensities for hPrP ₉₀₋₂₃₀ ; blue (red) bars represents the changes observed on day 4 (7) relative to their initial intensities and normalized to internal phthalimide (\$) as standard. Blue and red lines represent the running average over 7 residues.	

* and # indicates prolines for which no backbone assignment can be obtained and unassigned residues, respectively. YY(Q)R and palindrome AGAAAAGA are marked in red in sequence. The changes in intensities for YYR motif 149-151 is shown in the box. - 92 -

Figure 3.16: 1D ^{13}C MAS (magic angle spinning) spectra of hPrP $_{90-230}$ fibrillar state. hPrP $_{90-230}$ aggregates into fibres and forms with time a sample of gel-like texture. This sample was transferred from the liquid-state NMR tube into a 4mm MAS NMR rotor by centrifugation. At a spinning rate of 10 kHz, ^{13}C spectra were recorded using direct polarization (DP) and cross polarisation (CP). The DP spectrum (a) reveals well-resolved resonances with line widths of down to 0.5ppm. A signal loss is observed under CP conditions. This indicates high molecular mobility, which makes dipolar-based magnetization transfer as in CP inefficient. Spectra were recorded at a Bruker Avance 600WB spectrometer using a 4mm DVT probehead at 25°C. In both cases, ^1H decoupling of 90 kHz was applied and 2048 transients were accumulated. For CP, a contact time of 2ms was used. The FIDs were processed using exponential line broadening of 20Hz. - 94 -

Figure 3.17: Overlay of ^1H ^{15}N HSQC spectrum of hPrP $_{90-230}$ (green) and hPrP $_{166-230}$ (black) acquired in the denatured state at 8 M urea, pH 2.0, 25°C. - 95 -

Figure 3.18: Structural properties of Tyr-Tyr-Arg (YYR) motifs. (a) Secondary structure representation of hPrP $_{90-230}$ showing the distribution of tyrosine residues. Tyrosines appearing in pairs have been encircled. (b) ^1H ^{15}N HSQC spectra of hPrP $_{90-230}$ at 298K in 8M urea, pH 2 at a concentration of 200 μM in 10% D_2O . The signals correspond to the Tyr225-Tyr226-Gln227 in α -helix-3 of hPrP. The changes in the chemical shift are indicated by the arrow. The graph in the inlay shows changes in the intensity of the signals observed with respect to the first day of sample preparation (normalized to internal phthalimide). - 96 -

Figure 3.19: Schematic presentation of fibril core of recombinant prion hPrP $_{90-230}$ amyloid fibrils as investigated by mass spectrometry (Lu et al., 2007), electron paramagnetic resonance (EPR) spectroscopy (Cobb et al., 2007, Cobb et al., 2008) and solution-NMR spectroscopy (our data). The charged cluster (CC), hydrophobic core (HC), helices (H1, H2 and H3) and single disulfide bridge (S-S) from native structure (Zahn et al., 2000) are indicated. - 98 -

Figure 3.20: an example of α - β polymorphism observed. Cryo-EM reconstructions of 12 individual α - β (1-40) fibrils. (a) Electron micrographs of the 12 individual α - β (1-40) fibrils from the same sample. (b and c) Side (b) and top (c) views of the reconstructed fibrils shown in (a); the image is adapted from (Fandrich et al., 2009, Meinhardt et al., 2009). - 101 -

Figure 3.21: EMgraph of recombinant prion protein fibrils, these fibrils formed on long incubation at room temperature, and samples were not agitated. The EMgraphs clearly display a population of long twisted fibrils, which are having twisted about every 80nm and 20 nm in diameter. There are other fibrils presents, which are relatively thinner. - 103 -

Figure 3.22: The EMgraph of freshly prepared recombinant prion fibrils, samples were non-agitated and clearly display that sample is full of small worm-like fibrils, the length of these fibrils are relatively short and about 100nm.	103 -
Figure 3.23: The EMgraph of recombinant prion fibrils (non-agitated) display the presence of classic rod-like fibrils along with some twisted fibrils.....	104 -
Figure 3.24: The EMgraph of recombinant prion protein fibrils (agitated) displaying long-straight fibrils appearing in bunches for low protein concentration.	104 -
Figure 3.25: The EMgraph is showing a possible presence of high-order oligomers in the sample.	105 -
Figure 3.26: These EMgraphs reveal the presence of very-thin fibrils which are bundled together. These images are in accordance with the fibrils morphology observed for unglycosylated mouse prion fibrils (Sim and Caughey, 2009).	105 -
Figure 3.27: The view of EM grid.	106 -
Figure 3.28: The EMgraph for fibrils, which were dialyzed against water, pH2. These are long unbranched straight fibrils.....	106 -
Figure 3.29: The EMgraph for fibrils generated from a synthetic peptide containing residues from 174-184.	106 -
Figure 3.30: The electron diffraction pattern for fibrils formed of hPrP peptide 174-184.....	107 -
Figure 3.31: The high -resolution AFM images of recombinant human prion fibrils at two different magnifications (5 μm and 1.5 μm). The left panel shows height data, while amplitude images are shown on right panel. The upper image shows couple of non-fibril aggregates, and fibrils are branching out from there in spun and woven manner. The dense fibrils show variable heights. The detailed view in lower panel shows that most of fibrils are straight but different diameters. A small population of oligomers is also visible.....	109 -
Figure 3.32: The high resolution AFM images of recombinant human prion fibrils at a high magnification (700 nm). The left panel shows height data, while amplitude images are shown on the right panel. The image shows fibrils of variable length but similar height profile. Interestingly, the fibrils are arranged in bead like manner, which probably reflect twist in fibrils.....	110 -
Figure 3.33: The high -resolution AFM images of recombinant human prion aggregates; there are curvy fibril weaving out from those clusters of protein.	111 -
Figure 3.34: The high -resolution AFM images of recombinant human prion aggregates, which were dissected by urea crystal formed at 4 °C, two different dilution of preparations shows presence of large number of oligomeric species.	112 -
Figure 3.35: The high - resolution AFM images of recombinant human prion aggregates, the upper image shows amorphous aggregate formed, oligomers are visible in high number as well. The lower image shows a single straight fibril with a number of oligomers around.....	113 -
Figure 3.36: The distribution of carbon chemical shift in a typical solid state spectrum.....	114 -

Figure 3.37: The carbon chemical shift for recombinant human prion fibrils, A) and B) HP-MAS spectra of fibrils in water and urea respectively while C) D) and E) are decoupled spectra. The spectra A) and C) are for same sample and display flexible threonine C β and aromatic side chain C atoms, the signals in MAS spectra are weak, indicating flexible nature of fibrils. Spectra A) C) and E are of fibrils in 8 M urea, displaying highly flexible nature of residues in fibrils.....	- 116 -
Figure 3.38: The schematic presentation of sample preparation for HDX experiments.....	- 117 -
Figure 3.39: Protection plot for deuterium (70%) exchanged fibrils. Most of the residues show about 40% protection. There is a dip around TTTT sequence (189-192) showing that these amide protons are completely exchangeable.	- 119 -
Figure 4.1: outline of various fibrillation studies performed with unfolded recombinant prion protein constructs.....	- 120 -
Figure 4.2: Paths of molecular assemblies in a cell, a native monomer adopt to association prone monomer conformations in the suitable environments, these monomers then assemble into early oligomers with variable lag time in the formation of oligomers, and finally lead to end product like amorphous aggregates, globular oligomers, annular oligomers or to amyloids through the formation of nucleus.....	- 122 -
Figure 4.3: With new knowledge about strains and substrains, the energy landscape of amyloid formation should be broaden to include substrain phenomena of amyloid, which is largely depending upon the local environment.	- 125 -

LIST OF ABBREVIATIONS

1D, 2D, 3D	one dimensional, two dimensional, three dimensional
AFM	atomic force microscopy
ANS	1-anilino-8-naphthalene sulfonate
APS	ammonium persulfate
BME	β -mercaptoethanol
BMRB	biological magnetic resonance bank
BPI	base pair insertions
BS	bio-safety level
BSE	bovine spongiform encephalopathy
CARA	computer aided resonance assignment
CD	circular dichroism
CJD	Creutzfeldt-Jakob disease
CM	carboxy methyl
CNS	central nervous system
CPMG	Carr-Purcell-Meiboom-Gill Sequence
CSA	chemical shift anisotropy
CSF	cerebrospinal fluid
CSI	chemical shift index
C-ter	carboxyl terminal of a protein

CWD	chronic waste disease
DIPSI	decoupling In the presence of scalar interactions
DNA	deoxyribonucleic Acid
DSC	differential scanning calorimetry
DSS	4,4-dimethyl-4-silapentane-1-sulfonic acid, a NMR standard
DTT	dithiothreitol
<i>E.coli</i>	<i>Escherichia coli</i>
EDTA	ethylenediaminetetraacetic acid
EM	electron microscopy
EtOH	ethyl alcohol
FFI	fatal familial insomnia
FPLC	fast protein liquid chromatography
FRET	fluorescence resonance energy transfer
FTIR	fourier transform infrared spectroscopy
GdHCL	guanidine hydrochloride
GMM	genetically modified microorganisms
GSS	Gerstmann-Sträussler-Scheinker syndrome
hetNOE	heteronuclear NOE experiment
HMQC	heteronuclear multiple quantum correlation
HMBC	heteronuclear multiple bond correlation
HSQC	heteronuclear single quantum correlation

HPLC	high-performance liquid chromatography
haPrP	hamster prion protein
hPrP	human prion protein
hPrP ₁₂₁₋₂₃₀	truncated recombinant human prion protein polypeptide from residue 121 to 230
^{His} hPrP ₁₂₁₋₂₃₀	truncated recombinant human prion protein polypeptide from residue 121 to 230 with N-terminal hepta-hisdine tag
hPrP ₁₆₆₋₂₃₀	truncated recombinant human prion protein polypeptide from residue 166 to 230
hPrP ₁₇₄₋₁₈₄	synthetic human prion protein polypeptide from residue 174 to 184
hPrP ₉₀₋₂₃₀	truncated recombinant human prion protein polypeptide from residue 90 to 230
^{His} hPrP ₉₀₋₂₃₀	truncated recombinant human prion protein polypeptide from residue 90 to 230 with N-terminal hexa-histide tag
iCJD	iatrogenic Creutzfeldt-Jakob disease
INEPT	insensitive nuclei enhanced by polarization
IPAP	In-phase anti-phase (HSQC)
kDa	kilo-Dalton (= 10 ³ g/mol)
MAS	magic angle spinning
CP	Cross Polarization

IPTG	isopropyl β -D-1-thiogalactopyranoside
IUPAP	International Union of Pure and Applied Physics
LB	Luria Bertani broth
M	molar
ml	milliliter
mM	millimolar
μ l	microliter
μ M	micromolar
μ s	microseconds
MS	mass spectrometry
MWCO	molecular weight cut-off
NMR	nuclear magnetic resonance
NOE	nuclear Overhauser effect
NOESY	nuclear Overhauser effect spectroscopy: inter-nuclear cross relaxation
N-ter	amino terminal of a protein
OD ₆₀₀	optical density at 600 nm
PCR	polymerase chain reaction
PDB	protein data bank
PFG	pulse field gradient
PG-SLED	pulse gradient stimulated echo longitudinal encode decode

pH	negative log of the concentration of the hydrogen ions
PI	protein isoelectric point
π - π	stacked arrangement of aromatic molecules
PK	proteinase-K
PMCA	protein misfolding cyclic amplification
PMSF	phenylmethanesulfonylfluoride
ppm	parts per million
PrP 27-30	major scrapie prion protein
PrP 33-35	precursor prion protein
PrP ^{res}	proteinase-K resistant prion protein
PrP ^C	cellular prion protein
PrP ^{Sc}	scrapie prion protein
PrP ^{senin}	proteinase-K sensitive prion protein
R ₁	longitudinal or spin-lattice relaxation rate
R ₂	transversal or spin-spin relaxation rate
R _H	hydrodynamic radius
RDC	residual dipolar coupling
RNA	ribonucleic acid
rpm	rotation per minute
ROESY	rotational nuclear Overhauser effect spectroscopy
SAXS	small-angle X-ray scattering

sCJD	sporadic Creutzfeldt-Jakob disease
SDS	sodium dodecyl sulfate
SDS-PAGE	sodium dodecyl sulfate polyacrylamide gel electrophoresis
SEM	scanning electron microscope
ssNMR	solid state NMR spectroscopy
T ₁	longitudinal or spin-lattice relaxation time
T ₂	transversal or spin-spin relaxation time
TEM	transmission electron microscopy
TEMED	tetramethylethylenediamine
TFA	trifluoroacetic acid
TFE	trifluoroethyl alcohol
ThS	thioflavin S
ThT	thioflavin T
TMS	trimethylsilyl propionate, a NMR standard
TMSP	trimethylsilyl propionate, a NMR standard
TOCSY	total correlated spectroscopy
Tris	tris(hydroxymethyl)aminomethane
TSE	transmissible spongiform encephalopathy
UV	ultraviolet
UV-Vis	ultraviolet-visible spectroscopy
vCJD	variant Creutzfeldt-Jakob disease

w/v	weight/volume percentage
WHO	world health organization
WALTZ	A broad-band composite pulse decoupling scheme
τ	Correlation time for the electron-nuclear interaction
wt	wild type

Abstract

Transmissible spongiform encephalopathies (TSEs) are rare but fatal neurodegenerative diseases affecting human and animals. The prion protein which is the causative agent, according to “protein-only” hypothesis misfold in to rogue amyloid conformer. Despite several years of studies, the atomic structural details of the rogue conformers have not been clearly understood. This study focused on developing an *in-vitro* conversion method, which allows us to monitor the transition from unfolded state of prion protein to fibril state. In order to reach maximal unfolded state, we have used 8 M urea as chemical denaturant, pH 2 and prion fragment 90-230 as the model. It has been demonstrated earlier that acidic pH and mild denaturant induce the fibril formation. The mechanism underlying the structural transition from monomeric state to polymeric form is largely unknown. We have confirmed by EM and AFM that fibrils are formed in our conditions, which resemble to naturally occurring fibrils in morphologies observed. The agitation accelerates the rate of fibril formation and, which allow us to do time-resolved NMR on these preparations.

The conformational flexibility is inherent to amyloid fibrils and has been observed in our preparations. We aimed to map the important segment of prion protein, which forms the rigid core in its fibrillar structured form. Our time-resolved NMR studies allowed us to monitor the changes happening from unfolded state to fibrillar state. Analysis of data identified the segment between residues 145 to 223 forming the rigid core in these fibrils, which correspond to β strand 2, helix 2 and major part of helix 3 of native prion monomeric structure. Most of the point mutations which are associated with hereditary prion disease are part of rigid core, which undergo a refolding on fibril formation. The C-terminal residues from 224 to 230 displayed

peak shifting and therefore, indicate the adaptation to a fibril specific conformation. The major part of N-terminal 90-144 segment, remains dynamic, which can be understood by their accessibility to amyloid specific antibodies. This provides novel structural insight to the amyloid formation from unfolded state of prion protein fragment 90-230, which represents the proteinase-K resistant part naturally occurring prions. Earlier studies have established the core to 160-220 where hydrogen-deuterium exchange mass spectrometry or site-directed spin labeling EPR spectroscopy was used for analysis. Those studies have been initiated from either native-like or partially unfolded state of recombinant prion protein, and therefore, it is quite striking to find out that fibrils initiated from unfolded monomeric state share the same “amyloid core”. This structural insight has important implications for understanding the molecular basis of prion propagation

Chapter 1

Protein Misfolding, Amyloid and Prion Diseases

The "Central Dogma of Molecular Biology" (Crick, 1970) refers to the flow of genetic information in biological systems. The genetic information flows from DNA to RNA to protein. DNA (deoxyribonucleic acid) encodes the genetic information for most species. In order to use this information to produce proteins, the DNA must first be converted into a messenger RNA (ribonucleic acid) through a process called transcription. The information carried by the mRNA is then used as information transfer to code for a specific protein (or polypeptide) through a process called translation. Each polypeptide then performs a specific function in the cell. Retroviruses, like HIV, carry an RNA genome which is converted into DNA prior to its insertion into the human genome. In order to carry out this conversion, the RNA must be reverse transcribed into DNA. Retroviruses produce a special enzyme called reverse transcriptase which, conveniently, performs the process of reverse transcription (RNA \rightarrow DNA). Once the viral DNA is inserted into the human genome, the standard rules of the central dogma apply (Figure 1.1).

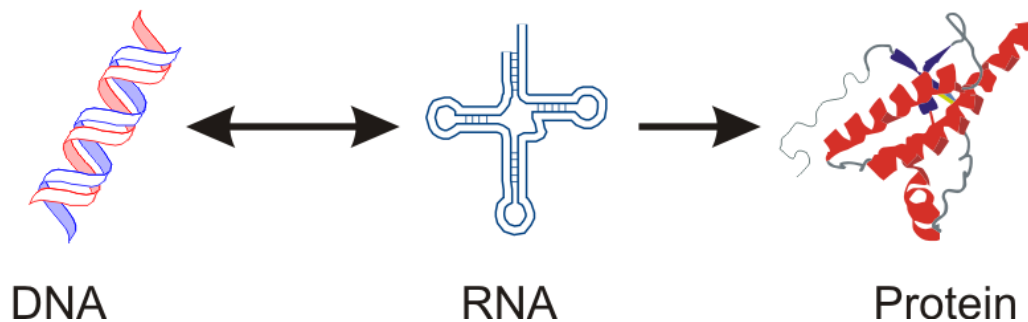


Figure 1.1: Schematic representation of central dogma of molecular biology: the flow of biological information.

The prions as called by Nobel laureate S. Prusiner to define “proteinaceous infectious agent” are protein molecules which are infectious agents. Since prions are proteins, they do not carry a genome. Prion diseases, such as Mad Cow, result from the interaction of misfolded, i.e. rogue prion proteins with normal prion proteins. These interactions result in the misfolding of the normal prion proteins and, ultimately, the typical spongiform encephalopathy associated with prion diseases (Hunter, 1999, Keyes, 1999a, b, Morange, 2007). The native structure of protein is the unique, stable and kinetically accessible minimum of the free energy. How these proteins reach their native structure is studied as "protein folding". These prions exist in more than one stable conformation (prion strains) and, which defy the presence of single minimum energy structure. These structures are usually macromolecular ordered assemblies, known as protein fibrils. It therefore, studies on prion proteins and alike a new field of study called “Protein misfolding and aggregation”. In this chapter, we discuss about understanding of protein folding, misfolding and aggregation, human prion protein and its conformations, structures of amyloid fibrils and finally NMR methods to explore amyloid fibril assemblies and its formation.

Protein folding, misfolding and aggregation

Protein folding is defined as the physical process by which a newly expressed nascent polypeptide chain adopts its characteristic and functional conformation. This process includes structural modification in the endoplasmic reticulum and the Golgi in eukaryotic organisms. The stable structural conformation exposes hydrophilic elements on the surface, while hydrophobic elements form the interior of the protein (Crick, 1970). This process is crucial as the correct fold is a prerequisite for a protein’s stability and the functionality to make it able to interact

with its partner biological macromolecules (Dobson, 2003). How do these proteins adopt the correct structure? What is the mechanism of folding? How is folding regulated in a living cell? These are the fundamental questions of protein folding. In 1968, Levinthal (Levinthal, C., 1968) was the first to notice the protein puzzle that even though proteins have vast conformational spaces, proteins can search and converge quickly to native states, on a microsecond time scale. The pioneering work of Anfinsen on protein folding in the 1970s (Anfinsen, 1973) inferred that the three-dimensional structure is encoded by the amino acid sequence of the polypeptide chain and this functional fold represents a global minimum on the energy landscape. Based on this finding, enormous effort has been put to understand the process of folding. How to achieve a minimum energy state and tracing the trajectory of folding has been of major interest in protein folding studies. The folding funnel hypothesis is a specific version of the energy landscape theory of protein folding, which assumes that a protein's native state corresponds to its free energy minimum under the solution conditions usually encountered in cells. It became evident that a random search for the right conformation cannot be performed on a microsecond to a millisecond biological timescale of protein folding, and the protein is “funneled” down through the energy landscape by energy barriers, kinetic traps and narrow pathways (Figure 1.2) (Wolynes et al., 1995, Dill and Chan, 1997). The cross-sectional view of energy funnel; shows presence of the myriads of unfolded states at the edges of the funnel, where potential energy and entropy are large. The native state is found at the funnel's bottom and has minimal energy and almost zero

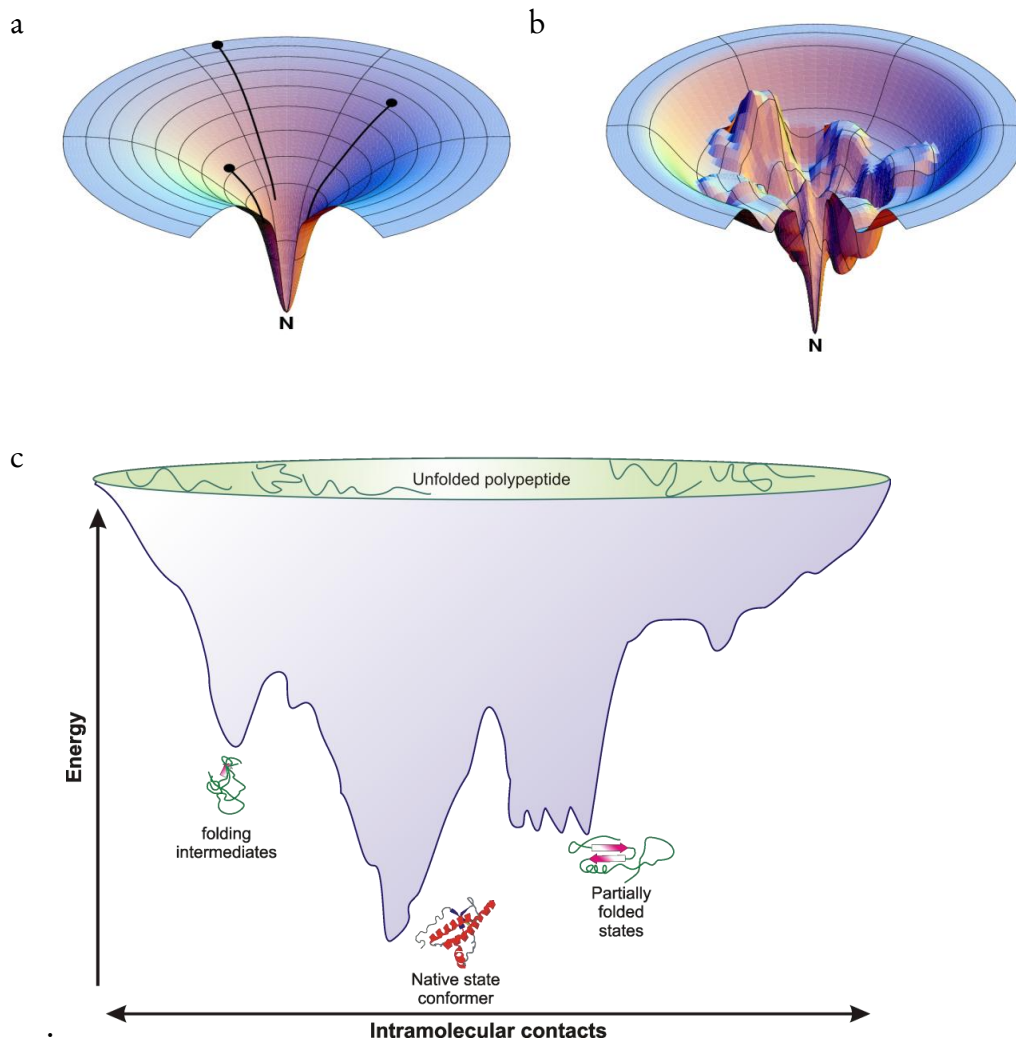


Figure 1.2: Schematic representation of folding energy landscapes. (a) Smooth funnel model: An idealized funnel landscape. As the chain forms increasing numbers of intrachain contacts, and lowers its internal free energy, its conformational freedom is also reduced (b) Bumpy bowl model which display that native structure N is achieved through intermediate stages with kinetic traps, energy barriers, and some narrow throughway paths (c) a cross-sectional view of funnel. (adapted from (Dill and Chan, 1997)).

entropy. Folding, therefore, advances by a trade-off between energy and entropy as protein moves down the energy landscape its energy decreases, but so does its entropy. This folding process takes place by different routes connecting unfolded and native state of protein. The concept of a folding funnel can be understood as ensembles of unfolded nascent polypeptide chain flowing through many diverse parallel microscopic routes to the native state ground state. Therefore the folding pathway is an ensemble of multiple microscopic folding trajectories and these microscopic folding routes may be grouped into several macroscopic pathways. Any state except the native (unfolded and intermediate) is an ensemble of microstates (i.e., microscopic conformations). *These microstates are meta-stable and microscopic trajectories initiate from unfolded ensembles. These conformational trajectories are driven either by native, nonnative or a blend of both interactions.* The presence of nonnative interactions in the transition state is supported by all-atom simulations using a Charmm-based effective energy function, where it was found that 20%–25% of the energy in the transition state arose from nonnative contact (Paci et al., 2002). Recently; a computational study on β -Hairpin peptide shows that its folding to native structure channeled through nonnative structuring (Figure1.3). This is one of the examples to show the importance of nonnative interactions in protein folding (Thukral et al., 2009), which is in accordance to the data published from our group stating that nonnative contacts stabilize early formed structures to prevent degradation or aggregation (Klein-Seetharaman et al., 2002).

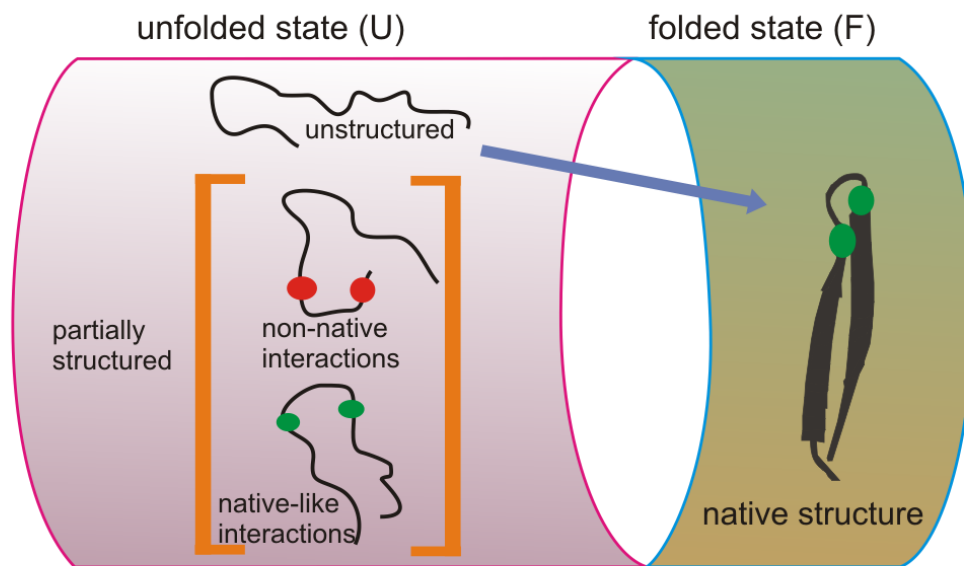


Figure 1.3: Folding of β -Hairpin Peptide routing through nonnative structures.
(Adapted from (Thukral et al., 2009))

On the other hand, the living cells are composed of very dense environment having about 300 g/L of protein and other macromolecules (Ellis, 2001b, a). This macromolecular crowding is considered as an important cause for these nonnative interactions which lead to intermolecular interactions between the unfolded domains of unstable or partially stable intermediate states. These intermolecular interactions results in self-association leading to formation of large ordered or disordered assemblies broadly called “aggregates” (Dobson, 2003, Brockwell and Radford, 2007). It is necessary for a cell to avoid these aggregate formations and therefore folding should happen in a regulated manner to prevent misfolding (Figure 1.4). In biological state, this is achieved by molecular chaperones (e.g. Hsp/Csp) they guide protein to adopt correct functional fold while the ubiquitin proteasome pathway directs degradation of abnormally folded conformations (Jahn

and Radford, 2005). The failure or disruption of any of these safeguarding systems results in malfunctioning of the living organism causing the disease (Dobson, 2001, Horwich, 2002). The nonnative states of proteins are considered as potential entry points for folding or misfolding pathways of protein thus it is important to characterize the residual structure in these states. Nonnative states of proteins can be produced *in-vitro* by denaturizing the native protein. This denaturation is achieved by putting protein under physical or chemical stress; physical methods include pressure and temperature variation while chemical stress is created by varying pH to highly alkaline or acidic, by chaotropic agents such as urea or guanidine hydrochloride, by detergents like sodium dodecyl sulfate and by other reducing agents like 2-mercaptoethanol or dithiothreitol. This denaturation process is often reversible.

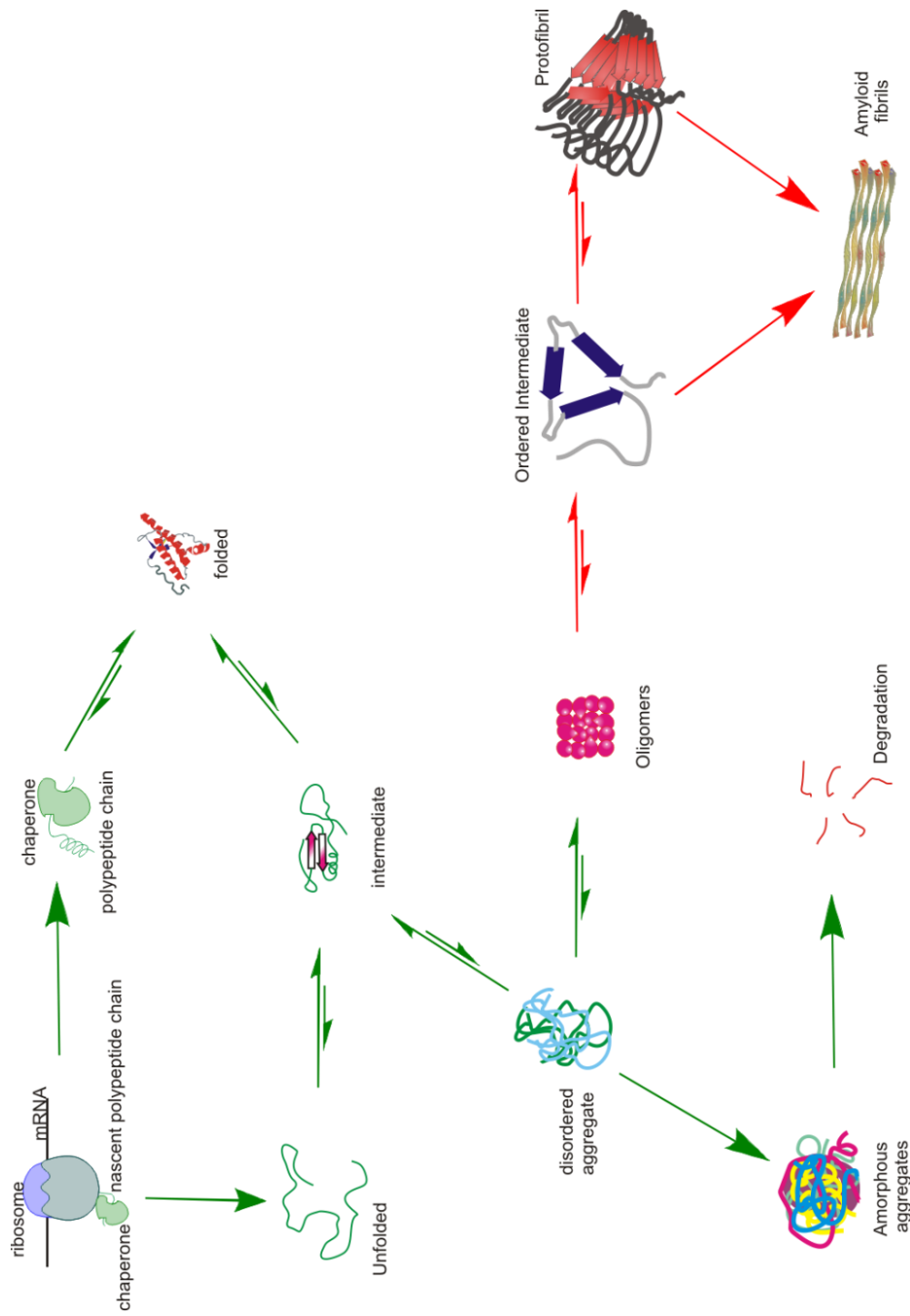


Figure 1.4: Outline of protein folding, misfolding and aggregation in living cell: in the normal path (green arrows), molecular chaperones regulate the folding and proteasomal degradation pathway prevents protein misfolding. In abnormal conditions (red arrows), failure in these mechanisms results in increased protein aggregation by self-association of partially folded ensembles which lead to formation of small oligomers, protofibrils and mature fibril deposits (adapted from Jahn and Radford, 2005)).

Amyloidosis: a protein conformational disease.

„Es gibt fast kein Problem in der allgemeinen und speziellen Pathologie, das sich über Jahrhunderte in einer so sphinxhaften Weise verhalten hat wie die Amyloidose.“ [There is almost no problem in general and systemic pathology that over the centuries has behaved in such a sphinx-like way as amyloidosis.] From Letterer (1966)(Westermarck, 2006)

The term amyloidosis refers to a group of diseases caused by abnormal deposition of aggregated proteins in organs and/or tissues (Ghiso et al., 1986, Abrahamson et al., 1992, Westermarck et al., 2005). Amyloidosis can be either local or systemic, where the amyloid deposits are localized to a particular organ or found in the whole body, respectively. So far, 24 (or more) different proteins have been isolated from amyloid deposits associated with different forms of human amyloidoses (Westermarck et al., 2005, Westermarck, 2005). A brief summary of some amyloidogenic proteins and related amyloid diseases is given in Table 1 (Westermarck, 2006). Among these disorders, prion diseases distinguish themselves by their transmissibility, which is believed to be a serious threat to the public health.

Table 1 : Amyloid fibril proteins and their precursors in human (Westermark, 2006).

Amyloid	Precursor protein		Systemic (S) or localized (L)	Syndrome or involved tissues
AL	Immunoglobulin chain	light	S, L	Primary myeloma associated
AH	Immunoglobulin chain	heavy	S, L	Primary myeloma associated
ATTR	Transthyretin		S	Familial senile systemic
A β 2M	β 2-microglobulin		L	Tenosynovium Hemodialysis Joints
AA	(apo)serum AA		S	Secondary, reactive
AApoAI	Apolipoprotein AI		S	Familial
AApoAII	Apolipoprotein AII		L	Aortic
AGel	Gelsolin		S	Familial
ALys	Lysozyme		S	Familial
AFib	Fibrinogen α chain		S	Familial
ACys	Cystatin C		S	Familial
ABri/AD an	ABriPP/ADanPP		S/L	Familial British/Danish senile
AApoAIV	Apolipoprotein AII		S	senile
A β	A β protein precursor		L	Alzheimer's disease
APrP	Prion protein		L	Spongiform encephalopathies
ACal	(Pro)calcitonin		L	C-cell thyroid tumors
AIAPP	Islet amyloid polypeptide		L	Islets of Langerhans insulinomas
AANF	Atrial natriuretic factor		L	Cardiac atria
APro	Prolactin		L	Aging pituitary prolactinomas
AIns	Insulin		L	Iatrogenic
AMed	Lactadherin		L	Senile aortic, media
AKer	Kerato-epithelin		L	Cornea; familial
ALac	Lactoferrin		L	Cornea; familial

Amyloid

The term amyloid was introduced in 1854 by the German doctor Rudolph Virchow to define an abnormal macroscopic appearance in cerebral corpora amylacea after staining with iodine. These macroscopic deposits had properties similar to cellulose and starch (Puchtler and Sweat, 1966). Virchow also detected proteins in these deposits, but the protein fraction was not considered to be a part of the amyloid. Later, it was established that main component of amyloid is protein (Sipe and Cohen, 2000). In 2006 the *Nomenclature Committee of the International society of Amyloidosis* defined amyloid as intra- and extracellular protein deposits, mainly consisting of protein fibrils with typical X-ray diffraction pattern and a particularly affinity for the dye Congo red resulting in green birefringence. It was based on earlier studies using electron microscopy, which displayed that amyloids of different origins share similar fibrillar ultrastructure (Cohen and Calkins, 1959). Similarly, the optical microscopic studies of Congo red-stained amyloid revealed that it shows apple-green birefringence under polarized light (Puchtler and Sweat, 1966). The following X-ray diffraction analysis of amyloid revealed that amyloid fibrils present characteristic “cross- β ” structure, i.e. continuously stacked β strands are oriented perpendicular to the axis of the fibril (Eanes and Glenner, 1968). First, atomic level insight into this “cross- β ” motif has been obtained by Nelson et al. using microcrystals formed by short amyloidogenic peptides thought to reflect certain structural properties of amyloid fibrils (Nelson et al., 2005).

In classical sense, amyloid is an extracellular deposit of proteinaceous fibrils, with specific “cross- β ” structure, characterized by green birefringence after being stained by Congo red (Westermarck et al., 2005). However, it has been shown that many synthetic proteins and peptides form amyloid-like fibrils *in vitro*. Thus,

biophysically, the definition of amyloid may be extended to any ordered protein or peptide aggregate with a “cross- β ” structure. The concept of protein folding funnel was extended to “dual-funnel” to allow the aggregation states of proteins (Figure 1.5). Partially folded states on this landscape may be intrinsically prone to aggregation, and favorable intermolecular contacts drive their association towards fibrillar state and eventually to protein-misfolding diseases. The mechanisms, specific to aggregation process have not been fully understood. A general understanding about misfolding and aggregation is that intermolecular contacts are required to drive *unfolded polypeptide ensembles* towards many disease causing fibril assemblies while intramolecular contacts lead to right functional conformation.

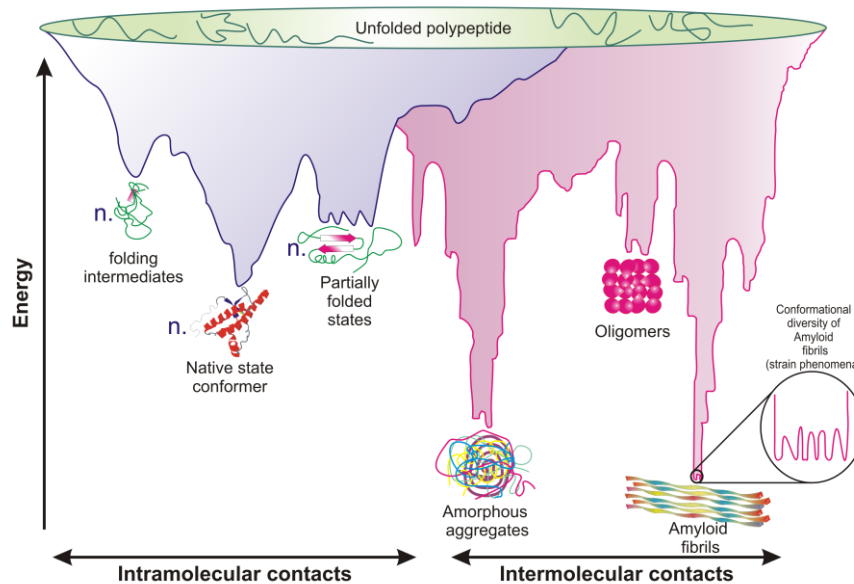


Figure 1.5: extension of protein funnel with addition of aggregation funnel in magenta, when extended ensembles trap to form aggregates or amyloids. adapted from (Jahn and Radford, 2005).

Prion diseases

Prion diseases correspond to pathologically defined transmissible spongiform encephalopathies (TSEs) of infectious, genetic or sporadic nature and are characterized by neurodegeneration and protein aggregation. They are known as TSEs because of the sponge-like holes they leave in infected brains. These diseases are a relentlessly progressive and fatal in nature. The human and animal neurodegenerative conditions associated with prion diseases include the deposition of abnormal Prion Protein (PrP^{Sc}) in the brain that affects the central nervous system. A list of various Prion diseases is given in Table 1.2 (Prusiner, 1998). The pathology of TSE may vary from case to case, but generally result in similar neurological features such as vacuolation, astrocytosis, and neuronal loss (Jeffrey et al., 1995), giving the brain a “spongy” appearance. Scrapie is the first prion disease ever studied, it was first described in sheep and goats more than two hundred and fifty years ago (Woolhouse et al., 2001). In 1936, scrapie was demonstrated as transmissible by Cuille and Chelle (Detwiler, 1992). In 1959, Hadlow reported that scrapie and Kuru have common histopathological and clinical traits, making a link between an animal and a human form of TSE for the first time (Hadlow, 1959, 1995). In the same year, Gajdusek managed to transmit Kuru from brain material of deceased humans to chimpanzees by intracerebral injection. In 1976, Gajdusek received the first Nobel Prize to be given to researchers in the TSE-field. The scrapie transmission to goats and mice successfully demonstrated a few years later (Chandler, 1961, 1962, Detwiler, 1992). In 1947, the second animal TSE, Transmissible Mink Encephalopathy (TME), was recognized in ranch-raised mink by Gaylord Hartsough (Marsh and Hadlow, 1992). In many midwestern states of the United States, some elk and mule deer carry a form of TSE called Chronic Wasting Disease (CWD) (Salman, 2003).

Human TSEs can be classified into three different forms: sporadic, inherited, or acquired by infection. Around 85% of TSE cases occur sporadically, in absence of any obvious trigger (Sy et al., 2002). The inherited forms include Gerstmann-Sträussler-Scheinker syndrome (GSS), fatal familial insomnia (FFI) and around 15% of the cases of Creutzfeldt-Jakob disease (CJD) (Eggenberger, 2007). Kuru is the first identified infectious human TSE; its transmissibility was linked to the practice of ritualistic cannibalism, confined to the Fore highlanders of Papua New Guinea (Liberski and Gajdusek, 1997). Human-to-human transmission of TSEs was confirmed by iatrogenic CJD cases caused by direct contact of the central nervous system with contaminated material during medical treatment (Johnson and Gibbs, 1998).

Prion diseases are rare in humans, and until 1980s the knowledge of these diseases was limited to a small community of neuroscientists. Since 1986, a new form of TSE, Bovine Spongiform Encephalopathy (BSE), also known as “mad cow disease,” had started to spread in Great Britain and infected more than 180,000 cattle (Brown et al., 2001). BSE is also believed to have been transmitted to humans resulting in outbreak of a new form of CJD, variant CJD (vCJD) by consumption of contaminated beef products (Bruce et al., 1997). Since then, TSEs have attracted enormous attention from both scientists and the public. A special concern is the potentially long incubation period for prion diseases, infected individuals may be carriers (pre- and subclinical) and similarly CJD-infection can be spread by blood transfusion or tissue transplants. Infective rogue proteins are resilient molecules; they are very difficult to destroy by routine sterilization methods and carry their infectivity. The presence of unnoticed subclinical infections in animal and human populations is continuous concern for health and food control authorities.

Table 2: Prion Diseases of mammals

<i>Species</i>		<i>Prion Disease</i>
Human	Sporadic	sCJD
	Inherited	fCJD, GSS, FFI, BPI
	Acquired	iCJD, Kuru, vCJD
Sheep		Scrapie
Cattle		BSE
Mink		TME
Felidae		FSE
Cervids		CWD

Protein-only hypothesis

Development of prion concept. Initially, until 1950s, scrapie, kuru, and CJD were studied independently, without realizing the interconnection among these disorders. In 1959, William Hadlow pointed out the likenesses between kuru and scrapie, and suggested that experimental transmission of kuru should be performed on chimpanzees, since they are genetically very close to humans (Liberski and Gajdusek, 1997). In 1966, Gajdusek et al. efficiently infected chimpanzees with kuru by injecting brain homogenates from diseased human into the recipient's brain

(Gajdusek et al., 1966, 1967). Later, the same group (Gibbs Jr et al., 1968, Masters et al., 1981b, a) showed the transmissibility of sporadic CJD and some forms of GSS indicating that the infectivity of a TSE is not related to if it is sporadic, inherited, or acquired by infection.

Once the transmissibility of TSEs was established, efforts were made to identify the causative pathogen. At first, based on the unusually long incubation periods between the exposure to the infectious agent and the onset of symptoms (Becker, 1977), it was suggested that TSE diseases were caused by a “slow virus” (Gajdusek et al., 1966, 1967), a term coined by Bjorn Sigurdsson in 1954 while he was working on scrapie disease of the sheep in Iceland (Palsson, 1994). However, subsequent studies showed that the infectious TSE agent might not be a virus, or any other known type of infectious pathogen, because the minimum agent necessary for infectivity was found to be too small (Alper et al., 1967). Furthermore, investigations revealed that the infectious agent from scrapie had extraordinary resistance to inactivation by UV and ionizing radiation, which would normally destroy DNA or RNA (Alper et al., 1967, Latarjet et al., 1970). Later, a similar resistance was found for the CJD agent (Gibbs et al., 1978).

All these investigations led scientists to conclude that causative TSE agents were devoid of nucleic acid, leading to many proposals on the nature of these pathogens (Gibbons and Hunter, 1967, Griffith, 1967, Pattison and Jones, 1967, Hunter et al., 1968, Field et al., 1969, Hunter, 1972). In 1967, Griffith proposed, for the first time, that a self-replicating protein instead of a virus was responsible for the transmission of scrapie (Griffith, 1967). In 1979 Stanley Prusiner started to work on the concept of an infectious agent completely devoid of DNA and based on his results, he hypothesized that TSE agents are primarily made of protein and called them

“prion” (Prusiner et al., 1980a, Prusiner et al., 1980b, Prusiner et al., 1980c, Prusiner et al., 1980d).

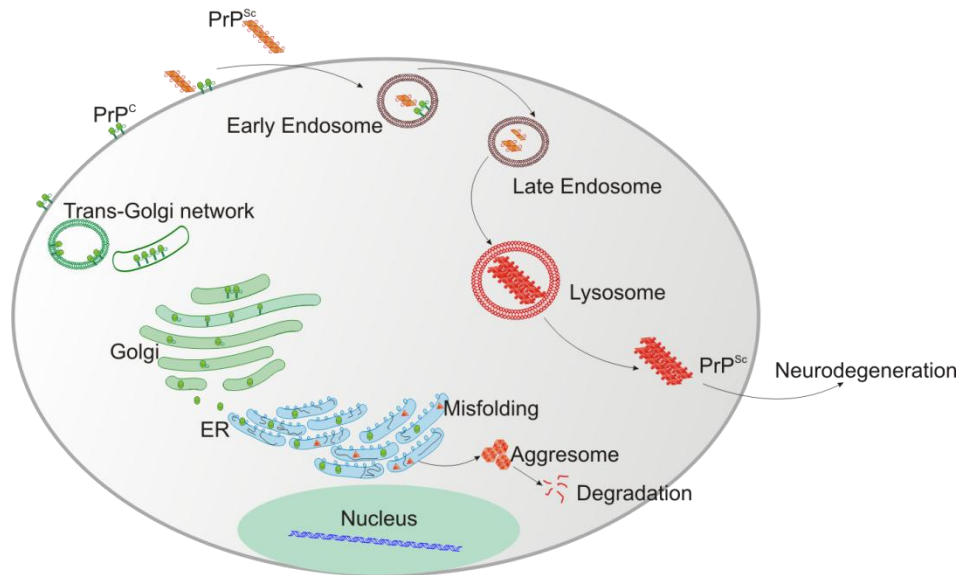


Figure 1.6: Prion cycle in cell. Prion proteins are synthesized and processed in ER and Golgi and transported to cell membrane (green) while, when they come in contact with rouge conformer (red), conversion of normal PrP to rouge conformation happened at cell surface and cell intake misfolded protein by endocytosis. These misfolded prions pile up in lysosome and where they grow in volume leading to cell death.

“Protein-only” hypothesis. In 1982, Prusiner and his colleagues successfully isolated the infectious agent from scrapie-infected hamster brains (Prusiner, 1982, Prusiner et al., 1982a, Prusiner et al., 1982b), and concluded that the agent was devoid of any detectable nucleic acid and was mainly, if not entirely, composed of protein. To describe this unusual pathogen, Prusiner coined the term “prion,” derived from “proteinaceous infectious particle.” Therefore, that protein was named prion protein, PrP. Since then, prion diseases have been considered synonymous with TSEs. Later, Prusiner was awarded the Nobel Prize for his work on Prions in 1997.

The studies revealed that prions often have typical amyloid features, including a rod-like shape in electron micrographs and apple-green birefringence under polarized light after staining with Congo red (Prusiner et al., 1982a, Prusiner et al., 1983). Prions are partially resistant to proteolytic digestion by proteinase K (PK), and Western blotting analysis showed the PK-resistant core of prions shows a molecular weight of 27-30 kDa, named PrP²⁷⁻³⁰ (Bolton et al., 1982, Prusiner et al., 1982a, McKinley et al., 1983). All of the aforementioned findings were summarized in the revolutionary “protein-only hypothesis.” *It states that the infectious particles, responsible for the transmissible forms of prion diseases are composed of an abnormal isoform of the normal cellular prion protein designated PrP^{Sc}. Conversion from the normal form of prion protein designated PrP^C to PrP^{Sc} can be catalyzed by introducing PrP^{Sc}.* Therefore a native prion protein go through conformational conversion, when it comes in proximity with misfolded prions (Figure 1.6), those misfolded proteins get deposited into lysosome through endocytosis.

Evidences supporting the protein-only hypothesis. Since prions are entirely different from other known infectious pathogens, the protein-only hypothesis is very controversial (Chesebro, 1998, Manuelidis et al., 2007), but colossal amount of biochemical data were published to support this model. Evidences in favor of the hypothesis include:

- 1) A few years after purifying PrP²⁷⁻³⁰, the gene encoding PK-resistant PrP was detected and identified as a host gene, designated PRNP in humans and Prnp in animals (Oesch et al., 1985, Basler et al., 1986, Sparkes et al., 1986). The PRNP gene is mapped to the short arm of chromosome 20, and the exact location of the Prnp gene varies from species to species. Further, the translated product from the Prnp gene was found to be widely expressed, even in a noninfected host, and showed no

difference in the primary structure, nor did it show any posttranslational chemical modification different from that of PK-resistant PrP. However, the translated product was highly soluble and very sensitive to PK digestion (Oesch et al., 1985, Basler et al., 1986, Stahl et al., 1993).

2) Transgenic studies of mouse provided another important evidence to support protein-only hypothesis (Bueler et al., 1992, Prusiner et al., 1993). PrP knockout mice were resistant to the scrapie infection, demonstrating that PrP^C expression is crucial to the propagation of prion diseases.

3) Genetic studies of familial prion diseases also strengthened the essential role of PrP, and provided important support to the protein-only hypothesis (Collinge, 2001). To date, more than twenty mutations in the PRNP gene have been connected to inherited prion diseases.

4) A number of studies on prion-based inheritance in yeast and fungi have proven the principle that proteins alone can be infectious (Uptain and Lindquist, 2002, Chien et al., 2004).

5) Further evidence came from the success in generating infectious PrP^{Sc} in vitro. Since the cell-free conversion of PrP^C to PrP^{Sc} was first reported in 1994 (Kocisko et al., 1994), in vitro generation of prions has been studied extensively, which finally led to a new cell-free conversion system called *Protein Misfolding Cyclic Amplification* (PMCA)(Soto et al., 2002b, Castilla et al., 2005). In 2004, Legname et al. successfully infected transgenic mice by inoculating them with in vitro generated amyloid fibrils from recombinant PrP (Legname et al., 2004). However, some scientists expressed reservations about the conclusions, because the transgenic mice used in these studies over-expressed by 16 times, the normal

amount of PrP, while mice which overexpressed PrP only 10 times the normal amount were found to show symptoms of prion disease without any inoculation (Couzin, 2004, Weissmann, 2005). To date, scientists are still looking for final proof of the protein-only hypothesis: using *in vitro* produced PrP^{Sc} to infect normal experimental animals.

Prion strains and species barriers: Although many results support the protein-only hypothesis, there are still some arguments against it (Kimberlin, 1982, Prusiner, 1998). One of these arguments is the existence of prion strains, where PrP^{Sc} can result in several distinct phenotypes which are faithfully propagated (Bruce and Fraser, 1991). First noted in early interspecies transmission experiments (Pattison and Millson, 1961), prion strains differ in the following three characteristics: *incubation period, histopathological lesion profiles, and clinical symptoms* (Morales et al., 2007). As well as these differences, prion strains can also be distinguished by biochemical and physical properties, such as PK resistance, to locate PK cleavage sites (Bessen and Marsh, 1992, 1994), and the ratio of unglycosylated, monoglycosylated and diglycosylated PrP within the infectious PrP^{Sc} aggregate (Khalili-Shirazi et al., 2005). Although distinct pathologies of disease are more easily reconciled with pathogens containing nucleic acid, prion strains can still be accounted for by the protein-only hypothesis. Recent evidence suggested that prion strains are encoded in the different conformational forms of PrP^{Sc} (Bessen and Marsh, 1994, Aguzzi, 2004, Priola and Vorberg, 2004). Other factors that would likely influence the strain phenotype include PrP^C glycosylation and differential binding of additional components to PrP^{Sc} (Weissmann, 1991, Khalili-Shirazi et al., 2005).

In most cross-species transmission experiments, prions transmitted between species resulted in longer incubation periods and/or weakened pathology. This phenomenon is called the “species barrier”, and reflects the observed limited infectivity of prions of one species towards another species. To determine the molecular basis for this barrier, Prusiner et al. developed transgenic mice expressing Syrian hamster PrP, which were found to be highly susceptible to hamster prions in contrast to normal nontransgenic mice (Scott et al., 1989, Prusiner et al., 1990). These studies were able to link the species specificity of prions with PrP sequence. Later, in vitro cell-free conversion studies limited the species specificity to a couple of amino acid residues (Kocisko et al., 1995).

PrP^C

The structure of PrP^C. Mammalian PrP^C is a glycoprotein attached to the cell surface by a C-terminal glycosylphosphatidylinositol (GPI) anchor. The original translated product consists of 253 amino acids. During processing in the endoplasmic reticulum, residues 1-22 are cleaved as a signal peptide that targets the protein to the plasma membrane, and residues 232-253 are replaced by a GPI anchor (amino acid numbering according to human PrP), so mature PrP^C contains 209 residues spanning from 23 to 231. PrP^C has three types of posttranslational modifications: two N-glycosylation sites at Asn181 and Asn197 (Caughey et al., 1989, Haraguchi et al., 1989), a single disulfide bond between Cys179 and Cys214 (Turk et al., 1988), and a C-terminally attached GPI anchor (Stahl and Prusiner, 1991, Stahl et al., 1993). In the human brain, the molecular weight of PrP^C varies among different glycoforms: 27 kDa for the unglycosylated form, 29 kDa for the monoglycosylated form and 33-42 kDa for the diglycosylated form.

Before 1996, high-resolution structural studies of PrP^C were hampered by the limited source of the protein. The problem was finally resolved by the successful expression of PrP in *E. coli* ((Hornemann and Glockshuber, 1996, Mehlhorn et al., 1996, Zahn et al., 1997). Since then, the three-dimensional structures of PrP from different species have been determined by nuclear magnetic resonance (NMR) spectroscopy (Riek et al., 1996, Donne et al., 1997, Zahn et al., 2000). All structures are very similar which is consistent with the fact that most known mammalian PrPs share a high degree of sequence identity (Wopfner et al., 1999). Different from the NMR structures, the crystal structure of human PrP was reported as a dimer (Knaus et al., 2001). However, the solution structure of human PrP (as shown in Figure 1.7) is believed to be more representative of the native structure *in vivo*. In this structure, full-length human PrP^C can be divided into two regions: the folded C-terminal segment (126-231) contains three α -helices and two β -strands, while the N-terminal segment (23-125) is flexible and unstructured. An octarepeat region between residues 51-91 contains four glycine-rich repeats (PHGGGWGQ) and one similar sequence (PQGGGTWGQ).

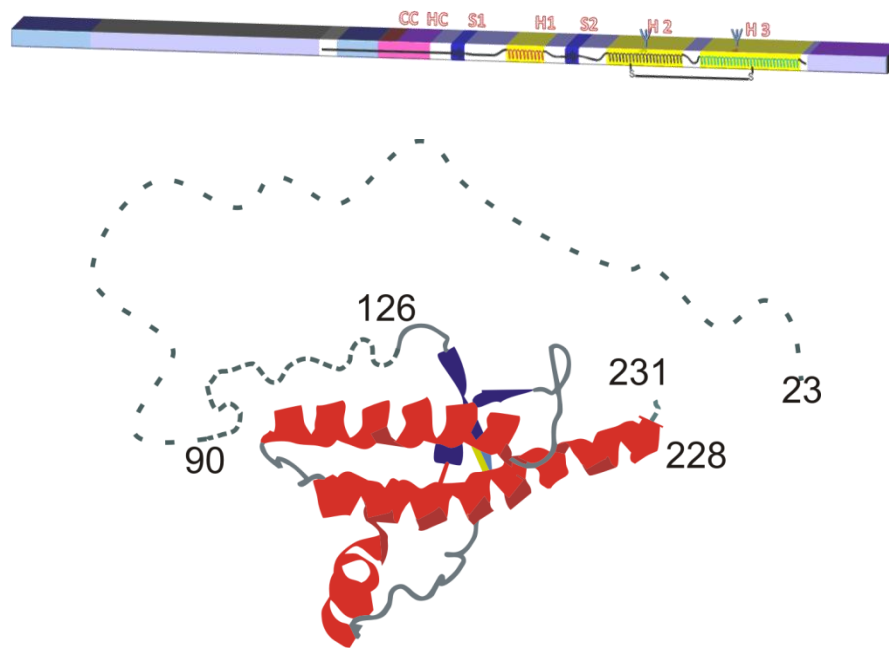


Figure 1.7: NMR structure of human prion protein (PDB:1QM0), C-ter 23 to 125 are unstructured while N-ter 126 -228 have well-defined structure having three α -helices and two β -strands forming an anti-parallel sheet. The N-ter unstructured part consist of five octapeptide repeats followed by charge cluster (CC), hydrophobic cluster (HC), while structured part is having two β -strand (S1 & S2) and three α -helices (H1, H2 & H3)

The cellular function of PrP^C: Despite many years of research, the exact physiological function of PrP^C remains unclear. Surprisingly, PrP knockout mice were found to behave normally, without any apparent defects (Bueler et al., 1992). So far, many hypotheses have been proposed for the physiological function of PrP^C, varying from protection against apoptotic and oxidative stress, to transmembrane signaling, to formation and maintenance of synapses (Hu et al., 2007, Westergard et al., 2007, Hu et al., 2008). Besides these proposals, the only clear feature of PrP is its ability to bind copper (II) ions. Most studies found the major copper-binding site was the octarepeat region of PrP^C, a region highly conserved in mammalian and avian PrP ((Hornshaw et al., 1995, Viles et al., 1999, Jackson et al., 2001). All these results

appear to suggest the involvement of PrP in brain copper metabolism, a hypothesis first proposed by Brown and Kretzschmar (Brown et al., 1997).

The strongest evidence for this hypothesis came from studies of PrP knockout mice, where the copper content in their synaptosomes was found to be much lower than that of wild-type mice (Brown et al., 1997, Herms et al., 1999). However, the above results were challenged by a following study, which proved that the amount of ionic copper in subcellular fractions or in whole brain were similar in the mice with different PrP expression levels (Waggoner et al., 2000). Taken together, a more likely hypothesis is that PrP^C can buffer copper ions in the synaptic cleft, so PrP^C can only alter the distribution of the copper content in the brain (Vassallo and Herms, 2003).

Mutations associated with the PRNP gene.

The inherited prion diseases are linked to mutations in the PRNP gene. These mutations can be classified into the three categories (Mead, 2006).

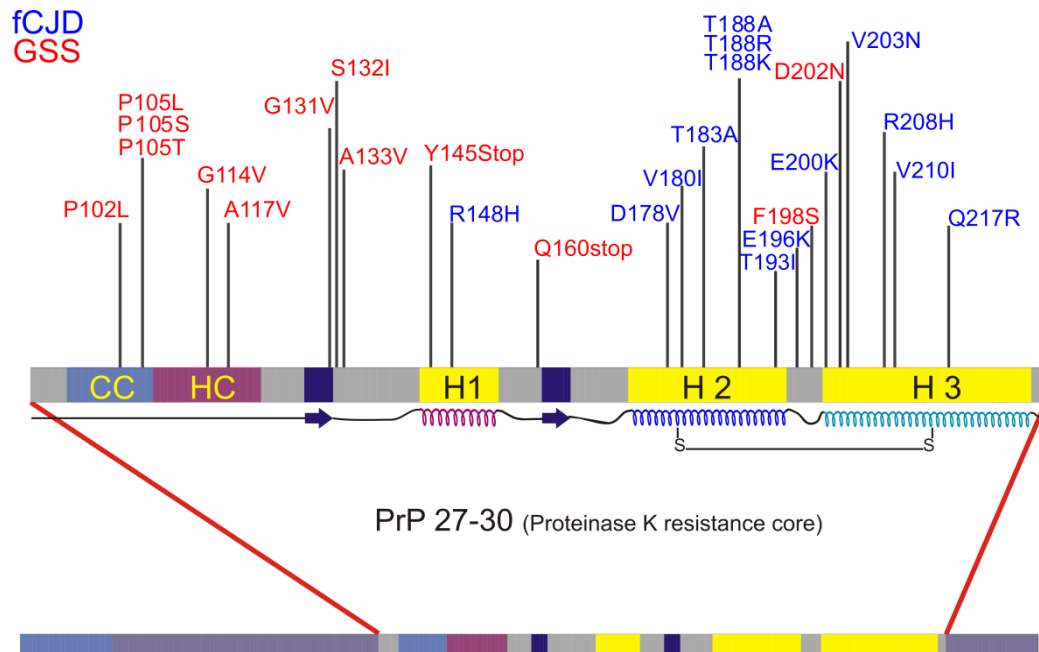


Figure 1.8: The pathogenic point mutations associated with hereditary prion diseases in PrP 27-30 region. (Prusiner, 1998, van der Kamp and Daggett, 2009)

1) Insertions of extra octapeptide repeats. Since the octapeptide region is not required for prion infection (Fischer et al., 1996), the mechanisms by which these mutations cause the diseases remain unclear.

2) Point mutations leading to a premature stop codon. One of these mutations is to substitute tyrosine with a stop codon at position 145, which results in a familial prion disease with the deposition of prion amyloid in cerebral vessels (Ghetti et al., 1996)

3) Point mutations leading to an amino acid substitution. So far, more than 25 of these mutations have been found within the 90-231 region of PrP (Figure 1.8) (Prusiner, 1998, van der Kamp and Daggett, 2009).

The connection between mutations and diseases is not fully understood. However, Surewicz lab's previous stopped-flow studies have revealed the existence of a partially folded intermediate on the pathway of PrP refolding (Apetri and Surewicz, 2002, Apetri et al., 2004). Compared to wild-type PrP, most disease-associated mutations result in an increase of the thermodynamic stability and thus to populate the intermediate, suggesting its possible role in the conformational conversion of PrP.

The rogue conformations: PrP^{Sc}

Prion Conversion Models

Nucleation dependent polymerization model

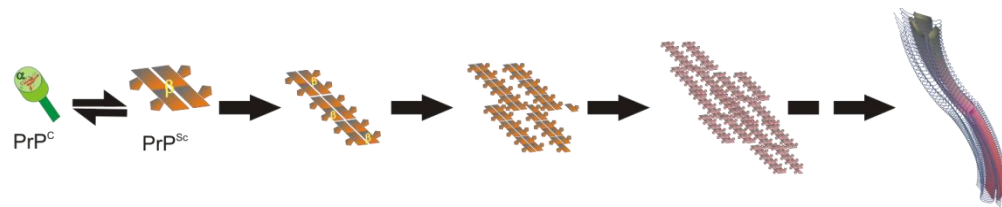


Figure 1.9: Nucleation dependent polymerization model of prion propagation, early conversion to β -rich structure is reversible and slow, therefore rate-limiting step.

The slow onset of neurodegeneration is a characteristic of the human prion diseases (Figure 1.9). (Jarrett and Lansbury, 1993) The prion amyloid exists as ordered noncrystalline polymers; which can be defined as a one-dimensional crystal in which the intermolecular packing in the plane vertical to the direction of fibril growth is nonuniform. Amyloid is capable of forming different types of insoluble, amorphous aggregates which can form rapidly when the protein concentration exceeds the solubility. *There is a kinetic barrier to amyloid formation caused by a lag in forming an amyloid nucleus which can subsequently multiply.* This

nucleation formation is rate-determining step and was proposed to be mechanistically relevant to that speeded up by the presence of infective agent during amyloid formation. This led to the hypothesis of a possible replication mechanism for converting PrP^C into PrP^{Sc} which assumes that PrP^{Sc} is an aggregate in which an alternative conformer of PrP is stabilized by intermolecular interactions. In this model, the initial *slow reversible formation* of a nucleating PrP^{Sc} multimer leads to a seeding process, during which PrP monomers are added to the growing polymer in an abnormal PrP conformation. The growing polymers can break apart, producing new seeds. PrP^{Sc} acts as a nucleation seed in the infectious form of disease and inherited mutations might contribute to the increase in affinity of the abnormal conformation of PrP for the polymer seed. Nucleation-dependent polymerization is common among many well-characterized processes including protein crystallization, flagellum assembly, microtubule assembly, sickle-cell hemoglobin fibril formation and actin polymerization. The process is similar to crystallization from a metastable supersaturated solution. Three distinctive features are characteristic of a nucleation-dependent polymerization mechanism. *First, there is a time lag before the aggregates become detectable. Second, there is a critical concentration. After completion of polymerization, the solution contains mainly monomers and high polymers at equilibrium.* The monomer concentration at this point is referred to as the critical concentration, below which polymerization will not occur. *Third, a supersaturated solution can be seeded by a preformed nucleus, resulting in immediate polymerization.* In contrast, the growth of a linear polymer neither requires nucleation nor can be seeded. Linear polymerization is characterized by the accumulation of intermediates in a sequential manner: no time lag is observed, and supersaturated solutions are unstable and rapidly aggregate.

Heterodimer (template assisted) model

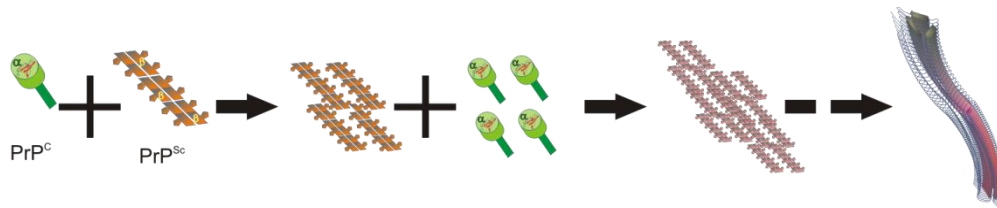


Figure 1.10: Template assisted model of prion propagation; first external misfolded conformer act as seed, which drive native PrP to misfold.

This conformational model (Figure 1.10) (Cohen et al., 1994) proposes that random fluctuations in the structure of PrP^C result in the reversible generation of a partially unfolded monomer, an intermediate designated PrP*, involved in forming PrP^{Sc}. The concentration of PrP* would normally be low and PrP^{Sc} formed in insignificant amounts. Exogenous prions containing PrP^{Sc} act as templates to induce the conversion of PrP* into PrP^{Sc} in the infectious form of prion disease. However, the insolubility of PrP^{Sc} renders this process irreversible and so the formation of PrP* followed by PrP^{Sc} promotes increasing concentration of PrP^{Sc}. Mutations in PrP could cause destabilisation of PrP^C, inducing its conversion into the intermediate PrP* state resulting in formation of PrP^{Sc}. In the case of sporadic prion diseases, the production of PrP^{Sc} could result from sufficient accumulation of PrP* under rare situations. Indeed, the development of spongiform degeneration is observed in transgenic mice overexpressing the wild-type PrP gene (Telling, 2000, Castilla et al., 2003). Somatic mutations could also play a part in this form of disease by destabilizing PrP^C and promoting its conversion into PrP^{Sc} through PrP*. For instance, both Met and Val are commonly found at amino acid 129 in human PrP. Homozygosity (Met-Met) at codon 129 was found to predispose to sporadic CJD in these studies. Further experiments showed that those patients carrying the Asp178

to Asn mutation would have insomnia if the codon 129 specifies Met in the mutant allele; if the codon 129 specifies Val, they would have dementia.

Current knowledge about PrP^{Sc} structure.

Although PrP^C and PrP^{Sc} have identical covalent structures (Stahl et al., 1993) they differ markedly in biophysical properties. PrP^C is monomeric, proteinase-sensitive and soluble in nonionic detergents, whereas PrP^{Sc} is partially resistant to proteinase K digestion and insoluble, forming amyloid-like fibrils (Prusiner, 1982, 1998, Caughey and Chesebro, 2001, Collinge, 2001, Polymenidou et al., 2004, Weissmann, 2004). These differences in physical properties seem to reflect different conformations of the two protein isoforms.

Indeed, low-resolution optical spectroscopic data suggests that PrP^C from normal brain is rich in α -helical structure, whereas PrP^{Sc} contains a high proportion of β -sheet (Caughey, 1991, Pan et al., 1993). Besides, recent studies show the degree of polymerization affects biological properties of the protein, with infectivity residing in oligomeric and not monomeric forms of PrP (Silveira et al., 2005).

According to the “protein-only” hypothesis, the conformational transition from PrP^C to PrP^{Sc} plays the central role in prion propagation. Thus, structural studies of PrP^{Sc} are the key step to understanding of the molecular basis of prion diseases. Unfortunately, in contrast to high-resolution data for monomeric PrP^C, the understanding of the structure of PrP^{Sc} or synthetic PrP^{Sc}-like aggregates is very poor, which is mainly caused by the low solubility of PrP^{Sc}.

New tools have recently emerged for studying the architecture of ordered protein aggregates (Tycko, 2004, Nelson and Eisenberg, 2006), however, these approaches

have not yet been used to probe the structure of mammalian prion amyloids. So far, very few direct observations have been made regarding the detailed structure of PrP^{Sc}. Roder and coworkers investigated the structural characteristics of the fibrils formed by the fragment of the mouse prion protein, mPrP₁₀₆₋₁₂₆ (Kuwata et al., 2003). However, the relevance of this short peptide to PrP conversion is controversial, so further structural studies are needed to probe amyloid fibrillar core structures formed by different mammalian prion proteins.

in-vitro conversion studies.

in-vitro generation of infectious prions from recombinant PrP is considered to be the final proof of the “protein-only” hypothesis. In addition, compared to slow and costly conversion experiments in animals and cell culture (Prusiner, 1998), cell free conversion systems simplify the experimental environment, and open an opportunity to understand the mechanism of the conversion. Thus, many scientists endeavored to study *in vitro* PrP conversion, beginning with short, synthetic PrP peptides (Gasset et al., 1992, Forloni et al., 1993, Tagliavini et al., 1993). Although these short peptides were found to form amyloid fibrils under certain conditions, their relevance has always been questioned since these fibrils were never found to be infectious *in vivo*.

In 2003, group of Surewicz successfully converted the recombinant protein huPrP₂₃₋₁₄₄, which corresponds to the Y145stop variant, from a monomeric state to amyloid fibrillar state *in-vitro* (Kundu et al., 2003). Furthermore, using this model they demonstrated species barrier and strain diversity in mammalian prion propagation (Vanik et al., 2004, Jones and Surewicz, 2005). However, the PK-resistant fragment of PrP^{Sc}, PrP 27-30, had been found to span residues ~90-231

(Prusiner, 1998), Y145stop, a disease-linked mutation, remains an artificial model for PrP conversion as it does not cover the full PK-resistant core.

Recently, it has been shown that the recombinant prion protein (PrP₂₃₋₂₃₁), or a biologically-relevant fragment PrP₉₀₋₂₃₁, can be converted into a variety of oligomeric forms that are rich in β -sheet structure and have increased resistance to PK digestion (Swietnicki et al., 2000, Baskakov et al., 2002, Apetri et al., 2005, Bocharova et al., 2005). These aggregates include amyloid fibrils, a form of PrP recently reported to be infectious in a transgenic mouse model overproducing PrP^C (Legname et al., 2004).

Another *in-vitro* conversion system, PMCA, was developed by Soto's group (Soto et al., 2002b, Castilla et al., 2005). This amplification is equivalent of the polymerase chain reaction (PCR) for DNA and applicable to prion protein, this technology replicates the conformation of PrP^{Sc}. During the procedure, minute amounts of brain-derived PrP^{Sc} and a large excess of cellular PrP^C are incubated with brain homogenate and a low concentration of detergents, resulting in the growth of PrP^{Sc} templates. Then these PrP^{Sc} aggregates are broken down by ultrasound to generate more units capable of replication. By the cyclic repeating of incubation and sonication, most PrP^C is rapidly converted into PrP^{Sc}. Healthy hamster brain homogenate was first used as the source of PrP^C, and the PMCA-generated PrP^{Sc} shared similar PK resistance, autocatalytic conversion activity and biological infectivity with the brain-derived templates (Castilla et al., 2005, Weber et al., 2006). However, brain homogenate contains many exogenous factors which may play a role in generation of infectivity. Recently, Supattapone and colleagues were able to simplify the components present during amplification of native hamster PrP^C (Deleault et al., 2007). Infectious PrP^{Sc}-like aggregates were produced using

only co-purified lipid molecules and a synthetic polyanion. In addition, the authors found infectious PrP^{Sc} could also be generated without any preexisting templates, which offers an opportunity to understand the mechanism of sporadic human prion diseases. Although recombinant PrP from *E. coli* has been widely used in other *in-vitro* conversion system, it has been rarely used as an amplification substrate of PMCA since it lacks glycosylation and the GPI anchor. Lately, Caughey's group succeeded in utilizing the recombinant hamster PrP as a PMCA substrate, and the PK digestion of the final product generated the similar bands as PK-digested unglycosylated scrapie PrP^{Sc} (Atarashi et al., 2007).

Toxicity of in-vitro generated prions

In recent reports, bacterially expressed recombinant prion protein has shown toxicity to host after fibril formation. These fibrils were either formed under denaturing conditions (Makarava et al., 2010) or using PMCA (Kim et al., 2010, Wang et al., 2010) method as shown in Figure 1.11. Although these fibrils prepared from recombinant protein lacked post-translational modification they proved to be infectious to hamsters upon serial transmission. (Makarava et al., 2010) However, recent data suggest that recombinant prion fibrils have different globular structure than the disease associated prion fibrils (Wille et al., 2009) and it is hypothesized that recombinant prion fibrils undergo a conformational adaptation during the process of conversion to disease-associated prions (Makarava et al., 2010). In the studies by Wang et al., they have used endogenous cofactors in prion conversion. Therefore it is likely that they probably constrain PrP structure and influence the properties of different prion strains in cells. It is more likely that endogenous

cofactors are catalyzing the formation of prions exclusively composed of PrP as it has been later demonstrated by the group of Surewicz (Kim et al., 2010).

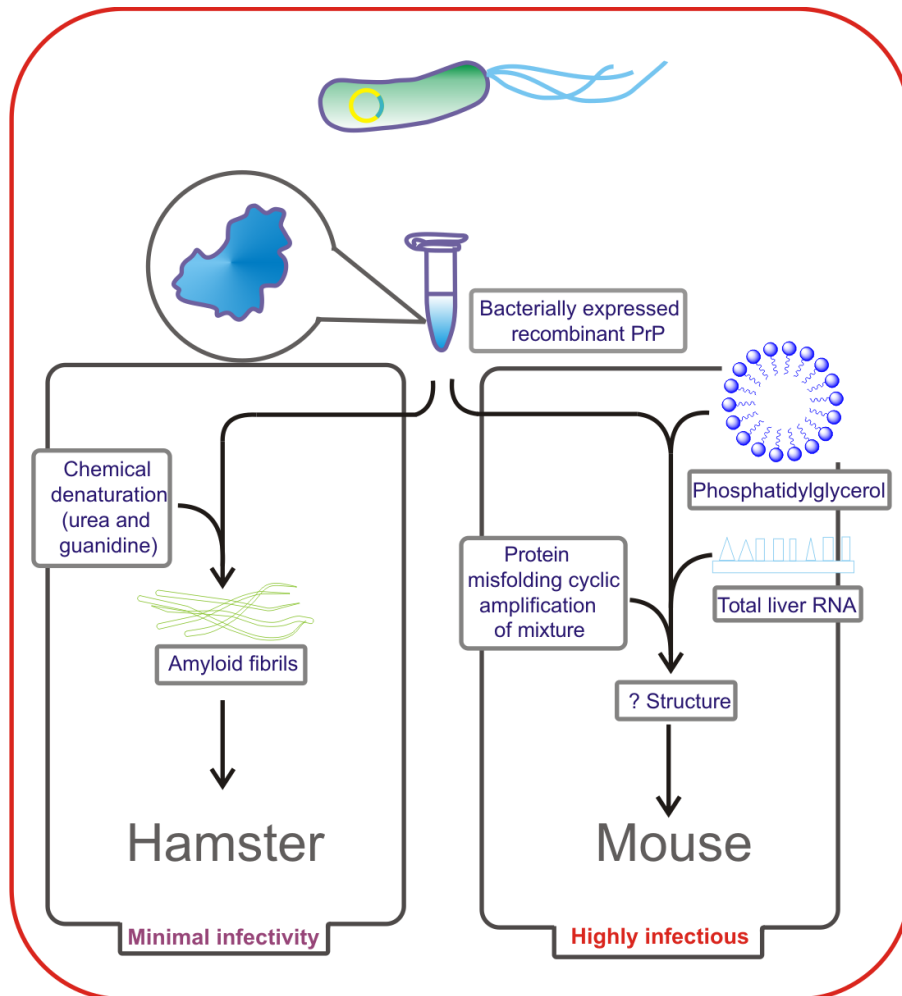


Figure 1.11: Two different biochemical protocols yield recombinant PrP with different level of infectivity. The amyloid fibrils, which are formed by incubating recombinant PrP with chemical denaturants were less infectious (left) while mixing recombinant PrP with phospholipid and RNA produces highly infectious prions (right). Adapted from (Supattapone, 2010).

Current structural models for PrP^{Sc}.

The structure of PrP^{Sc} is still unclear since it is insoluble and inaccessible to conventional methods of protein structural biology, such as NMR spectroscopy or X-ray crystallography. In 2002, Cohen and coworkers used electron microscopy to study the structure of two-dimensional crystals of PrP 27-30, and the reconstructed images shown that the repetitive unit of the samples is having hexagonal symmetry (Wille et al., 2002). Assuming PrP^{Sc} had a similar structure to currently known proteins, the authors suggested that the hexagonal symmetry came from a trimeric structure, and proposed a “left handed β -helical model,” as shown in Figure 1.12 (Govaerts et al., 2004). In this β -helix model, the N-terminus of each monomeric subunit (residues 89-175) formed left-handed β -helices in the core part of the trimer, whereas the C-terminus (residues 176-227) largely preserved the disulfide-linked α -helices at the outer part with the glycosyl groups pointing away from the center.

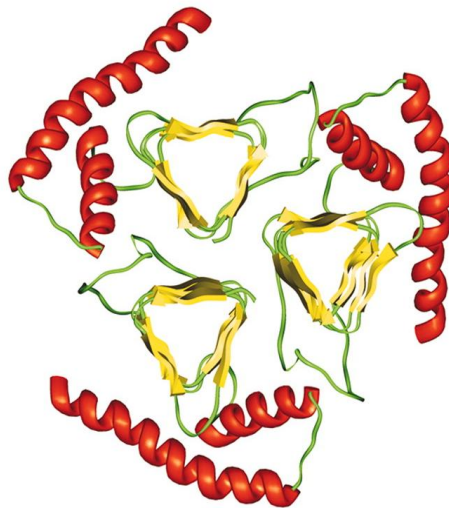


Figure 1.12: The left handed β -helical model adapted from (Govaerts et al., 2004).

At same time, DeMarco and Daggett utilized molecular dynamics to simulate PrP conversion, which resulted in another theoretical model, the “*spiral model*”, as shown in Figure 1.13 (DeMarco and Daggett, 2004). In this model, each monomeric subunit in PrP^{Sc} preserves all three α helices, but has increased β -sheet content in the 116-164 region, consisting of a three-stranded sheet and one isolated strand. The first new strand proposed (116–119) is N-terminal to the first β strand, other extended structures represent extension of the original two β strands. During polymerization, each isolated strand is connected with the adjacent monomer’s three-stranded sheet to form a continuous four-stranded sheet, which leads to a spiraling protofibril. Our findings which will be discussed later in the thesis identified amyloid core region, which is strikingly different from the discussed *in silico* models.

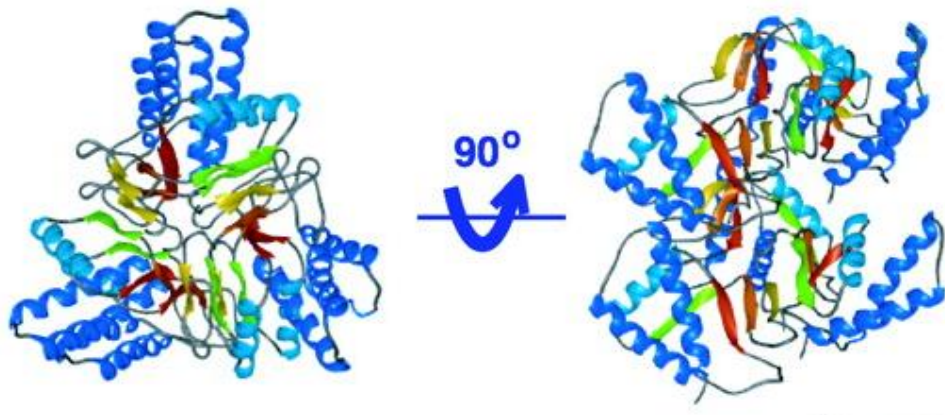


Figure 1.13: spiral model of prion fibrils, adapted from (DeMarco and Daggett, 2004)

Fungal prions

In 1994, Reed Wickner proposed that two non-Mendelian genetic elements of yeast *Saccharomyces cerevisiae*, [PSI⁺] and [URE3], were caused by a self-propagating conformational conversion of protein (Wickner, 1994), and therefore it extended the prion concept from the infectious agent of TSEs to heritable elements of yeast. So far, six prions in yeast and other fungi have been identified (Wickner et al., 2007). These fungal prions do not share amino acid sequence identity with mammalian PrPs, however fungal proteins display prion-like mechanisms of propagation. The aggregation of soluble fungal prion proteins into amyloid fibrils changes the phenotype of cells, and these characteristics can be cytoplasmically transferred from mother to daughter cell, showing that the altered phenotype is heritable. Studies on these fungal prion proteins have been proven extremely valuable (Chernoff et al., 2002). For example, one of the best-studied fungal prion proteins, the translation termination factor Sup35p, can aggregate into distinct forms of amyloid fibrils *in-vitro* under different experimental conditions (Glover et al., 1997). Infection of normal yeast cells with these distinct amyloid fibrils was found to generate different [PSI⁺] strains, providing an opportunity to understand the molecular basis of this phenomenon (King and Diaz-Avalos, 2004, Tanaka et al., 2004).

Methods to study protein aggregation and amyloid structure

The biophysical investigations are aim to resolve the three fundamental questions linked to prion amyloid assemblies:

- 1: fibril structure determination (rigid core),

2: the mechanism of fibril formation and

3: understanding the kinetics of fibril formation.

As far as the strategy of targeting protein misfolding is addressed, most preliminary studies are carried out *in vitro* both for mechanism elucidation and for inhibitors' discovery. Several physical methods are available to study protein aggregation *in vitro*. They are distinguished from being direct or indirect methods (when a property that is directly or indirectly involved in the aggregation process is measured) and from being or not being capable of giving some information on the characteristics and morphology of aggregates (morphological or non morphological techniques). Each approach shows a few advantages and disadvantages. Therefore, in order to get a complete picture of the aggregation phenomenon, the simultaneous of multiple techniques is often used to cross-validate the results.

Direct non-morphological techniques

The easiest direct approach is absorbance spectroscopy, which can be used if the monomer shows an absorption profile somehow different from the oligomers. However, since this requirement is not easily met, an alternative application is to follow the disappearance of soluble species from the solution by monitoring the decrease of absorbance of an aggregating mixture (e.g. in combination with sedimentation). Intrinsic fluorescence spectroscopy is also a direct method to measure protein aggregation. It is based on the measurement of intrinsic fluorophores (e.g. indole side chain of tryptophans) to gain information on conformational changes occurring in the protein upon aggregation. The advantage is that it is a directly applicable and sensitive methodology, which requires pM-nM concentration of peptide/protein and can monitor the kinetics of aggregation. Another technique, which has the advantage of correlating signal and concentration

through the Lambert and Beer's law, is circular dichroism (CD) spectroscopy (Han and Hill, 2008). By measuring the selective absorbance of dextro or levo circularly polarized monochromatic wavelength over the range of the UV spectrum related to the absorption of the carbamidic function of peptide/protein (190-230 nm), the secondary structure of the protein can be characterized. CD spectropolarimeters can monitor the formation of amyloid structures of proteins in solution in real time. Therefore, the time course CD spectrum changes provide useful kinetic information on the conformational transitions over oligomerization and aggregation. A universally applicable method for obtaining kinetic data is calorimetry. The direct measurements of the temperature changes (e.g. microtritation calorimetry) accompanying protein aggregation can provide thermodynamical information such as the free energy, enthalpy, entropy, equilibrium constant and heat capacity of the protein aggregation process.

Solid-state and liquid nuclear magnetic resonance (NMR).spectroscopy are powerful, direct methods that can be used to characterize all the intermediate species in protein aggregation. By solid-state NMR, the amount of fibrils that precipitate can be monitored, as well as the conformational changes upon aggregation (Tycko, 2006a, Naito and Kawamura, 2007). However, the required protein concentrations typically higher than that required with other techniques (mM versus nM). Moreover, NMR requires the use of labeled amino acid residues. *Solution phase NMR can be used to monitor the aggregation process*, however, at the high concentration required, proteins quickly tend to become insoluble. At this regard, two dimensional (2-D) and polynuclear NMR techniques are better suited. Concerning fibrils characterization, Fourier Transform Infrared spectroscopy (FTIR) is directly used to characterize the β -sheet orientation of fibrils, determining whether they are in a parallel or anti-parallel configuration. However,

no evidence is yet available for intermediate oligomeric or amorphous protein aggregates.

Indirect Non-morphological techniques

Among the spectroscopic techniques, indirect colorimetric or fluorometric methods are widely employed due to the high sensitivity of these techniques. These indirect methods involve the use of dyes such as congo red and thioflavin T (Khurana et al., 2001, Khurana et al., 2005). By interacting with aggregates (which usually have a high content cross- β structure) the former gives rise to a specific absorption band in the visible region of the UV-Vis spectrum, the latter to a fluorescence spectrum; whose intensities are proportional to the amount of aggregates/fibrils and therefore can be used for protein aggregation kinetics in solution and for quantitative studies.

Morphological methods

Despite being useful for quantitative studies, *the spectroscopic and calorimetric methods cannot allow the discrimination of different aggregate species*, which all together contribute to the measured property in a combined averaged way. Therefore, methods capable of defining characteristics of the oligomeric/fibrillar species in the aggregation kinetics are described. Turbidity directly measures aggregation by revealing the particles with a hydrodynamic radius greater than the wavelength of the incidence light. The solution turbidity has been shown to be proportional to the number concentration (equal to the number of entities of a mixture divided by the volume of the mixture) multiplied by the length of the aggregates in dilute solution; consequently, turbidity is proportional to the total number of monomeric units in solution. Therefore, if the sample is homogeneous, the turbidity is directly related to the concentration, and the oligomeric size can be

determined. However limitations exist in detecting some intermediates if their hydrodynamic radius is smaller than the wavelength and in determining the size of aggregates in heterogeneous samples. To follow fibril size as a function of time, light scattering has been extensively used. By assuming that all particles are of identical size, then the scattering intensity, $R_{(Q)}$, is dependent upon the particle concentration, C_p (g/L), the molar mass of the particles, M_p (g/mol), the particle form factor, $P_{(Q)}$, and the structure factor of the dispersion, $S_{(Q,C_p)}$, according to the following equation:

$$R_{(Q)} = KC_p M_p P_{(Q)} S_{(Q,C_p)}$$

where K is a constant dependent upon the instrumentation and upon the difference in refractive index of particles and solvent. Therefore, the molecular weight of a polymeric species can be determined by the Einstein-Stokes relation:

$$M = 4\pi r^3 N_A / 3v$$

where M is the molecular weight of the polymer, r is the radius, N_A is the Avogadro's number, and v is the partial specific volume of the polymeric molecule. Light scattering depends upon Brownian motion and the speed at which particles move, or the diffusion of the molecules, which is inversely proportional to the cubic root of the molecular weight. Therefore, a correlation between the extent of light scattering measurement and fibril size is feasible.

Mass spectrometry, in particular matrix-assisted laser desorption coupled to ionization time of flight mass spectrometry (MALDI-TOF) can be used to monitor the formation of protein complexes at specific time intervals (Kheterpal et al., 2006). By optimizing buffer, cosolvent and matrix conditions, oligomeric and larger aggregate proteins can be detected and their mass derived in the molecular range up

to approximately 300,000 g/mol. X-Ray diffraction (XRD) can help in elucidating fibrils structure at the end of the aggregation process. Important information such structure (fibrils morphology) and packing in crystalline fibril sample can be acquired; however, the interesting intermediate and amorphous species cannot be examined by XRD. Morphology in terms of shape and dimensions of oligomers and fibrils can be defined by using microscopic techniques.

The *atomic force microscope* (AFM) is a surface biophysical probe capable of generating high-resolution topographical images of surfaces and exploring the interactions between molecules within a sample (Anderson et al., 2006, Gosal et al., 2006). In addition force spectroscopy experiments can be performed using the AFM whereby the forces between the tip and sample or interactions between individual molecules can be investigated. The principle of AFM imaging is analogous to a record player where sound is generated when the stylus moves across the surface of the record. In the AFM, a stylus is attached to a flexible cantilever; at the end of the stylus is a sharp tip, which interacts with the surface of the sample. As the cantilever raster scans backwards and forwards across the surface of the sample, a map of the surface features is generated in the x and y direction. In the simplest imaging method, to build up a topographical map of the sample surface details of variations in the height of the surface are recorded by the movement of the cantilever in the z direction, thus producing a two-dimensional image of the surface topography (Figure 1.14). The deflections of the cantilever are monitored with atomic-scale sensitivity by an optical lever system; a laser beam directed onto the cantilever is reflected via a mirror to a position sensitive photodiode. A piezoelectric ceramic scanner controls the motion of the cantilever by an electronic feedback mechanism. As the probe raster scans across the surface, the flexible cantilever undergoes deflections due to the attractive and repulsive

forces experienced by the tip as a result of the overlapping electron orbitals between the atoms of the sample and the tip. Consequently the deflection of the cantilever is a measure of the forces experienced by the tip.

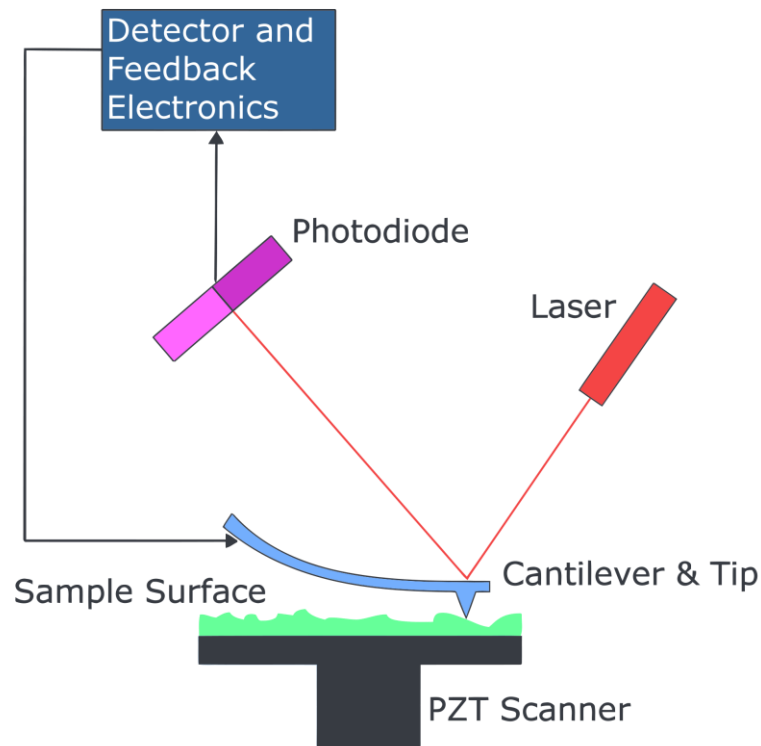


Figure 1.14: schematic diagram of atomic force microscopy (AFM) setup, showing cantilever & tip. (Adopted from wikipedia)

AFM cantilevers for biological imaging are very flexible structures with spring constants of less than 1 N/m for contact mode and 2 to 42 N/m for tapping mode imaging. Typically cantilevers are silicon or silicon nitride with lengths ranging

from 100-250 μm and tip apexes with radii of curvature of 5 to 40 nm. The optimum resolution of an image is greatly affected by the shape and apex of the tip. Currently the most commonly used commercially available tips are oxide-sharpened pyramid shaped. However, the low aspect ratio and shape of these tips may result in the contact occurring between the sides of the tip and the sample feature before the apex of the tip. This causes a tip broadening artifact whereby features appear larger than their true size, in addition two structures lying adjacent might be perceived as one. A solution to this limitation is under development, in which long and narrow carbon nanotubes with high aspect ratios, replace the pyramidal tip.

Electron microscopy (EM) is a non solution method for visualizing the surface morphology of the fibrils being studied (Shirahama and Cohen, 1967). The EM (including scanning electron microscopy (SEM) and transmission electron microscopy (TEM)) is capable of generating very high-resolution images of biological samples. However there are limitations to studying amyloid using the EM: firstly, the requirement for extensive sample preparation in which samples must be dried and stained before imaging, and secondly the inability to image dynamic processes in situ; the images generated are of dehydrated samples in their non-native state. The greatest advantage, that EM offer over other structural or morphological techniques is that it does not require samples to be crystalline, it enables the study of transient quaternary intermediates, it requires a small amount of sample relative to NMR or crystallography and there is no upper limit for the size of molecule to be studied. Samples are usually preserved in a heavy metal stain (negative stain) or in a hydrated state at liquid nitrogen temperatures (cryoEM). Recent advances in cryo electron microscopy and image processing techniques have enabled detailed structural studies of large macromolecular

assemblies including protofibrils and amyloid fibrils. The negative staining EM is a simple method which allows rapid and routine morphological and structural examination of biological macromolecules and macromolecular assemblies. The negative staining EM offers several distinct advantages over other techniques: 1) it is technically simple to perform; 2) it produces high contrast images; 3) it is relatively insensitive to damage to the specimen by the electron beam; 4) samples are easy to prepare and 5) it requires only a small amount of sample (couple of μs). In this procedure, the sample is placed on an EM grid and stained with heavy metal solution and dried. Contrast is introduced by interaction of the electron beam with the sample regions having different scattering power, macromolecules scatter electrons weakly and the images are of low contrast. The thin shell of heavy metal atoms surrounding the sample scatters the electron beam. The problems associated with negatively stained specimens are the resolution is limited to about 25 Å. The structure is usually flattened due to drying of sample, different quaternary structures exhibit differential adsorption and orientation to the grid. The uneven staining could result in some image artifacts and the high ionic strength and non physiological pH of stain might alter the specimen. The cryo electron microscopy overcomes most of these limitations imposed by negative staining and has been used to achieve near atomic resolution in the most favorable cases. In this method, samples are preserved in their hydrated state in ice by quick freezing in liquid nitrogen or ethane and imaged at low to moderate dose by EM to minimize damage to sample. For separating aggregates of various size, Size Exclusion Chromatography (SEC), Capillary Electrophoresis (CE), sedimentation and flow Field-Flow Fractionation (FFF) in combination with other techniques have been used to detect and distinguish the aggregates. However, these techniques suffer from intrinsic potential effects on the aggregation phenomenon. In fact, in sedimentation studies, centrifugation time and sample concentration would require

controls, while interaction with the stationary phase, flow stress and electric field could induce changes in samples analyzed respectively by SEC, FFF and CE.

NMR methods

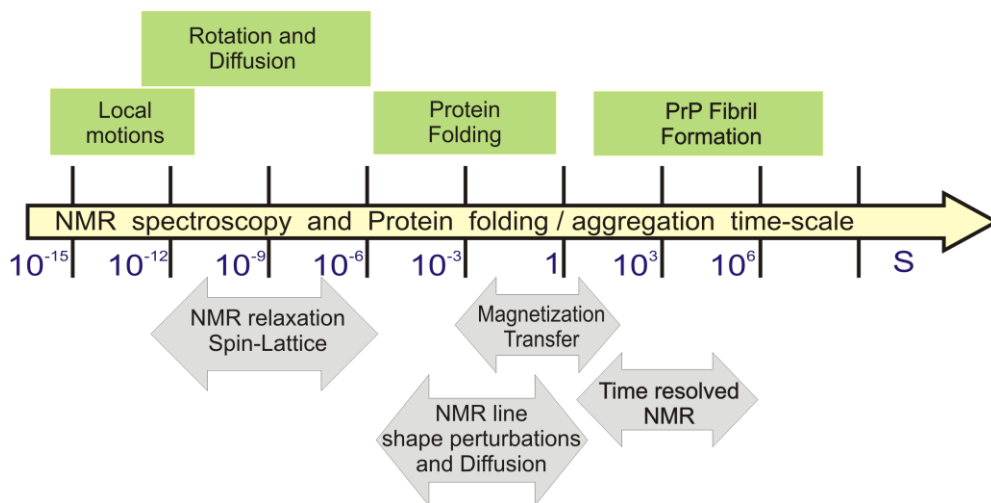


Figure 1.15: Time scales of molecular motions for the prion (PrP) protein and linked NMR-techniques.

For a protein, different dynamical features happen at different time-scale to carry out necessary biological activity of the protein. Therefore, protein cannot be completely rigid but should be containing flexible regions. For prion protein, these processes include formation of oligomers, protofibrils and mature fibrils. Amyloid fibril formation is a relatively slow process. The Figure 1.15 above represents the correlation between NMR observables and protein folding process.

Diffusion ordered spectroscopy

NMR spectroscopy is best suited for carefully purified single isoform compounds. But the nature's most challenging problems like amyloids are presented to us as mixture of populations as well as continuously changing globular shape. Diffusion-ordered spectroscopy (DOSY) answer to this limitation by separating the NMR signals of molecules of different sizes, so that the signals from different species can be distinguished. In DOSY, a series of experiments is performed in which pulsed field gradients are used to make the signals in a spectrum decay at a rate which depends on the rate of diffusion, and the set of spectra is then used to synthesize a two-dimensional spectrum in which Larmor frequency is plotted against diffusion coefficient. Where different species have NMR signals at the same frequency, it is extremely difficult to distinguish the different contributions the individual signals make to the overall decay of signal strength as a function of field gradient. Rotational and translational diffusion coefficients are given by

where ζ is an appropriate friction factor, k_B is the Boltzman constant and T is temperature. For small hard spheres, the translational friction factor is given by Stokes' law as $\zeta = 6\pi\eta r$, where η is the viscosity of the solution and r is the hydrodynamic radius of the sphere. The Einstein-Stokes equation is therefore:

H/D exchange methods

The aggregation process of proteins converting them into amyloid fibrils is complex. This conversion involves series of events during which various intermediate states are populated. The amyloid fibrils are highly dynamic in nature as evident from our Solid-state NMR data. Therefore hydrogen deuterium exchange experiments on amyloid-like fibrils are best to find out solvent accessibility in these fibrils. It was known more than 50 years ago that the isotopic exchange rates of peptide backbone amide protons are very sensitive to protein structure, which led to widespread use of hydrogen deuterium exchange (HDX) as a tool to probe protein structure, dynamics, and interactions (Engen and Smith, 2001, Hoofnagle et al., 2003, Englander, 2006). High-resolution multidimensional NMR is a dominant analyzing method of HDX. The HDX-NMR can provide direct information towards structural organization of fibrils. In all polypeptides, there are three groups of hydrogens: those attached to carbons are barely exchangeable under normal conditions; those on the polar amino acid side chains and on the N- or C- terminus exchange too fast to be trapped for measurement; only the backbone amide hydrogens have suitable exchange rates for most HDX studies. Amide hydrogens normally undergo rapid exchange with solvent hydrogens experience a slower exchange when involved in hydrogen-bonded structures or sterically inaccessible to the solvent. The rate of exchange is monitored by replacing hydrogens by deuterons. In an amyloid assembly, protein molecules assemble in repetitive arrays of β -sheets oriented parallel to the fibril axis. These arrangements of protein molecules form a core of residues, which becomes solvent-shielded. The HDX-NMR is a powerful tool for mapping the core structure of amyloid fibrils (Wagner et al., 1984, Wand et al., 1986) . Recent data have suggested that fibrils probably

represent a source of toxic oligomeric species that give rise to disease (Koffie et al., 2009). The mature fibrils are best to characterize the core structure of amyloids due to their long-life and highly ordered structure. The exchange rates of HDX are minimum at about pH 2.5 (Smith et al., 1997).

Aim of the thesis

There have been significant progresses made in the field of prion biology in last two decades. There has been significant advancement towards the final proof of “protein-only” hypothesis. Despite this progress, the key questions remain unanswered. These open questions are about transmission and structural characterization of prions and include questions like (1) what drives monomers to assemble into oligomers; (2) which segments or domain of a long polypeptide constitute the recognition motifs (3) are there any of these recognition motifs play key roles in amyloid fibril formation; (4) how the β -strands stack relative to one another; (5) what is the significance of π - π stacking; (6) there more a few possible arrangements other than “cross- β ” architecture, (7) what are most favored architecture of β -sheets and what are the intermolecular interactions between the layers that stabilize these; (8) what are the pathways and the intermediate states that are involved in seed and fibril formation; and, (9) how do strains carry structural information for transmission of disease? Several studies have demonstrated fibril formation from native-like and partially folded state of recombinant prion protein; however there is not much information available on fibril formation from another important state “the unfolded state”, while it has been postulated that protein has to undergo partial or complete unfolding for conformational switching as happen in prions. The unfolded state of the prion protein is an important conformational state apart from the native state. Urea has been used and provided substantial information of unfolded state of proteins. The main objective of my study is to establish and characterize the prion fibril formation from chemically denatured state (8 M urea, pH 2, 25 °C) and map the structural transition of the prion protein segments from its unfolded state to the fibril structure. Which thus enable us to draw an atomic picture of dynamics and misfolding events in prion protein.

Chapter 2

Material and methods

Materials

Plasmids

pJCTEV: The pJCTEV vector is a pJC40-derived expression vector for high-level prokaryotic expression controlled by the strong bacteriophage T7 promoter. Expression is induced by the production of T7 RNA polymerase in BL21(DE3) *E. coli*. Additionally, pJCTEV vector offers N-terminal polyhistidine (7xHis) tag for rapid purification with nickel-chelating resin and tobacco etch virus (TEV) protease cleavage site for removal of fusion tag. It is a high-copy number expression vector (Clos and Brandau, 1994).

pRSET A: The pRSET vector is a pUC-derived expression vector for high-level prokaryotic expression controlled by the strong bacteriophage T7 promoter. Expression is induced by the production of T7 RNA polymerase in BL21(DE3) *E. coli*. These cells also produce T7 lysozyme to reduce basal expression of target genes. Additionally, pRSET vector offers T7 gene 10 sequences, which provide protein stability, an N-terminal polyhistidine (6xHis) tag for rapid purification with nickel-chelating resin and thrombin cleavage site for removal of fusion tag.

pKM263: The pKM263 is a pGEX-cs derived expression vector having additionally N-terminal GST tag for rapid purification with nickel-chelating resin and tobacco etch virus (TEV) protease cleavage site for removal of fusion tag

Construct	Coding for	Source
pJCTEV/hPrP ₁₂₁₋₂₃₀	Human prion C-terminal structured fragment 121-230	Kindly provided by Dr. Susanne Grimme, Sanofi-aventis Cooperation, Goethe University, Frankfurt
pRSET A/hPrP ₉₀₋₂₃₀	Human prion C-terminal PrP 27-30 derived fragment 90-230	Kindly provided by Dr. Krishna Saxena, Sanofi-aventis Cooperation, Goethe University, Frankfurt
pKM263/hPrP ₁₆₆₋₂₃₀	Human prion C-terminal fragment 166-230	This work

Software

Following software were used for data acquisition, analysis and visualization of NMR experiments.

Topspin 1.3, 2.1, 2.5	Bruker Biospin, Karlsruhe, Germany
Xwin-NMR 3.5	Bruker Biospin, Karlsruhe, Germany
Sparky 3	Goddard and Kneller, University of California San Francisco
XEASY	Wüthrich group, ETH Zürich

CARA Rochus Keller, Wüthrich Group, ETH
Zürich

Protein Dynamics Center Bruker Biospin, Karlsruhe, Germany

Buffers and solutions

Lysis buffer:

Buffer 1A: 8M Urea, 100mM NaPi, 10mM Tris, pH 8.0

Buffer 2A: 8M Urea, 100mM NaPi, 10mM Tris, 10mM Imidazole, pH 8.0

Buffer 3A: 8M Urea, 100mM Tris-HCl, 10mM Imidazole, pH 8.0

Buffer 4A: 100 mM Tris-HCl, 500mM NaCl, 1% Triton-X-100, pH 8.0

Inclusion Body wash buffer

50 mM Tris-HCl, 23% sucrose, 1 mM EDTA, 1 mM benzamidine-HCl, 1 %
Triton-X-100, pH 8.5

Refolding and proteolytic cleavage buffer

10mM Tris, pH 8.0

Purification buffers

Buffer 1A: 8M Urea, 100mM NaPi, 10mM Tris, 10mM Imidazole, pH 8.0

Buffer 1B: 8M Urea, 100mM NaPi, 10mM Tris, 50mM Imidazole, pH 8.0

Buffer 1C: 8M Urea, 100mM NaPi, 10mM Tris, 200mM Imidazole, pH 8.0

Buffer 2A: 8M Urea, 100mM Tris-HCl, 10mM Imidazole, pH 8.0

Buffer 2B: 100mM Tris, 10mM Imidazole, pH 8.0

Buffer 2C: 100mM Tris, 50mM Imidazole, pH 8.0

Buffer 2D: 100mM Tris, 200mM Imidazole, pH 8.0

Buffer 3A: 8M Urea, 100mM NaPi, 10mM Tris, pH 8.0

Buffer 3B: 8M Urea, 100mM NaPi, 10mM Tris, pH 5.5

Buffer 3C: 8M Urea, 100mM NaPi, 10mM Tris, pH 4.5

Prion Protein Protocols

Safety considerations

The expression and purification of human prion protein constructs was carried out under S1 conditions, in the laboratory of Prof. Dr. Harald Schwalbe at the Institute for Organic Chemistry and Chemical Biology, at the Riedberg campus of Goethe University, Frankfurt, Germany.

The following procedures were used for inactivation of prions

Surfaces were cleaned with 1M NaOH (final concentration) applied for a minimum period of 30 minutes at 20 °Celsius. Devices and articles were dipped 2.5 % sodium hypochlorite with at least 2% free chlorine for >1 hour or 1M NaOH for > 1 hour. Liquids were treated by addition of a same volume 2 M NaOH and/or 5 % a sodium hypochlorite solution - 1h. This was followed by thermal inactivation in the autoclave (134 °Celsius for 5 minutes or 121 °Celsius for 20 minutes).

Constructs

Recombinant human PrP⁹⁰⁻²³⁰

Amino acid Sequence:

MRGSHHHHHGLVPRGSGQGGGTHSQWNKPSKPKTNMKHMAGAAAAGAVVGGLGGYMLGSA
MSRPIIHFGSDYEDRYRENMHRYPNQVYYRPMDEYSNQNNFVHDCVNITIKQHTVTTTTK
GENFTETDVKMMERVVEQMCITQYERESQAYYQRGS

(From Dr. Krishna Saxena, Sanofi-aventis cooperation)

Parent Vector: pRSETA

Promoter: T7

Purification: His-tag (underlined in amino acid sequence)/Ni-NTA

Protease Site for cleavage: Thrombin

Recombinant human PrP¹²¹⁻²³⁰

Amino acid Sequence:

MGHHHHHHASENLYFQGHMVVGGGLGGYMLGSAMSRPIIHFGSDYEDRYRENMHRYPNQV
YYRPMDEYSNQNNFVHDCVNITIKQHTVTTTTTKGENFTETDVKMMERVVEQMCITQYERES
QAYYQRGS

(From Dr. Sussane Grimme, Sanofi-aventis cooperation)

ParentVector: pJCTEV

Promoter: T7

Purification: His-tag (underlined in amino acid sequence)/Ni-NTA

Protease Site for cleavage: TEV

Recombinant human PrP₁₆₆₋₂₃₀

Amino acid Sequence:

MHRYPNQVYYRPMDEYSNQNNFVHDCVNITIKQHTVTTTTTKGENFTETDVKMMERVVEQMC
ITQYERESQAYYQRGS

Residues 166-230 were subcloned from pJCTEV PrP₁₂₁₋₂₃₀ construct in pKM263 vector with engineered TEV protease cleavage site using forward primer with Nco1 restriction site

5' AAACCATGGTGGTGGGGGGCCTTGGCGGCTACATG3' and backward primer with BamH1 restriction site

5' AAACCATGGTGGTGGGGGGCCTTGGCGGCTACATG 3'

Promoter: T7

Purification: His-tag/Ni-NTA

Protease Site for cleavage: TEV

Expression of prion protein for NMR

The authenticity of the clone construct was confirmed by nucleotide sequencing. Independent of the construct used, plasmid DNA was freshly transformed into BL21 (DE3) and cells were grown on selective agar plates. A single colony was picked from the plate and a 10 ml overnight culture in Luria-Bertani (LB) broth medium was started at 37 °C supplemented with 100 µg/ml ampicillin. Protein expression was induced with the addition of 1 mM isopropyl 1-thio- β -D-galactopyranoside (IPTG) when the OD₆₀₀ reached ~0.6. The culture was incubated in 5-liter Erlenmeyer flask for ~4 h with aeration (160-180 rpm) at 37 °C before the cells were harvested by centrifugation (5,000 × g, 15 min, and 4 °C).

Expression of isotope labeled protein

Procedure 1: The above procedure is used with minimal M9 media in place of LB media. ¹⁵N enriched NH₄Cl (1g/L) & ¹³C enriched Glucose (2g/L) are used to obtain uniformly labeled protein for NMR experiments.

Procedure 2: BL21 (DE3) *E. coli* cells with hPrP(90-230) were initially inoculated into two 10ml culture tubes of LB medium with 100µg/ml ampicillin. These cultures were grown with shaking at 37 °C for approximately 4 hours, inoculated into 90ml of LB/Amp each and then grown overnight for about 12 hours. One 2000ml flask of LB/Amp medium were then inoculated with 10% of the overnight

culture and grown at 37 °C until the absorbance at 600nm (OD₆₀₀) reach ~1.2, when the cells have reached the end of log phase of their growth. These cells were pellet down and washed twice with M9/Amp medium and then re-suspended into one 2000ml flasks containing M9/Amp medium (either with ¹⁵N or ¹⁵N & ¹³C enriched) along with addition of 1mM isopropyl-β-D-thiogalactopyranoside (IPTG) to induce the expression of PrP and allowed to grow at 37 °C until the absorbance at 600nm (OD₆₀₀) reach ~2.4.

Purification of prion protein:

The cells were harvested by centrifugation (5,000 × g, 15 min, 4 °C). The cell pellets obtained further processed by 4 different procedures to obtain the purified protein for NMR experiments.

Purification of His-tag free protein

Procedure 1:

Cell pellet was dissolved in Buffer 1A and sonicated (10×, 55-s pulse on, and 180-s pulse off) in an ice bath. This was followed by the centrifugation at 15000 ×g, 20 minutes, 10 °C. The cell debris was separated as pellet, while supernatant was used for another round of centrifugation (20000 ×g, 20 minutes) to remove urea-insoluble particles. The supernatant containing the protein was subjected to incubation with Ni-NTA resin for 30 minutes and then loaded on *disposable spin columns*. The column was washed thrice with Buffer 1A and then with buffer 1B having increased imidazole concentration of 50 mM, to washout non-specifically bound proteins. Protein was eluted with buffer 1C. The column resin was then

washed with 1M NaOH and 1% SDS with 4 column volume and equilibrated by buffer C by 10-15 column volume. Ni-NTA resin recharged with 1mM NiSO₄ and again equilibrated by buffer 1A by 10-15 column volume. The purified protein was refolded by gradual dialysis against refolding buffer for 16 hours. Purified protein was subjected to Protease cleavage in dialysis cassette and the His-tag was then removed by thrombin cleavage for 1 h at room temperature in cleavage buffer, using 0.1 unit thrombin/ml. Thrombin was removed using DE52 column and purified protein was pooled using 200mM NaCl gradient. This protein was again passed through recharged Ni-NTA column to remove residual His-tag tail, which gets bound to column, while cleaved protein came as flow through. The column was recharged again as described earlier. The protein was dialyzed against 8M Urea pH 8 for about 3-4 hours and further dialyzed against 8.8 M Urea pH 2 for experimental purposes. The protein was concentrated to variable concentrations of 200 μ M to ~2mM for experimental purposes. The usual concentration was ~1mM. . The NMR samples were prepared with addition of 10% D₂O.

Procedure 2:

Procedure 2 is almost similar as 1st but involving refolding on column as reported earlier (Zahn et al., 1997). This refolding is achieved by applying slow gradient from buffer 2A to 2B. The protein was eluted with buffer 2D. This process of refolding and elution was repeated thrice for maximum recovery of protein. The rest of the procedure was same as first.

Fast purification of his-tag protein

Procedure 3:

Since for many NMR experiments, protein purity of ~95% is satisfactory, a shorter purification protocol was developed, which effectively resulted in better

yield. In this method protein was purified by changing to acidic pH. (Buffer 3C). The pooled protein was then dialyzed against 8.8 M urea, pH 2 and used for experiments or used as same procedure as earlier to remove His-tag.

Procedure 4:

The prion protein is expressed in inclusion bodies and resolubilization of these inclusion bodies in NMR buffer was enough to obtain a good spectrum. In this procedure cell pellet was suspended in lysis buffer 4A and sonicated as described above. On centrifugation, pellet containing inclusion bodies and cell debris separated out. This pellet was washed thrice with wash buffer and then obtained inclusion bodies were suspended in 8.8 M Urea, pH 2 and put on dialysis against same for 1 hour.

Yield of protein varied from 8mg/L to 40mg/L of media, depending on the procedure. The concentration of purified protein was determined spectrophotometrically using the molar extinction coefficient, ϵ_{276} , of $21640\text{ M}^{-1}\text{ cm}^{-1}$

Fibril formation

To form amyloid fibrils for NMR investigations, hPrP (various constructs and concentrations) in 8 M urea, pH 2 was placed into 1.5 ml conical plastic tubes, each containing 0.5 ml. The protein concentration was determined by measuring the absorbance at 280 nm. The fibrillation reactions were carried out in 1.5 ml conical plastic tubes at a total reaction volume of 0.5 ml at 37 °C with continuous shaking at 600 rpm using Eppendorf plate shaker. A schematic diagram showing the fibril formation is shown in Figure 2.1. These samples were used for NMR measurement

at regular intervals. ^{15}N -Phthalimide ($\text{C}_8\text{H}_5\text{O}_2\text{N}_1$) was used as reference in NMR experiments.

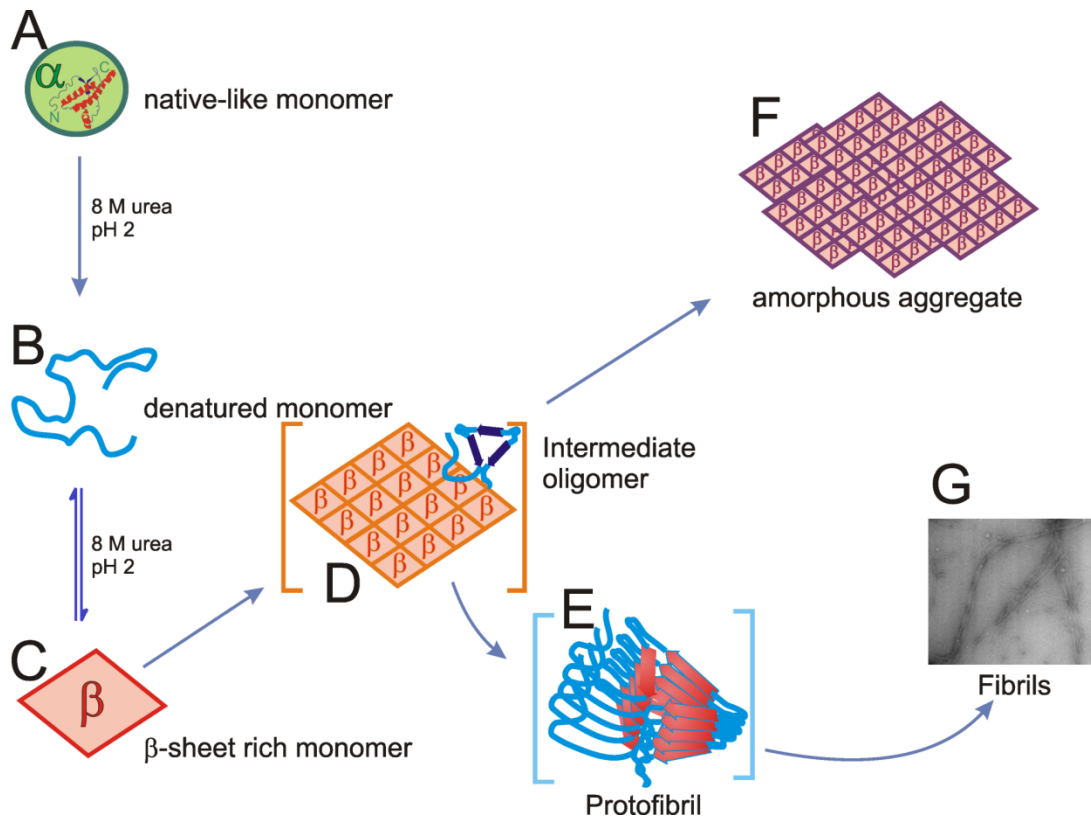


Figure 2.1: Model for *in vitro* prion fibrillation in denaturing environment. The native-like conformer (a) of recombinant hPr^{P90-230} consists of three α -helices and two β -strand forming anti-parallel sheet (PDB:1QM0) (Zahn et al., 2000). Addition of 8M Urea and acidic pH changes the equilibrium between unfolded extended conformation (b) and β -sheet rich conformation (c) (Baskakov, 2004). These β -sheet rich monomers lead to either amorphous aggregate (f) or fibril formation (g) when agitated at 600 rpm at 37°C; probably through formation of intermediate oligomer (d) and protofibrils (e).

AFM:

The AFM images were taken by Dr. Thorsten-Lars Schimdt in the Group of Prof. Dr. Alexander Heckel at Center of Excellence – Macromolecular Complexes, Frankfurt and taken on a Veeco (New York, NY, USA) Dimension 3100 AFM with a Nanoscope IIIa controller in dry tapping mode. 1 μl of the completed amyloid fibril formation reaction solution were diluted in 99 μl of TEA-Mg buffer (40 mM Tris/ acetic acid pH 7.5, 2.5 mM EDTA, 12.5 mM MgCl_2). From this solution, 2 μl were applied on freshly cleaved mica (muscovite grade, Plano, Wetzlar, Germany) and incubated for ca. 2 minutes. The surface was rinsed with a few ml of milli-Q water and dried with a stream of nitrogen. ACT probes (25-75 N/m) from APP Nano (Santa Clara, CA, USA) were used for imaging at an amplitude set point of 0.3 V. The AFM raw data was processed with Nanoscope 5.31 software (Veeco).

EM:

Electron microscopy has been performed by Dr. Janet Vonck at Max Planck Institute for Biophysics, Frankfurt. Electron microscopic images were obtained by negative staining with 1% uranyl acetate, pH \sim 4 using a Philips CM 120 at 120kV under low dose conditions at a magnification of 45,000 \times on Kodak SO-163 electron image film. Usually the samples for EM were diluted using distilled water by 100 factors.

NMR spectroscopy

Solid-state NMR spectroscopy

The solid-state NMR experiments have been done in the Group of Prof. Dr. Clemens Glaubitz, Institute for Biophysical Chemistry, Frankfurt. These experiments have been performed by Ines Lehner, Nicole Pflieger, Jun Yang and Jakob Lopez. Spectra were recorded at a Bruker Avance 600 WB spectrometer using a 4mm DVT probehead at 25°C. Usually ^1H decoupling of 90 kHz was applied and 2048 transients were accumulated. For CP, a contact time of 2ms was used. The FIDs were processed using exponential line broadening of 20 Hz.

Backbone resonance assignment

The backbone assignment is prerequisite for the analysis of protein dynamics, interactions by NMR. The assignment of backbone residues involves the isotope labeling of protein with NMR observable ^{15}N and ^{13}C nuclei. Therefore prion protein constructs were labeled as discussed earlier. The labeling of these nuclei along with abundant ^1H nuclei allows for intra- and inter-residual correlation of $^1\text{H}^{\text{N}}$, $^{15}\text{N}^{\text{H}}$, $^{13}\text{C}_{\alpha}$, $^1\text{H}_{\alpha}$ and $^{13}\text{C}'$ nuclei through scalar couplings along bonds in a series of three-dimensional NMR experiments, which permit to map resonances according to amino acid sequence of protein.

A set of three dimensional NMR experiments (Sattler et al., 1999) were performed to unambiguously assignment of residues. The core experiment of assignment was HNCACB; this experiment correlates the ^1H , ^{15}N of amide with $^{13}\text{C}_{\alpha}$ and $^{13}\text{C}_{\beta}$ of self and previous residue in polypeptide. The sign of α and β residues are opposite, and thus allow easier identification. The second experiment was CBCA(CO)NH, which correlates the ^1H , ^{15}N of amide with $^{13}\text{C}_{\alpha}$ and $^{13}\text{C}_{\beta}$ of previous residue in polypeptide. The sign of both α and β residues were same in this experiment. In an ideal situation, a protein backbone can be completely assigned with these two three-

dimensional experiments. However, prion protein in non-native environment showed low dispersion of signals, which lead to over-lapping of several signals. For start point of backbone assignments, backbone amide peaks were picked in a well-resolved ^1H ^{15}N HSQC spectrum. The chemical shift patterns in a HNCACB spectrum, is a good indicator of residue type. The denaturing conditions of 8M urea creates an environment where these shifts are closely resemble random coil chemical shifts available at NMR database BMRB. Few residues like alanine, glycine, threonine and serine are easier to identify based on their unique peak pattern and chemical shifts. These residues are suitable candidates for start of sequential backbone assignment. However, amino acid sequence of prion protein is having several repetitive sequences, which make it harder to identify them in the sequence, where each of these sequence appear similar due to high denaturing environment of 8M urea. Therefore additional three-dimensional experiments were performed to assign backbone residues unambiguously. Which includes HNCA, HN(CO)CA, HNCO, and (H)CC(CO)NH allowed better resolution for $^{13}\text{C}\alpha$ residues while HNCO was in particularly useful to resolve overlapping amide peaks in ^1H ^{15}N HSQC with additional resolution from ^{13}C dimension. The (H)CC(CO)NH experiment ^{13}C of previous residue with amide in a TOCSY-type transfer, therefore gives a unique peak pattern, which helps in determining the spin-system type for the residue. Another important three dimensional NMR experiment was HNN (Panchal et al., 2001), which correlates amide resonance with amide resonance of previous and next residue and offer another dimension to sequential assignment. All pulse programs were used from Bruker standard library, except HNN which was kindly provided by the group of Prof. Hosur, Mumbai.

MUSIC based HSQCs

The amino acid type selective experiments are developed to assign the residues which are difficult to assign unambiguously in manual or automated routine assignment procedure. Most assignment procedure use a ^{15}N -HSQC spectrum as a starting point and correlate the (^1H , ^{15}N) frequency pairs with carbon or proton frequencies in a third dimension to achieve a sequence-specific assignment. These experiments are based on the MUSIC (multiplicity selective in-phase coherence transfer) (Schubert et al., 1999, Schubert et al., 2001a, b) pulse sequence building block, which accomplishes a coherence transfer to or from the hetero-nucleus and which replaces the initial INEPT transfer and is selective for $X\text{H}_2$ or $X\text{H}_3$ (where X is either ^{15}N or ^{13}C). A distribution landscape for C_β and C_α chemical shifts is shown in Figure 2.2; this specific distribution is utilized for selection. It selects multiplicity via multiple-quantum filters and offers superior suppression of unwanted signals compared to sequences, which work solely by the appropriate tuning of delays to select for the number of coupling partners or the use of selective pulses.

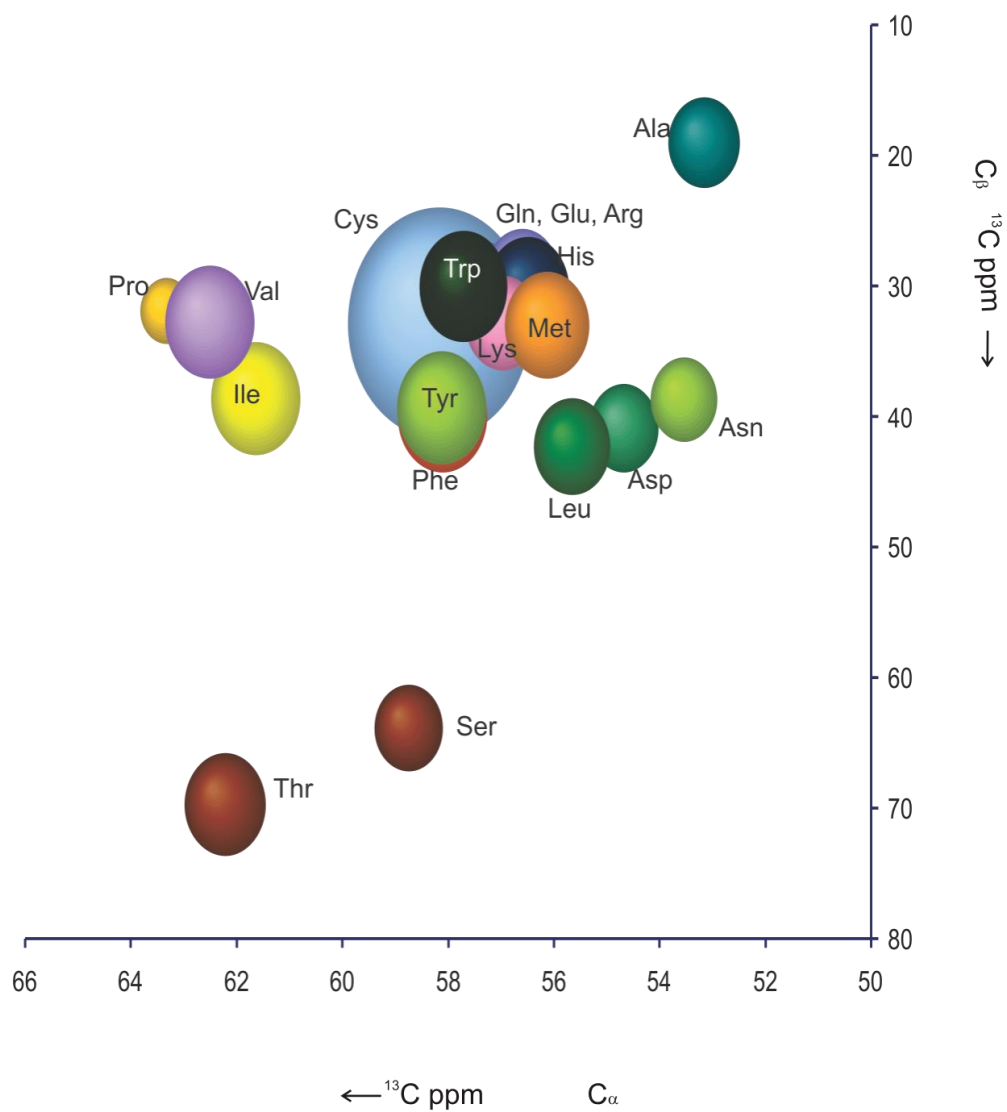


Figure 2.2: Two dimensional landscapes of C_{β} and C_{α} chemical shifts with characteristics areas for different amino acid types. The circle shows approximate areas with standard deviations of the chemical shift values found in Biological Magnetic Resonance Bank database (www.Bmrb.wisc.edu)

When MUSIC is implemented in the appropriate triple-resonance experiment, the signals of the desired amino acid types are selected based on the topology of the side chain. MUSIC does not lengthen the sequence compared to the standard triple-resonance experiments; therefore no loss of intensity occurs due to relaxation. MUSIC HSQCs provide the information in number of HSQCs (Figure 2.3), each one giving for a particular type of set of residues for example, selective for Ser (S-HSQC); Val, Ile, and Ala (VIA-HSQC); Leu and Ala (LA-HSQC); Asp, Asn, and Gly (DNG-HSQC), as well as Glu, Gln, and Gly (EQG-HSQC).

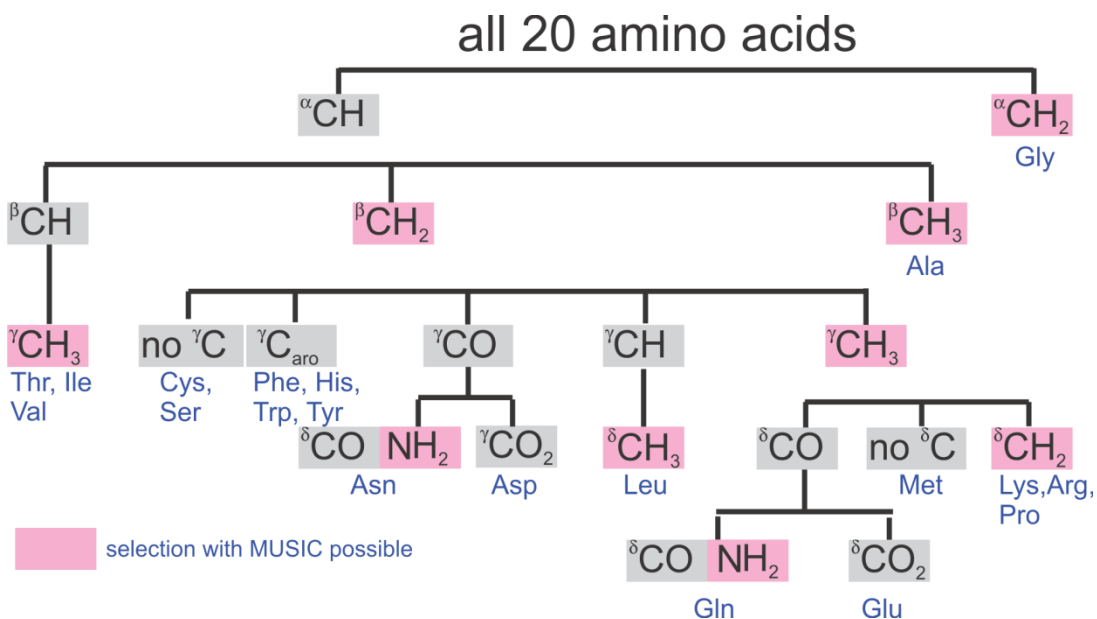


Figure 2.3: The distribution of MUSIC based selective HSQCs for all amino acids

Table 3: NMR acquisition processing parameters for the assignment of recombinant prion constructs.

Experiment	T(K)	B ₀ (T)	t ₁	SW ₁ (ppm)	t ₂	SW ₂ (ppm)	t ₃	SW ₃ (ppm)	ns	d1 (S)	p1 (μS)	¹⁵ N ω (ppm)	¹³ C ω (ppm)	SI ¹	SI ²	SI ³
hPrP₁₂₁₋₂₃₀																
¹⁵N, ¹H-HSQC	298	14.091	2048	14	256	24	-	-	8	1.3	12	117	-	2048	2048	-
HNCACB	298	14.091	2048	10	72	24	160	60	16	1.3	11.75	117	41.5	2048	256	512
CBCA(CO)NH	298	14.091	2048	14	72	24	140	70	16	1.3	10.15	117	39	2048	256	512
HNCO	298	14.091	2048	14	68	24	80	12	16	1.3	11.75	117	172	2048	128	256
HNCA	298	14.091	2048	14	70	24	140	30	8	1.3	11.75	117	51	2048	256	512

Table: NMR acquisition processing parameters for the assignment of recombinant prion constructs.

Experiment	T(K)	B ₀ (T)	t ₁	SW1 (ppm)	t ₂	SW2 (ppm)	t ₃	SW3 (ppm)	ns	d1 (S) p1 (μS)	¹⁵ N ω (ppm)	¹³ C ω (ppm)	SI ¹	SI ²	SI ³
(H)CC(CO)NH	298	21.137	2048	16	96	20	220	65	16	1.3	14.82	39	2048	256	512
¹⁵ N NOESY-HSQC	298	16.443	2048	12	100	23	180	12	8	1.3	11.25	-	2048	256	256
¹⁵ N TOCSY-HSQC	298	16.443	2048	14	128	24	256	14	8	1.3	11.4	-	2048	256	512
hPrP ₉₀₋₂₃₀															
¹⁵ N, ¹ H-HSQC	298	16.443	2048	14	128	25	-	-	2	1.5	14.3	-	2048	512	-
HNCACB	298	16.443	2048	14	64	25	104	75	16	1.2	11.75	39	2048	256	512

Table: NMR acquisition processing parameters for the assignment of recombinant prion constructs.

Experiment	T(K)	B ₀ (T)	t ₁	SW1 (ppm)	t ₂	SW2 (ppm)	t ₃	SW3 (ppm)	ns	d1 (S) p1 (μS)	¹⁵ N ω (ppm)	¹³ C ω (ppm)	SI ¹	SI ²	SI ³
CBCA(CO)NH	298	18.791	2048	14	80	20	140	60	8	1.3	13.62	40	2048	256	512
HNCO	298	21.137	2048	14	40	24	96	12	16	1.3	19.5	176	2048	128	256
HNCA	298	18.791	2048	16	72	20	140	22	8	1.3	13.62	51	2048	256	512
(H)CC(CO)NH	298	21.137	2048	16	40	20	124	60	16	1.3	16.38	40	2048	256	512
HNN	298	18.791	2048	14	104	23	104	23	16	1.1	14.75	60	2048	256	256
hPrP₁₆₆₋₂₃₀															
¹⁵ N, ¹ H-HSQC	298	16.443	2048	16	256	20	-	-	4	1.3	15.5	-	2048	1024	-

Diffusion ordered NMR spectroscopy

Diffusion coefficients obtained from PFGSE measurements can be directly related to the geometry of species under study via the friction factors. For an amyloid which represents a near rod kind shape, the motion is much restricted and therefore the length of fibrils influence significantly to the value of diffusion coefficient. The friction is different for rod shaped and spherical shaped assemblies. The translational, ζ_t , and rotational, ζ_r , friction factors, preexponential factors $C(l)$, and limiting preexponential functions $\zeta(l)$ for idealized geometries. η is the viscosity, r is the radius, and l is the rod length.

Geometry				
Sphere			—	
Rod			-	

In an amyloid sample, there will be a distribution of the lengths of rods or the diameters of spheres. The lengths are observed to vary over several orders of magnitude. Account must be taken of this variation if the model is used to analyze experimental data. And therefore, a prefactor $C(l)$ and the Stejskal-Tanner factor $\zeta(l)$ and the PFGSE signal intensity decay is given by

$$\ln \frac{S_i}{S_0} = \ln \frac{\sum_{l=0}^{\infty} C(l) \zeta(G, \delta, \Delta, l) \sigma(G, \delta, \Delta, l)}{\sum_{l=0}^{\infty} C(l) \lim_{G \rightarrow 0} \zeta(l)}$$

The DOSY experiments were performed using pulse field gradient stimulated echo (PFGSE) sequence with presaturation (Bruker pulse sequence: ledbpgppr2s) was used for diffusion experiments with $p30 = 2.2$ ms with variable diffusion delay Δ as

shown in Figure 3.14 (Baldwin et al., 2008) The resonances from amide and methyl regions were used for analysis.

Deuterium exchange

Preformed fibrils were visualized using EM and then gradually dialyzed against water, pH 2 for 2 days with 6 changes to remove urea from the solution. The dialyzed protein was concentrated and then divided in two parts. Those parts were diluted with D₂O to achieve 90% H₂O, 10%D₂O and 70%D₂O, 30% H₂O final solvent environment. Deuterium exchange was observed constantly for a day and then for 2weeks and 6 months interval.

Chapter 3

Results

A complete understanding of prion misfolding and aggregation process requires the characterization of all species populated along the aggregation coordinate in aggregation funnel, including the unfolded state, partially folded intermediate states, prefibrillar oligomers, protofibrils and mature amyloid fibrils. The unfolded state ensembles are of particularly importance as it is believed that prion or any other protein molecule, either partially or globally unfold in the course of misfolding pathway. Unfolded states of proteins, such as in high concentration of chemical denaturant, have been used as random coil models, where long-range interactions are considered to be absent and therefore local interactions of next neighbor amino acids dominate the conformational behavior. However, the high-resolution NMR studies with unfolded lysozyme (acid denatured with or without urea) in our group has been significant in providing evidence that unfolded states are not completely random (Klein-Seetharaman et al., 2002). The parameters and time-scales of these NMR experiments can provide considerable information about the ensemble-averaged structural properties of unfolded proteins. The most common structure element found in unfolded state is the presence of hydrophobic cluster. The studies on hen egg white lysozyme (HEWL) showed that the polypeptide chains contain residual structure involving long-range interactions between aromatic residues, importantly tryptophane residues. It has been also established that single-point mutations of the hydrophobic residue in the residual structure modulated the compactness and long-range interactions of reduced lysozyme (Wirmer et al., 2004),

resulting in the production of mutant HEWLs possessing various degrees of residual structure; these studies have contributed significantly in understanding of fibrillation of lysozyme. The heat-denatured (65 °C) HEWLs reported to form fibrils at acidic pH readily (Krebs et al., 2000, Xu et al., 2005) and established importance of denatured state in amyloid path of protein conformations.

Prion diseases are one of most lethal amyloid related disease and the spontaneous amyloid formation from recombinant prion protein has been studied extensively in recent years. The methods of choice utilized mild denaturing conditions at acidic pH. Under those conditions, the protein misfolds and misfolding is driven through both native and non-native contacts. The mechanism, therefore, appears complex, while the unfolded state should minimize the effect of native-like interactions and therefore allow us to get a better understanding of importance of non-native contacts in the process. Our result shows that fibrils can be formed from highly denatured state in 8M Urea, pH 2 with and without agitation, which clearly demonstrate the presence of mechanism of self-aggregation in highly denaturing environment. This mechanism may involve formation of fluctuating local structures which promotes intermolecular aggregation or long range interactions which define the architecture for aggregation. These contacts might be initiation site for misfolding eventually leading to amyloid formation. There are not many reports showing amyloid formation in highly denaturing conditions.

Assignments of recombinant prion fragments

The structural characterization of the unfolded state of recombinant prion protein by NMR is been most challenging due to complex nature of protein. In general, the NMR characterization is difficult due to the poor dispersion of amide and carbon resonances in unfolded or partially folded states. The aggregation process of prion

protein hampered the backbone resonance assignments severely. The 3D NMR experiments usually require 3 to 4 days of NMR measurement time, in which the ratio of monomer-oligomer population in NMR sample changes. The use of HNN (Panchal et al., 2001)- and MUSIC-based (*multiplicity selective in-phase coherence transfer*) HSQCs (Schubert et al., 1999, Schubert et al., 2001a, b) helped in unambiguously identifying and assigning the amide backbone resonances. The initial assignment of backbone amide resonances was performed using a series of triple resonance backbone experiments (HNCACB, CBCA(CO)NH, HNCA, HN(CO)CA, HNCO, HCCCONH) (Sattler et al., 1999). There have been significant numbers of overlap, which have been resolved using combination of two or more experiments.

Almost complete ^1H and ^{15}N backbone resonance assignments of recombinant prion protein fragments 90-230, 121-230 and 166-230 in 8 M urea at pH 2, 25 °C were obtained. Figure 3.1 shows comparative dispersion for amide resonances in ^1H ^{15}N HSQC spectrum with respect to spectrum at lower urea concentration or without urea. Figure 3.6 shows an illustrative sequential walk for the palindrome sequence 113-120 AGAAAAGA using HNN corresponding CBCA(CO)NH and strips are plotted in HNCACB in Figure 3.7. The complete backbone amide resonance assignments for unfolded recombinant prion protein is shown in Figure 3.2, all of ^1H amide resonance are distributed in narrow range of $\sim 0.8\text{ppm}$. Despite the small chemical shift dispersion and dynamic nature of protein, the almost complete assignment of disordered protein is satisfying. MUSIC (multiplicity selective in-phase coherence transfer) pulse sequence based HSQCs were helpful in determining the residues and $i+1$ selective manner for a number of amino acids (Figures 3.3, 3.4, 3.5) and helped in correct assignment of these residues.

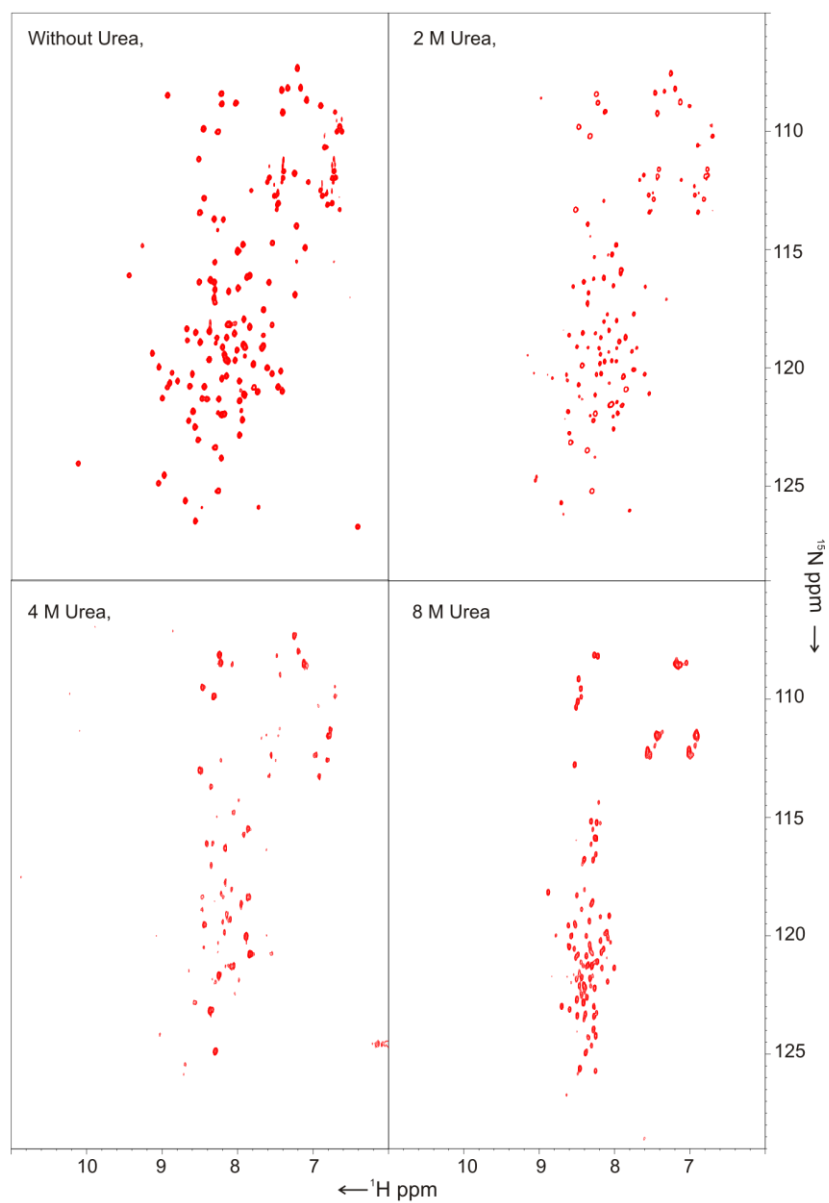
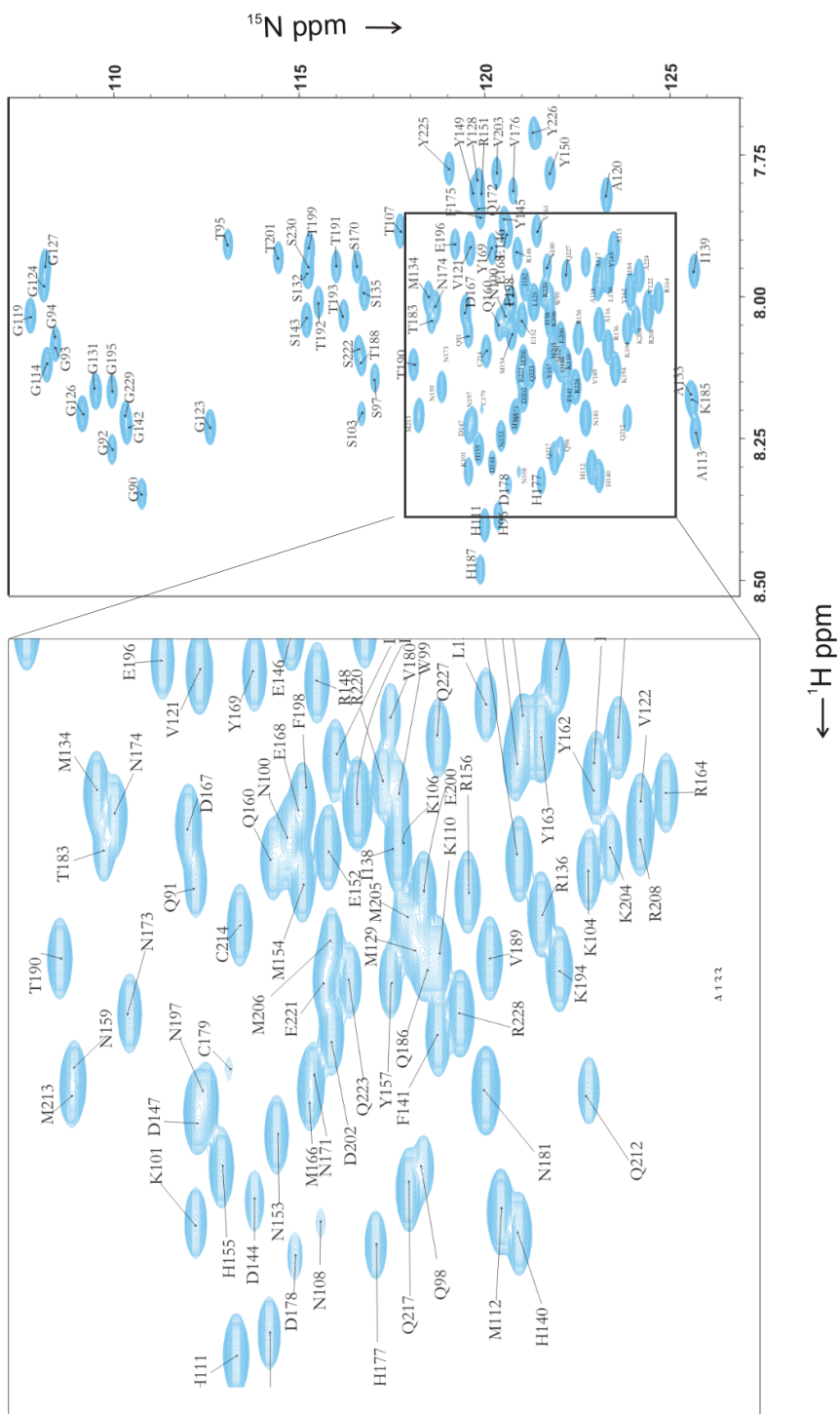


Figure 3.1: ^1H ^{15}N HSQC spectra for various urea concentrations recorded with recombinant human prion protein 121-230, the spectra for 4 M urea concentrations display line broadening and disappearance of signals, indicating molten globule state of protein, while spectra in 8 M urea, shows characteristics low dispersion of signals.

For a native protein structure, the $^{13}\text{C}_\alpha$ resonances for α -helices are shifted downfield typically by an average of 3.1 ± 1.0 ppm, while in β -sheets; they are shifted upfield typically by -1.5 ± 1.2 ppm. However, for the unfolded states of proteins, where conformational averaging takes place, the observed NMR parameters are a population-weighted average of all structures in the conformational ensemble; therefore the observed secondary shifts are considerably smaller. Nevertheless, deviations of chemical shifts from random coil values reflect the relative population of dihedral angles in α and β regions of conformational space. The *chemical shifts and J coupling constants* are the two most sensitive NMR parameters to detect small conformational propensities of the protein backbone in unfolded states, which otherwise cannot be detected by NOEs. Recently, also residual dipolar couplings have been utilized to derive local conformational preferences (Shortle and Ackerman, 2001). The cumulative chemical shift deviations (Kumar et al., 2008) indicate slight preference for β -sheet propensities in urea-unfolded state (Figure 3.8); while random coil index analysis and TALOS+ analysis predict the non-native state in 8 M urea as random coil with very little β -sheet preferences near to C-terminus residues (Figure 3.9 and 3.10).



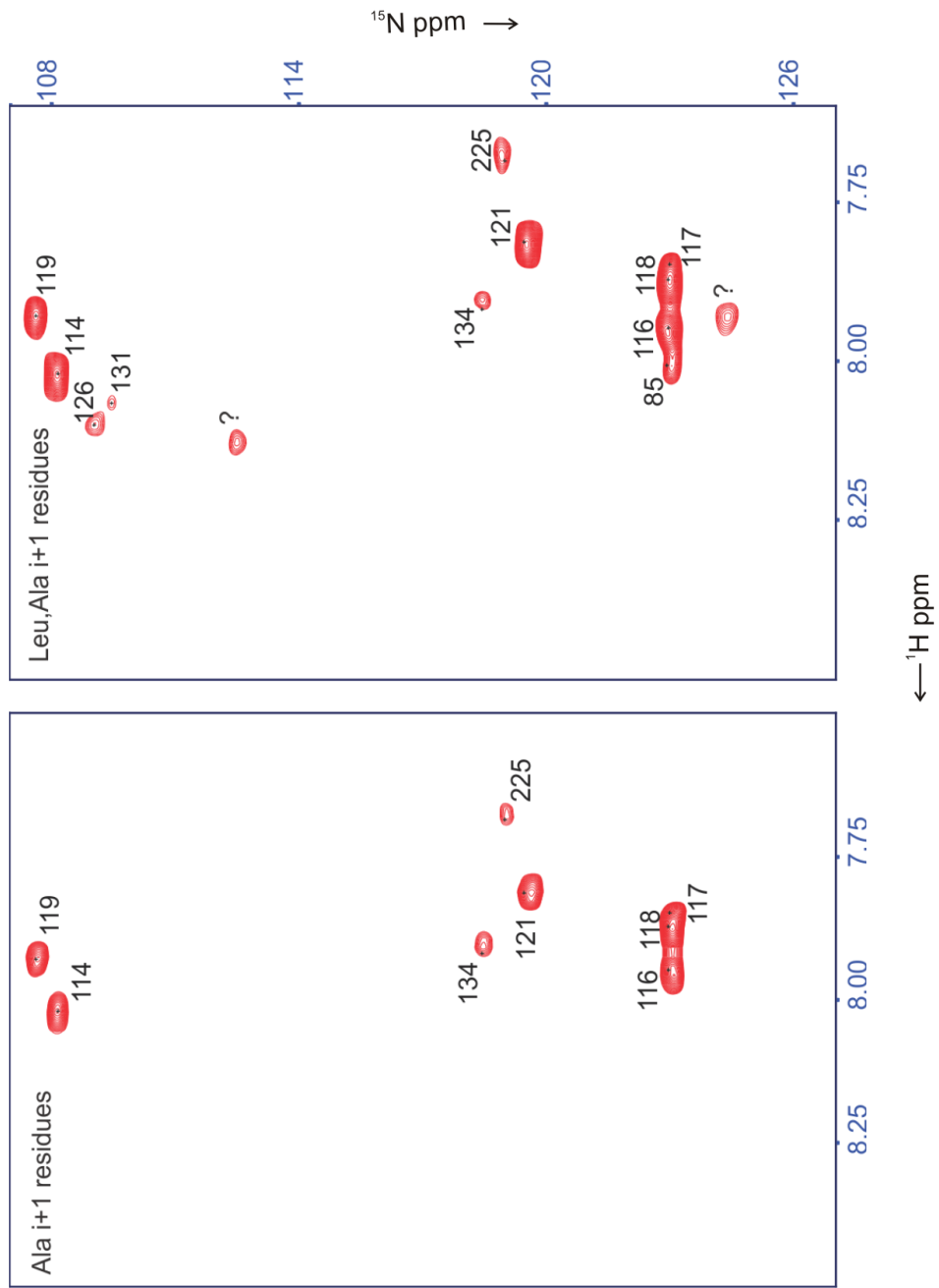


Figure 3.3: ^1H ^{15}N MUSIC based HSQC spectra in 8 M urea, pH 2 for recombinant human prion protein (90-230) for i+1 residues for Alanine (left) and either Leucine or Alanine (right).

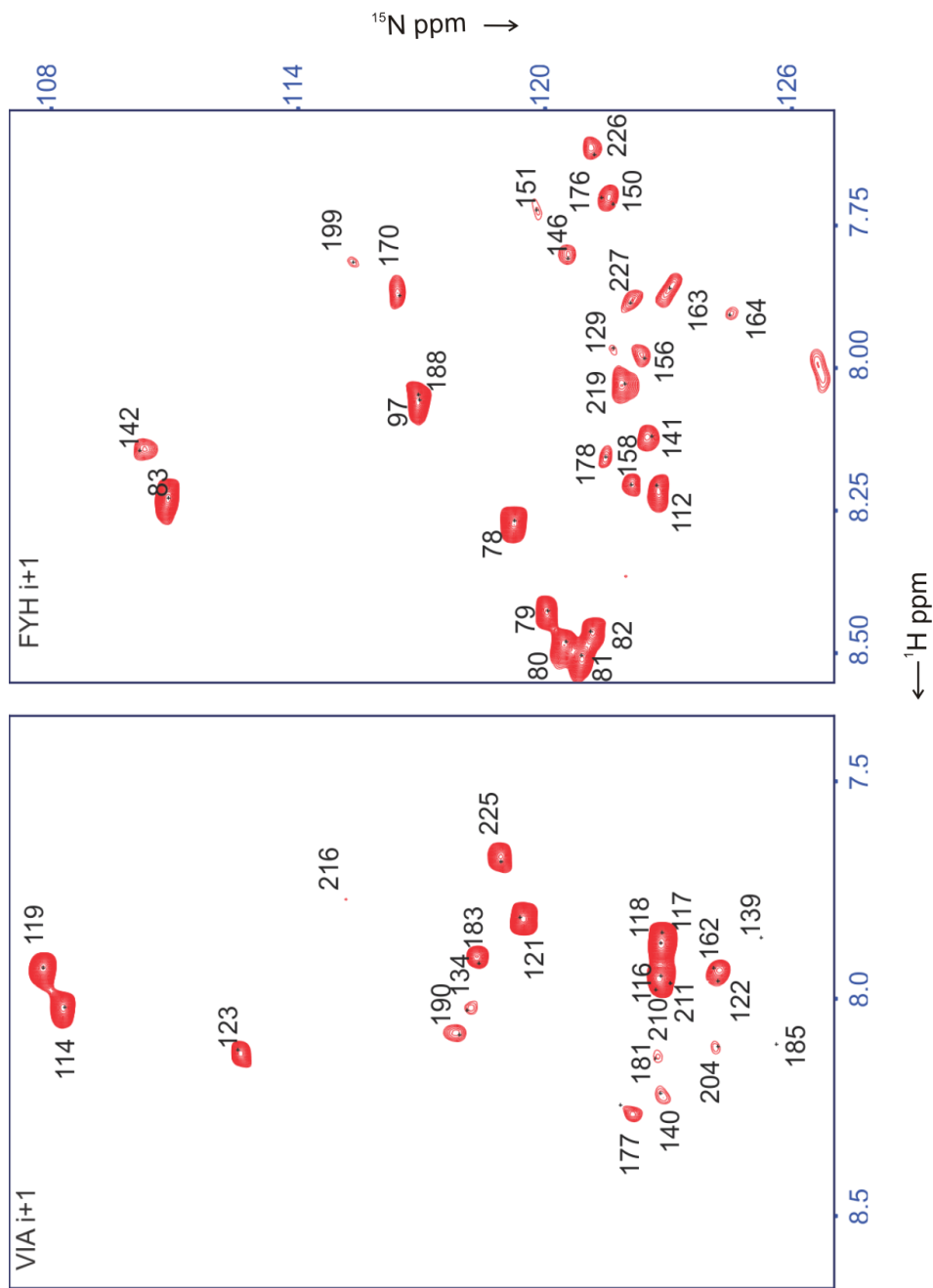


Figure 3.4: ^1H ^{15}N MUSIC based HSQC spectra in 8 M urea, pH 2 for recombinant human prion protein (90-230) for i + 1 residues for Valine, Isoleucine or Alanine (left) and either aromatic Phenylalanine, Tyrosine or Histidine (right).

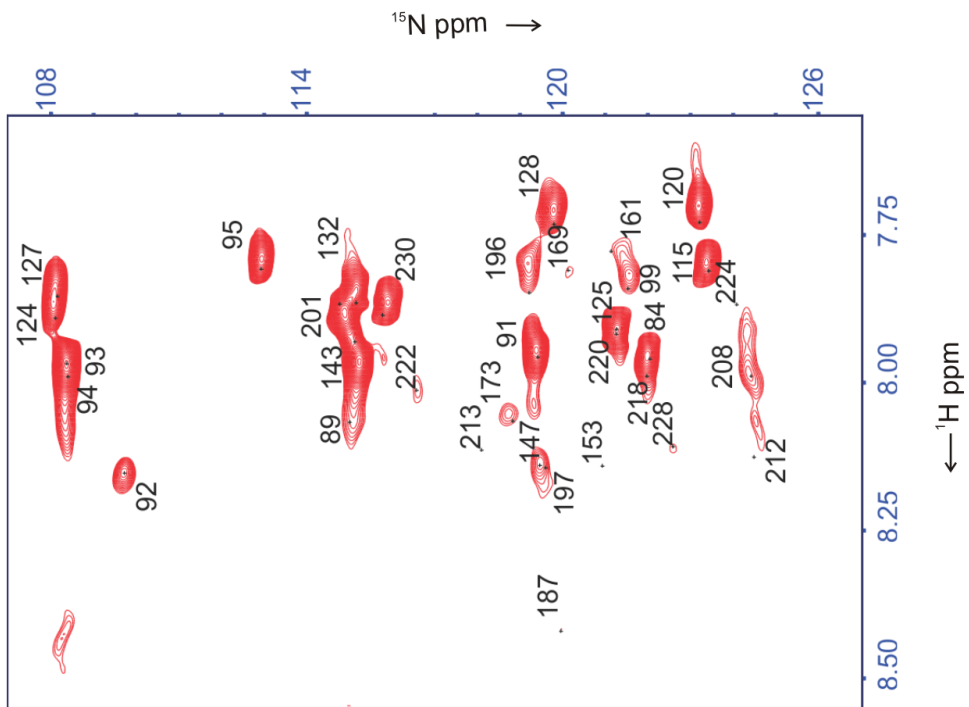


Figure 3.5: ^1H - ^{15}N MUSIC based HSQC spectra in 8 M urea, pH 2 for recombinant human prion protein (90-230) for $i+1$ residues for Glutamate, Glutamine and Glycine.

HNN

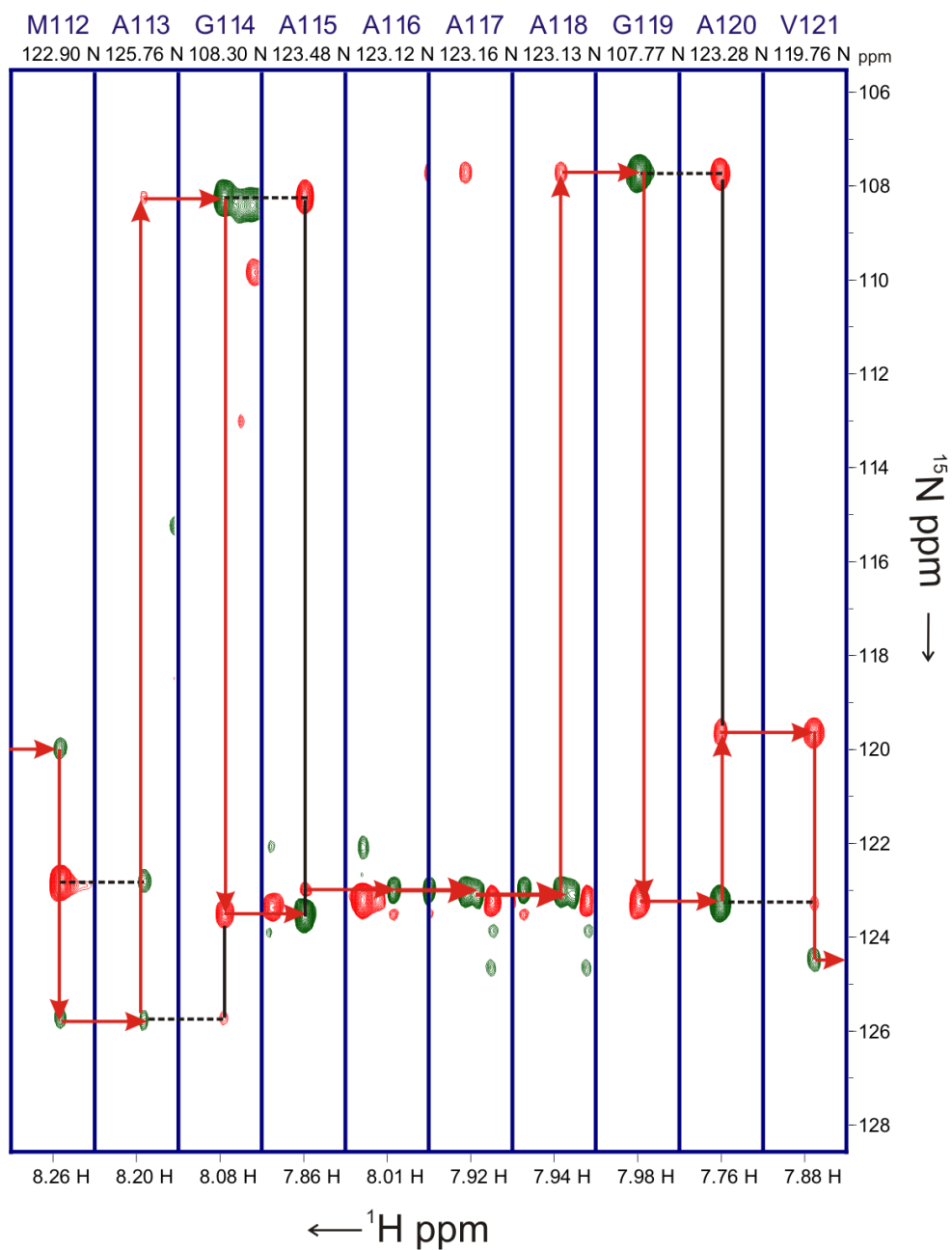


Figure 3.6: Strip plots for three dimensional HNN experiments for 10 residues long sequence (111-120) including palindrome sequence AGAAAAGA . (next page)

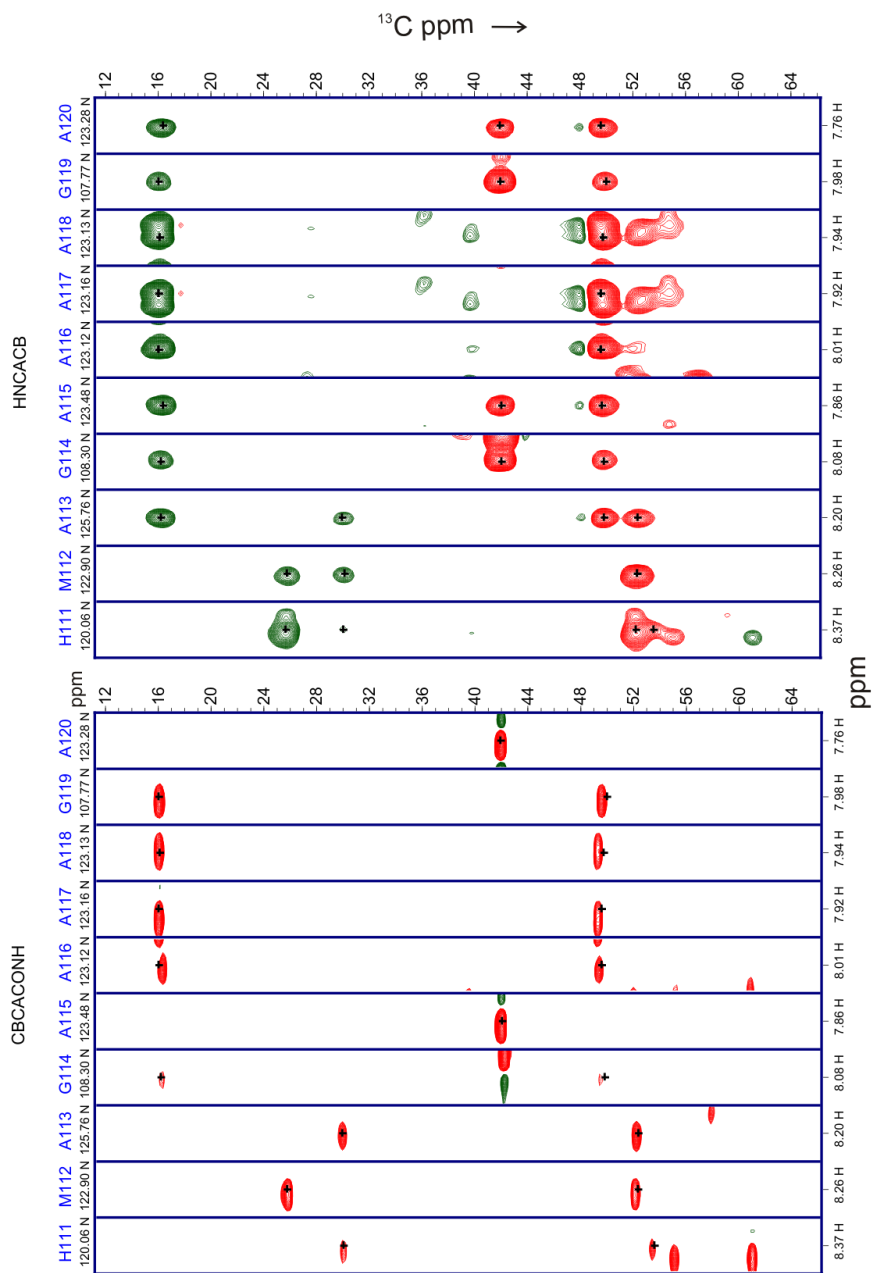


Figure 3.7: Strip plots for three dimensional HNCACB, and CBCA(CO)NH experiments for 10 residues long sequence (111-120) including palindrome sequence AGAAAAGA.

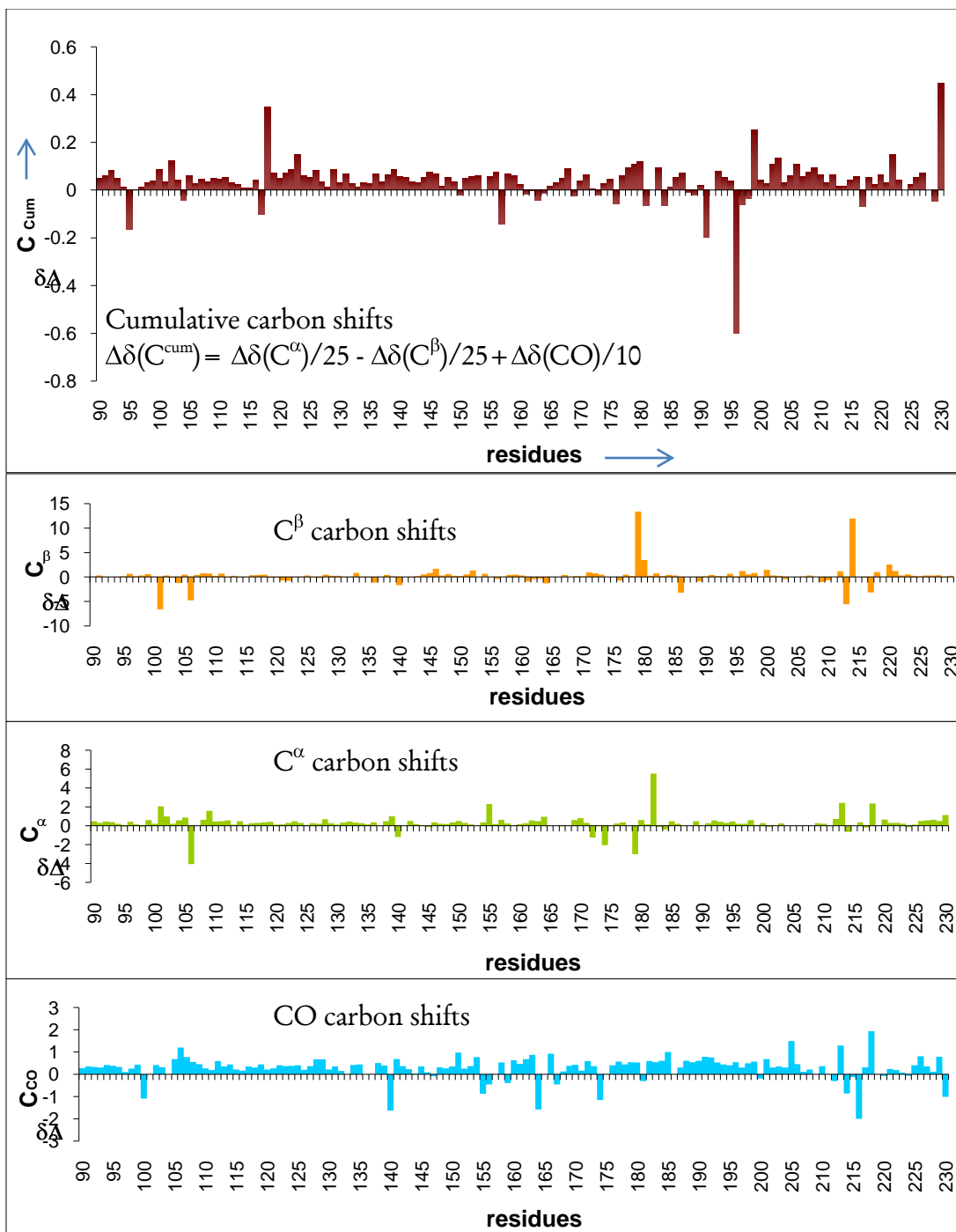


Figure 3.8: Chemical shift deviation plots for recombinant human prion protein 90-230 (previous page). The cumulative (Kumar et al., 2008) shift indicates random coil structure for whole sequence with slight preference for β -sheets.

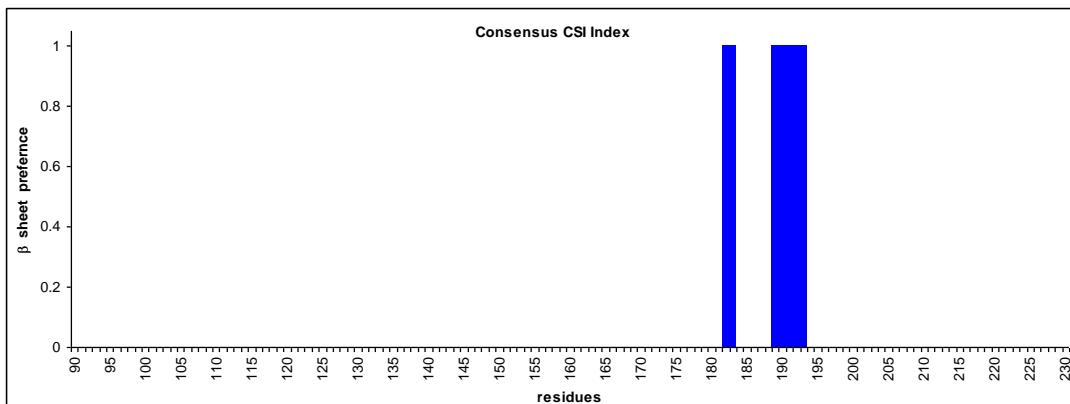


Figure 3.9: Chemical shift Index (CSI) (Berjanskii and Wishart, 2005) plots for recombinant human prion protein 90-230. The CSI values shows β -sheet preferences for residues 182-83 and 189-193, primarily consist of threonine residues.

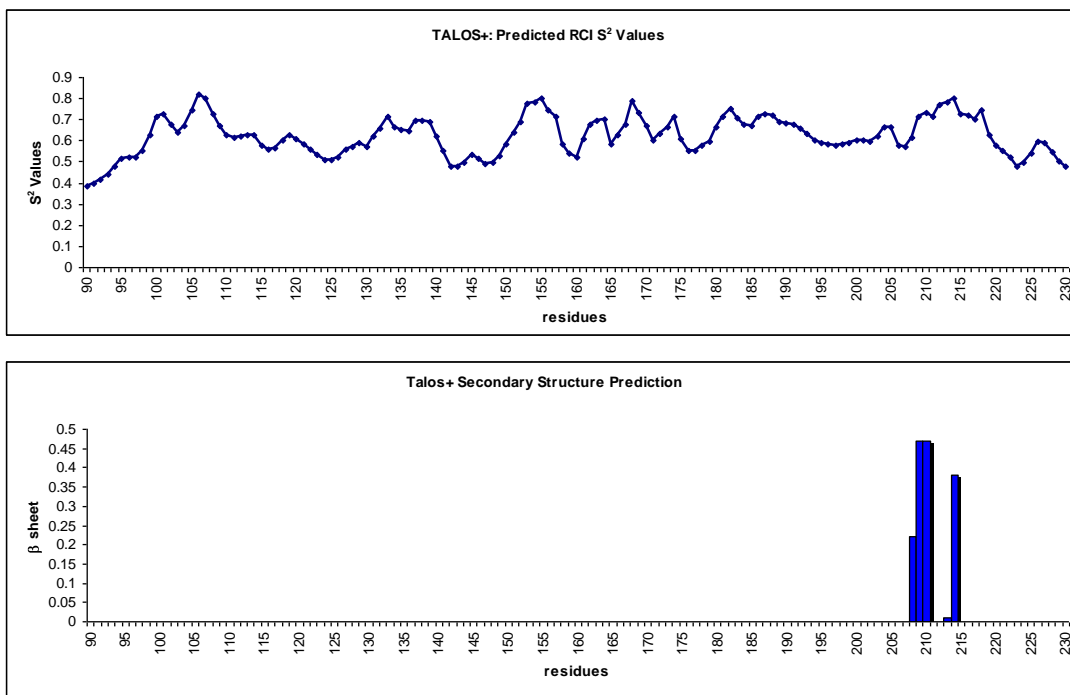


Figure 3.10: TALOS+ analysis; S^2 and β -sheet propensity (Shen et al., 2009) plots for recombinant human prion protein 90-230. The RCI values shows β -sheet preferences for residues 208-210 and 213-214, rest of chain shows random coil preferences.

Amyloid core residues in prion fibrils

We have analyzed the structural rearrangements of the urea-denatured state of recombinant human prion protein (residues 90-230) hPrP₉₀₋₂₃₀ to the fibrillar state by liquid-state NMR. This fragment is of particular importance as it represents the proteinase-K resistant core of prion protein and includes the widely studied amyloidogenic determinant 106-126 (Forloni et al., 1993, Gu et al., 2002, Singh et al., 2002). Over a period of seven days, protein preparations form high molecular weight fibrils. Their formations have been observed by subjecting the fibrils to electron microscopy (EM) (Figure 3.11). Consistently the observed images are similar to those described previously (Anderson et al., 2006).

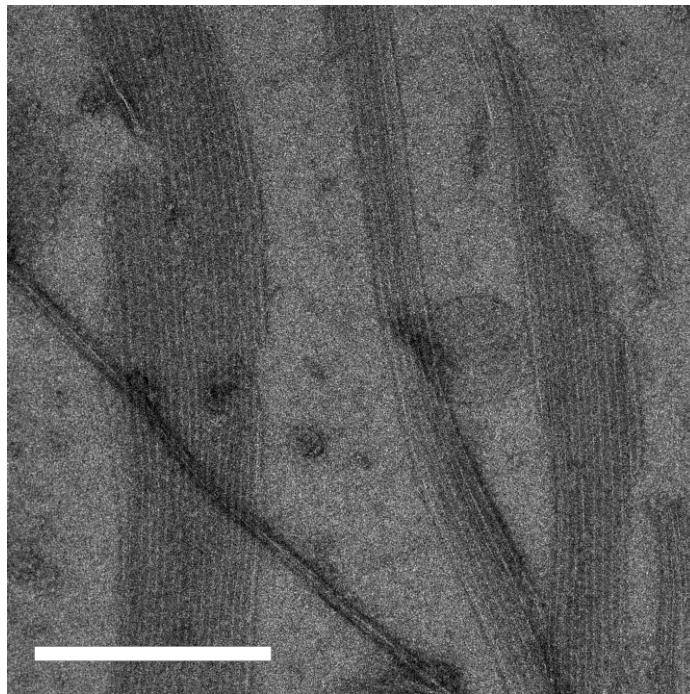


Figure 3.11: Electron micrograph of the hPrP₉₀₋₂₃₀ sample showing long straight fibrils.
Scale bar: 500 nm.

The ^1H ^{15}N HSQC of hPrP₉₀₋₂₃₀ with intact disulfide bond recorded immediately after purification under urea denaturing conditions (8M urea, pH 2.0) revealed the typical dispersion and narrow line width comparable to spectra of unfolded proteins (Figure 3.12a). The spectra for the same sample acquired after constant agitation on the 4th and 7th day showed a non-uniform loss of intensity of resonances, some of them disappeared (Figure 3.12b and 3.12c). By comparison with spectra of a construct containing residues 166-230 only, we can show that the disappearing signals originate mainly from residues corresponding to this region of hPrP (Figure 1.8) that is associated with hereditary point mutations (Collinge, 2001).

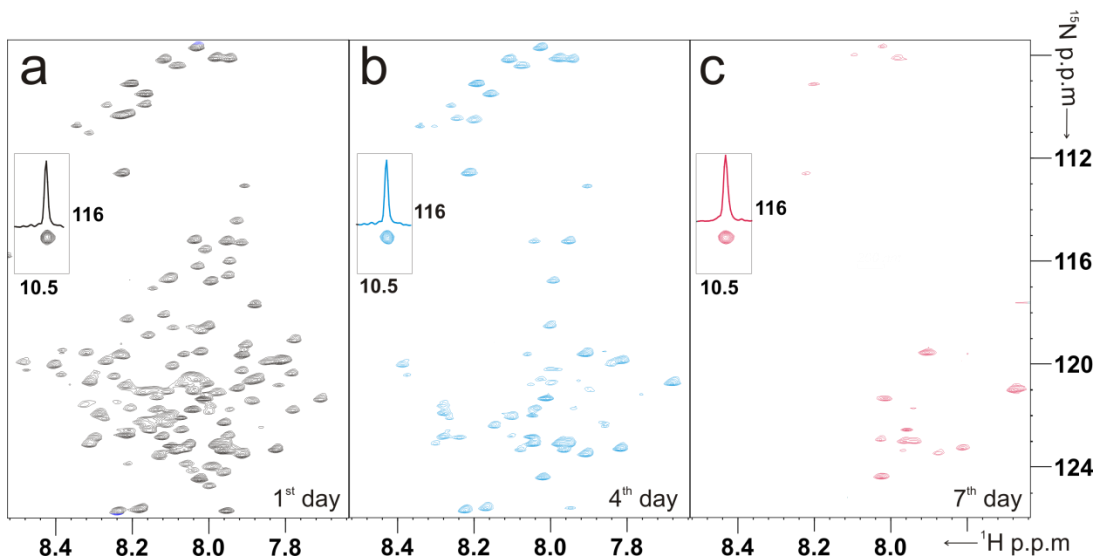


Figure 3.12: Solution NMR of human prion fibrils. (a) ^1H , ^{15}N -HSQC spectra of hPrP₉₀₋₂₃₀ at 298K in 8M urea, pH 2 at a concentration of 200 μM in 10% D₂O. Spectrum acquired 30 minutes after dissolving hPrP₉₀₋₂₃₀. The spectrum is well resolved and 135 out of 136 cross peaks are assigned (Figure 3.2). Spectra acquired (b) 4 days and (c) 7 days after dissolving hPrP₉₀₋₂₃₀ under constant agitation.

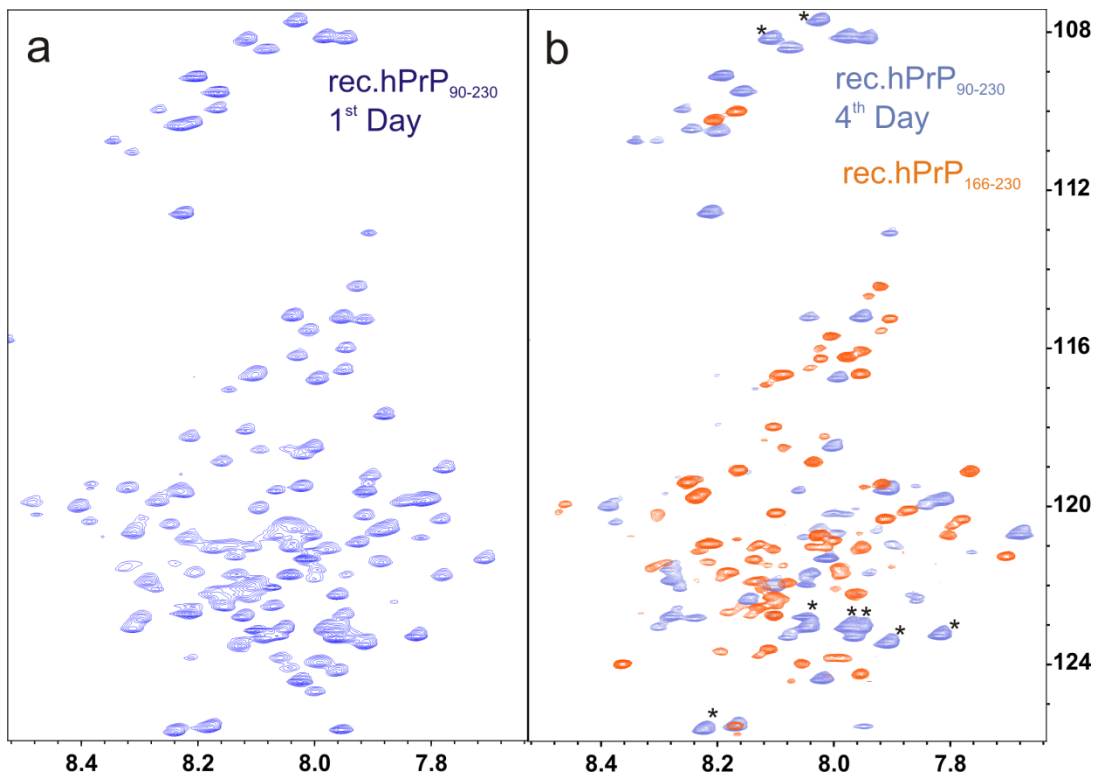


Figure 3.13: Disappearing signals include the region comprising the residues 166-230 of hPrP sequence. (a) ^1H , ^{15}N -HSQC spectrum of hPrP₉₀₋₂₃₀ acquired immediately after dissolving the protein in the denaturing conditions (8 M urea, pH 2.0, 25°C). (b) Overlay of the spectra in (a) acquired on the 4th day (blue) and the construct hPrP₁₆₆₋₂₃₀ (8 M urea, pH 2.0, 25°C) acquired immediately after sample preparation. The disappearing signals in the hPrP₉₀₋₂₃₀ include region 166-230, * represents signals for the palindrome sequence AGAAAAGA (113-120).

Apparently, even under conditions where fibrils form as evidenced by EM and AFM, we can observe some well-resolved resonances in solution-state NMR spectra. The observation of NMR signals from a high molecular weight fibril state has previously been attributed to either a residual monomer population (Platt et al., 2009) and/or has been thought to be due to the dynamic nature of the individual sub-domains stemming from the residues not rigidified in the amyloid fibrils

(Baldwin et al., 2008). The presence of fibrillar species in solution can be ascertained by pulse-field gradient (PFG) NMR quantifying rotational diffusion (Baldwin et al., 2008). These experiments when performed for the seven days old sample of hPrP₉₀₋₂₃₀ confirmed the presence of fibrillar species (Figure 3.14).

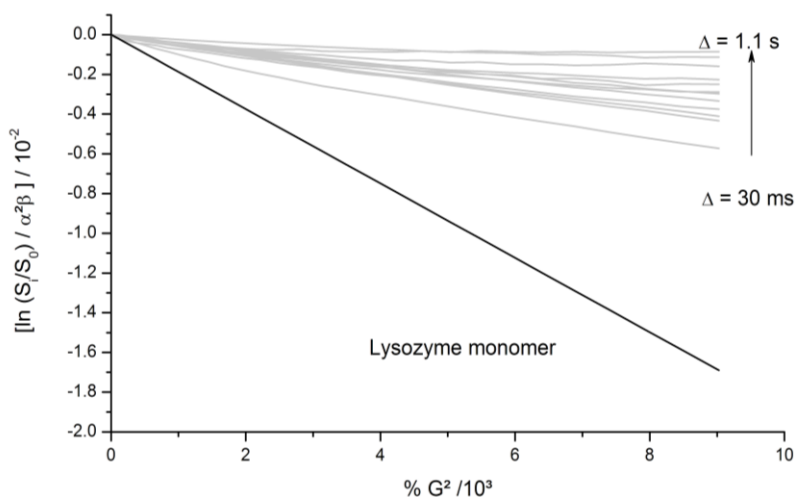


Figure 3.14: Integrated PFGSE profiles for prion protein in fibril state as a function of field strength. Data is plotted for a range of Δ . (in grey) with a lysozyme monomer (black). These values are in accordance with earlier reported values for SH3 fibrils (Baldwin et al., 2008) supporting the presence of large molecular structures like the fibrils, in solution.

We assigned the NMR backbone resonances of the hPrP₉₀₋₂₃₀ under denaturing conditions of 8M urea and pH 2. The assignment was complete with all the residues except for residues near Cys214 (Figure 3.2). The gradual loss of the intensities observed in the HSQC spectra between the 1st, 4th, and the 7th day is plotted against the residue numbers in Figure 3.15. The relative intensities observed can be broadly classified into three different categories: (I) peaks with a slow decrease (90-144), (II)

peaks with the fast decrease that finally disappeared (145-223). A few residues, namely 149, 150, 151, 177, decreased slower than others in this region until 4th day while residues 180 and 208 are still observable on the 7th day, and (III) peaks that change chemical shifts during the aggregation process (224-230) (Figure 3.18). The loss of signal intensities is caused by slow rotational reorientation, arising from the rigid parts of the fibrils while the signals that are still NMR observable stem from mobile regions of the fibrils. The presence of rigid and flexible regions in the fibrils is further supported by solid-state NMR experiments (Figure 3.16).

Running average as indicator of fibril formation

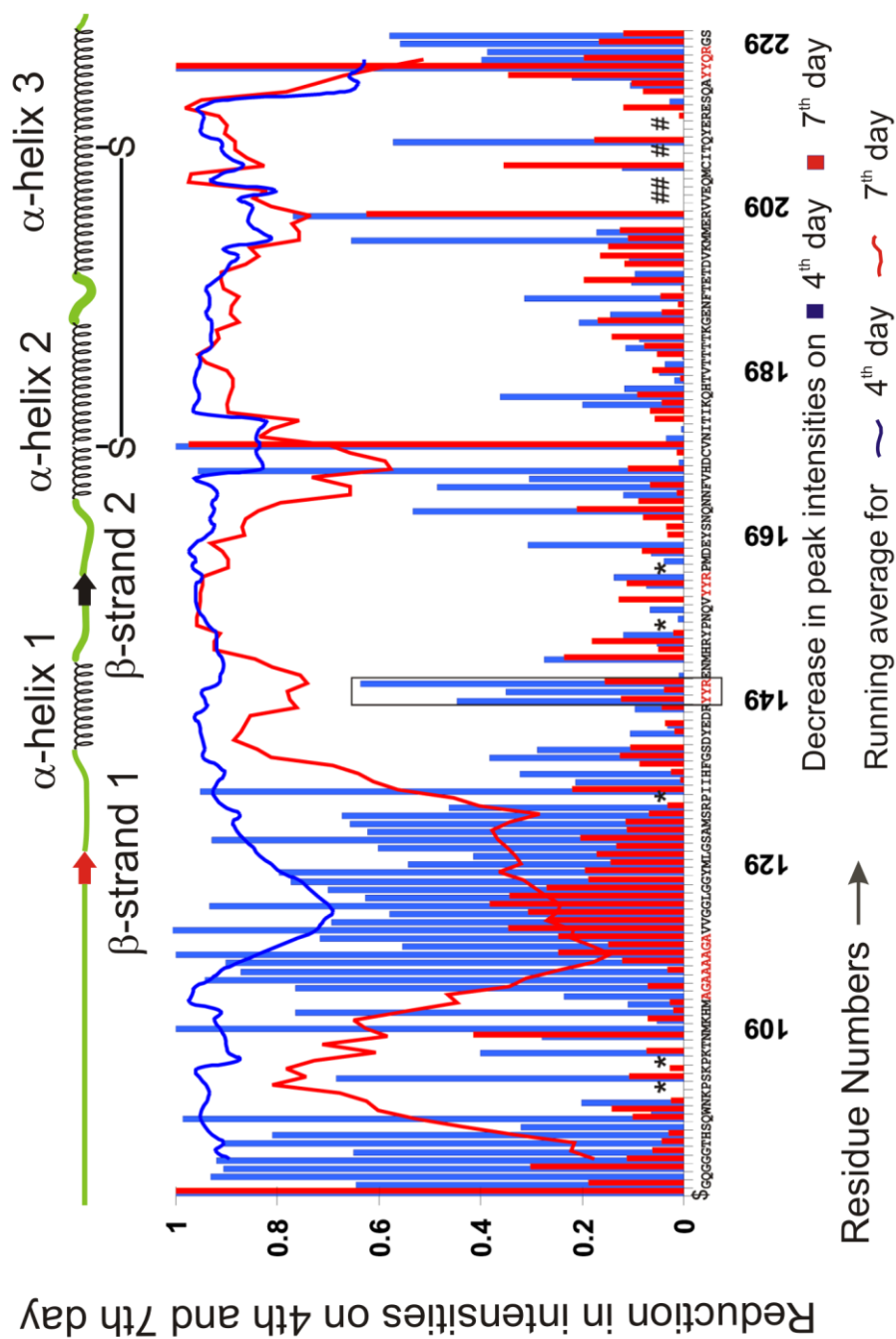


Figure 3.15: Bar diagram showing decrease in NMR peak intensities for hPrP90-230; blue (red) bars represents the changes observed on day 4 (7) relative to their initial intensities and normalized to internal phthalimide (\$) as standard. Blue and red lines represent the running average over 7 residues. * and # indicates prolines for which no backbone assignment can be obtained and unassigned residues, respectively. YY(Q)R and palindrome AGAAAAGA are marked in red in sequence. The changes in intensities for YYR motif 149-151 is shown in the box.

The region between residues 145-223 showed a significant decrease in signal intensities, indicating a major role in fibril formation. Although signal intensities for residues 144-156 (α -helix-I) are decreased, it has been reported that this region promotes aggregation but is not converted to β -sheet (Watzlawik et al., 2006). Recently, using mass spectrometry (Lu et al., 2007) and EPR spectroscopy, it has been proposed that the residues ranging from Gln160–Lys220 form the core of amyloid made of parallel in-register β -sheets (Cobb et al., 2007, Cobb et al., 2008). The amyloid form of the recombinant mouse prion protein of the full length mPrP₂₃₋₂₃₁ displays only two regions that are highly protected from hydrogen exchange (residues (24-98) and (182-212)) showing that the region in between is still flexible (residues 99-180) (Nazabal et al., 2009). We investigated the role of the residues 166-230. ^1H ^{15}N HSQC of hPrP₁₆₆₋₂₃₀ acquired immediately after the protein was dissolved in denaturing conditions (8M urea, pH 2) revealed line widths and chemical shifts comparable to the hPrP₉₀₋₂₃₀ (Figure 3.17). The HSQC acquired after six hours already showed remarkable disappearance of most of the signals, indicating formation of oligomers. This sample resulted in a thick gel, which when subjected to electron microscopy revealed an un-resolvable dense mass of amorphous aggregates. We concluded that a polypeptide chain comprising residues 166-230 does not form fibers under the denaturing conditions employed here. These residues, although being part of the amyloid core in our hPrP₉₀₋₂₃₀ preparations, do not form fibers in the shorter construct. We concluded that the aggregation promoting sequence in the 90-166 region seems to be required for the amyloid formation.

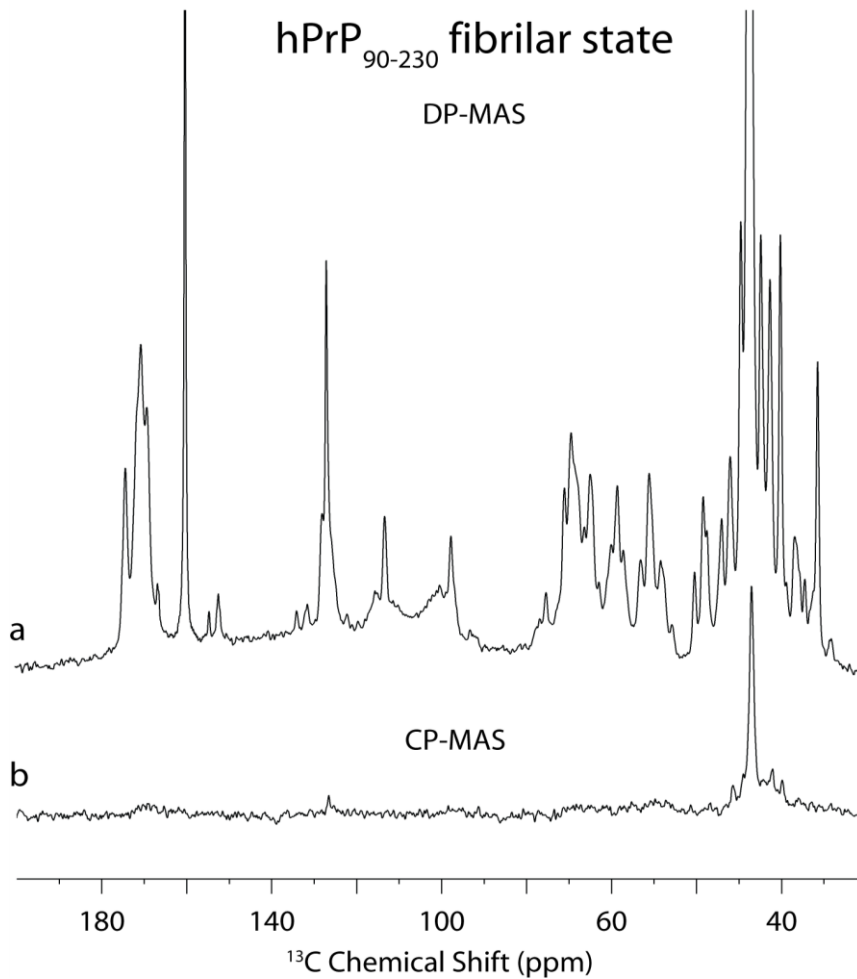


Figure 3.16: 1D ^{13}C MAS (magic angle spinning) spectra of hPrP₉₀₋₂₃₀ fibrillar state. hPrP₉₀₋₂₃₀ aggregates into fibres and forms with time a sample of gel-like texture. This sample was transferred from the liquid-state NMR tube into a 4mm MAS NMR rotor by centrifugation. At a spinning rate of 10 kHz, ^{13}C spectra were recorded using direct polarization (DP) and cross polarisation (CP). The DP spectrum (a) reveals well-resolved resonances with line widths of down to 0.5ppm. A signal loss is observed under CP conditions. This indicates high molecular mobility, which makes dipolar-based magnetization transfer as in CP inefficient. Spectra were recorded at a Bruker Avance 600WB spectrometer using a 4mm DVT probehead at 25°C. In both cases, ^1H decoupling of 90 kHz was applied and 2048 transients were accumulated. For CP, a contact time of 2ms was used. The FIDs were processed using exponential

line broadening of 20Hz.

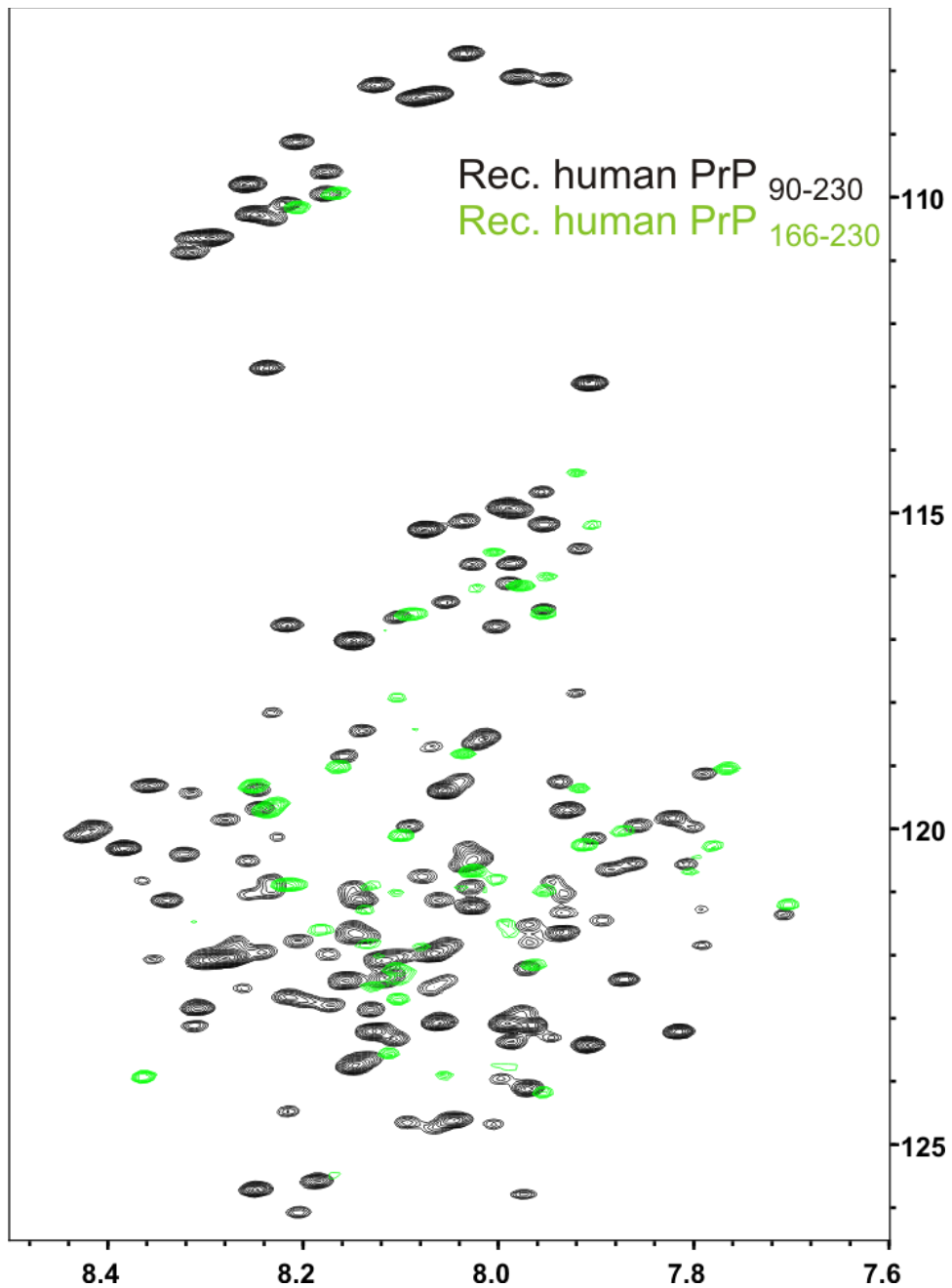


Figure 3.17: Overlay of ^1H ^{15}N HSQC spectrum of hPrP₉₀₋₂₃₀ (green) and hPrP₁₆₆₋₂₃₀ (black) acquired in the denatured state at 8 M urea, pH

2.0, 25°C.

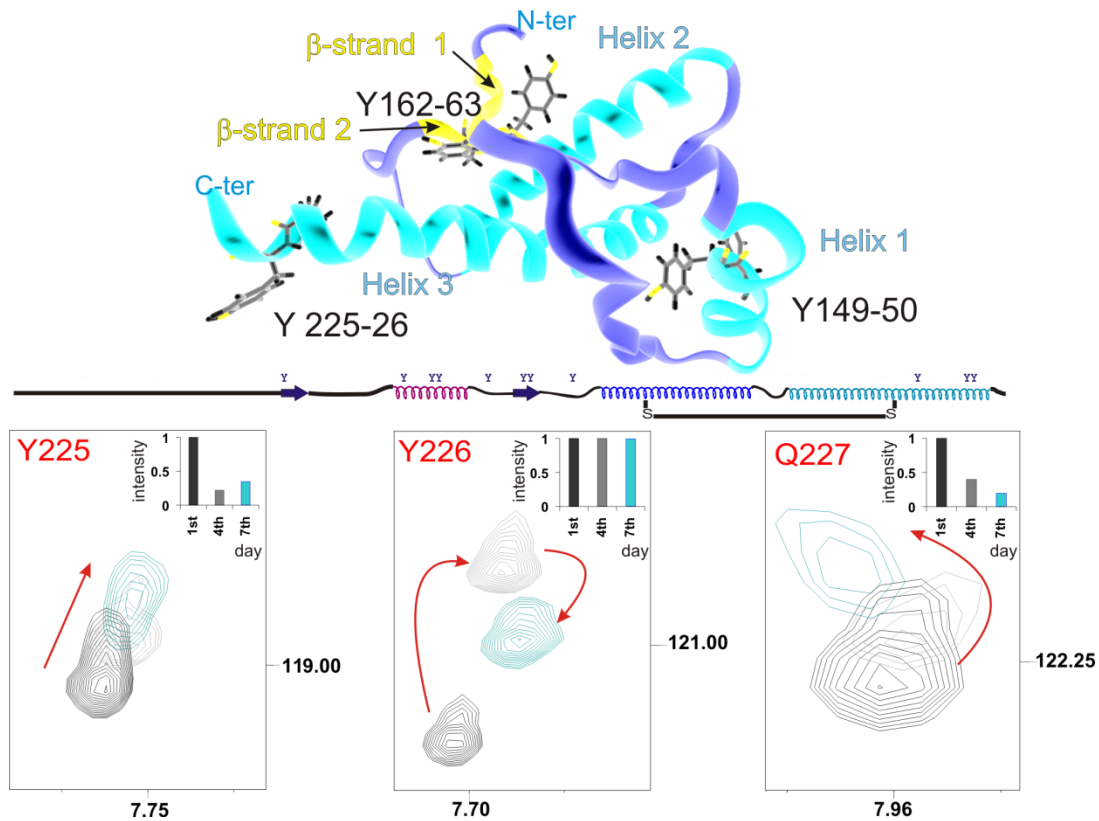


Figure 3.18: Structural properties of Tyr-Tyr-Arg (YYR) motifs. (a) Secondary structure representation of hPrP₉₀₋₂₃₀ showing the distribution of tyrosine residues. Tyrosines appearing in pairs have been encircled. (b) ¹H ¹⁵N HSQC spectra of hPrP₉₀₋₂₃₀ at 298K in 8M urea, pH 2 at a concentration of 200µM in 10% D₂O. The signals correspond to the Tyr225-Tyr226-Gln227 in α-helix-3 of hPrP. The changes in the chemical shift are indicated by the arrow. The graph in the inlay shows changes in the intensity of the signals observed with respect to the first day of sample preparation (normalized to internal phthalimide).

Residues 90-126 are unstructured in the native form (Zahn et al., 2000) and have been proposed as key region for the amyloid and toxic nature of PrP (Weissmann

and Flechsig, 2003). This region comprises a hydrophobic core (residues 106-126) and within this core an amyloidogenic palindrome sequence AGAAAAGA (residues 113-120). Our data show that the peak intensities of residues within the 90-126 region decrease only by 30-40% after day 4 and remain largely visible even after day 7 in comparison to the other regions of the protein, except for the region around the Pro102 and Pro105, which show complete decrease in NMR signal intensity (Figure 3.13b). The palindrome sequence (Gasset et al., 1992) remains visible in the NMR spectra (Figure 3.13) indicating that this region is flexible in the fibrillar state after the 7th day. Previously, solid state NMR investigations on hPrP₂₃₋₁₄₄ (a Gerstmann-Sträussler-Scheinker (GSS) syndrome-related Y145stop variant) identified a rigid core comprising of residues 112-141 (Helmus et al., 2008), while in our studies, residues 113-140 in hPrP₉₀₋₂₃₀ remain flexible. The palindromic sequence is not part of the rigid core of fibrils but likely promotes fibril formation. The amyloidogenic region comprising the residues 106-126 remains solvent accessible in the fibril state, which could explain for the specificity of the recently reported monoclonal antibody (variant-CJD (Creutzfeldt-Jakob disease) monoclonal antibody 3F4 (Barry and Prusiner, 1986) binds to epitope with residues from 109-112) against this region of the pathogenic prion protein.

The prion protein comprises 13 tyrosines and 11 of these tyrosine residues are in the structured domain (Figure 3.18). 6 tyrosines appear in pairs and are conserved across mouse, human, sheep, bovine and human PrP (Paramithiotis et al., 2003). Two tyrosine pairs, located in α -helix-1 and β -strand 2, are found in conjunction with a C-terminal arginine (hPrP residues 149-151 and 162-164, respectively), whereas the tyrosine pair at the C-terminus of α -helix-3 (residues 225-227) is flanked by a C-terminal aspartate in mouse and hamster or a glutamine in sheep, bovine and human PrP (Figure 3.18) (Paramithiotis et al., 2003). Several antibodies against Tyr-

Tyr-X motifs have been developed as a diagnostic tool specific to the prion protein, based on the assumption that these tyrosine residues are solvent exposed in the fibril state (Paramithiotis et al., 2003, Li et al., 2009). The same antibodies do not bind to the native PrP presumably because these tyrosine motifs are concealed to antibody recognition by tertiary structure elements (Riek et al., 1996, Liu et al., 2000, Zahn et al., 2000) and native post-translational modifications. Our data provide direct evidence for the solvent exposure of these tyrosine motifs in the fibril state by NMR. In the ^1H ^{15}N HSQC spectrum of the fibril state of the hPrP₉₀₋₂₃₀ signals for Tyr149-Tyr150-Arg151 in α -helix-1 can be observed, indicating that this motif remains flexible and solvent exposed (Figure 3.13). The disappearance of the signals for Tyr162-Tyr163-Arg164 in β -strand 2 shows that this motif is in the core of the fibril. Changes in the chemical shift observed for the residues Tyr225-Tyr226-Gln227 in α -helix-3 (Figure 3.18) indicates that this motif undergoes structural rearrangement during the formation of the fibrils. We conclude that two of the three tyrosine motifs are solvent-exposed in the fibril state.

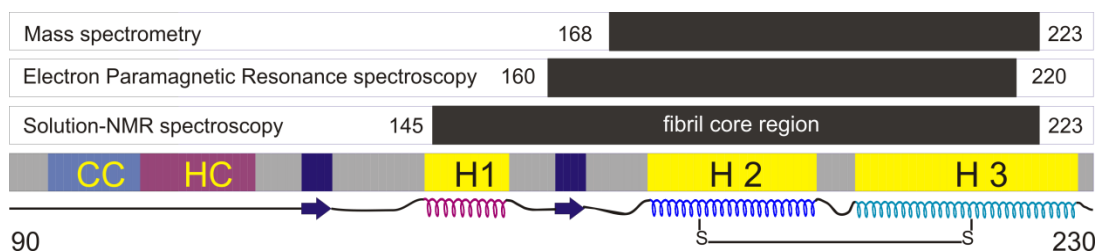


Figure 3.19: Schematic presentation of fibril core of recombinant prion hPrP₉₀₋₂₃₀ amyloid fibrils as investigated by mass spectrometry (Lu et al., 2007), electron paramagnetic resonance (EPR) spectroscopy (Cobb et al., 2007, Cobb et al., 2008) and solution-NMR spectroscopy (our data). The charged cluster (CC), hydrophobic core (HC), helices (H1, H2 and H3) and single disulfide bridge (S-S) from native structure (Zahn et al., 2000) are indicated.

In summary, the recombinant human prion fibrils formed under denaturing conditions (from 8 M urea at pH 2) comprise both rigid and dynamic parts and the NMR data presented here allows us to delineate these regions of the fibrils. Within hPrP₉₀₋₂₃₀, residues 145-223 (comprising from helix-1 to helix-3 in the native state) form the rigid core of the fibrils. Previous studies using fibrils prepared in denaturing conditions mapped the core region to 168-223 using H/D exchange (mass spectrometry) (Lu et al., 2007), whereas, the fibrils prepared in native-like environment at acidic pH (pH 4.0) mapped the core region to 160-220 using EPR spectroscopy (Cobb et al., 2007, Cobb et al., 2008) (Figure 3.19). It is striking that recombinant prion fibrils formed under the highly denaturing and native-like environment share a common core region. This information has a strong implication for presence of common fibril forming mechanism in variable chemical environments. Furthermore, recently it has been shown that recombinant hamster prion fibril induces disease in hamsters on serial transmission (Makarava et al., 2010). It has been hypothesized that recombinant fibrils undergo conformational adaptation in the process. Importantly these recombinant fibrils carry structural information to recruit native PrP^C and thus causing the disease (Makarava et al., 2010). Therefore, despite being potentially structurally different from infectious prion (Wille et al., 2009), these recombinant prion fibrils are having all the structural information for seeding and transmission of disease (Makarava et al., 2010). We further show that the amyloidogenic region around residues 106-126 is not part of the rigid core but remains flexible, a finding further supporting its role as aggregation promotor. The solvent accessibility of tyrosine motifs known in the fibrils is in line with the antibody binding specific to prion protein.

Polymorphism in prion fibrils

Understanding the molecular and high order architectural structural heterogeneity of amyloid fibrils is a major challenge to present day science. It is well known that for amyloid fibrils, nucleation and kinetics depend not only on inherent features such as the amino acid composition, sequence, and length, but also on environmental conditions such as temperature, concentration, pH, ionic concentration, agitation, and enhanced aggregation. Despite the knowledge about these factors, the self-assembly mechanism which leads to ordered fibril formation is not well understood. There are a number of open questions like (1) how the monomers assemble into oligomers; (2) which segments or domain of a long polypeptide constitute the recognition motifs and are there any of them play key roles in amyloid fibril formation; (3) how the β -strands stack relative to one another; (4) are there favored organizations between the β -sheets or there more a few possible arrangements, (5) what are the most favored architecture of β -sheets and what are the intermolecular interactions between the layers that stabilize these; and, (6) what are the pathways and the intermediate states that are involved in seed and fibril formation. The combination of these contribute to one of the most difficult problem in the field of protein aggregation which is known as aggregate or fibril polymorphism; the aggregates can have different preferred fibril architectures depending on (even slight) changes in any of these sequence or environmental factors. In our studies, where we started to observe fibril formation in highly denaturing environment of 8 M urea, pH 2; which essentially unfold the polypeptide chain, we were able to observe fibril formation. The fibrils formed under these conditions display structural polymorphism as reported for underglycosylated scrapie prion fibrils. The different morphologies of fibrils (Figure 3.20) are suppose to be initiated from different molecular structures and may be lead to

formation of different prion strains. Therefore, an understanding is necessary for gaining an insight into the phenomenon of prion strains, wherein the same prion protein adopts a range of infectious conformations differing in their specificity and transmission barrier. In this section, we try to bring together the data from electron microscopy (EM), atomic force microscopy (AFM), solid-state NMR spectroscopy (SS-NMR) and solution-NMR spectroscopy.

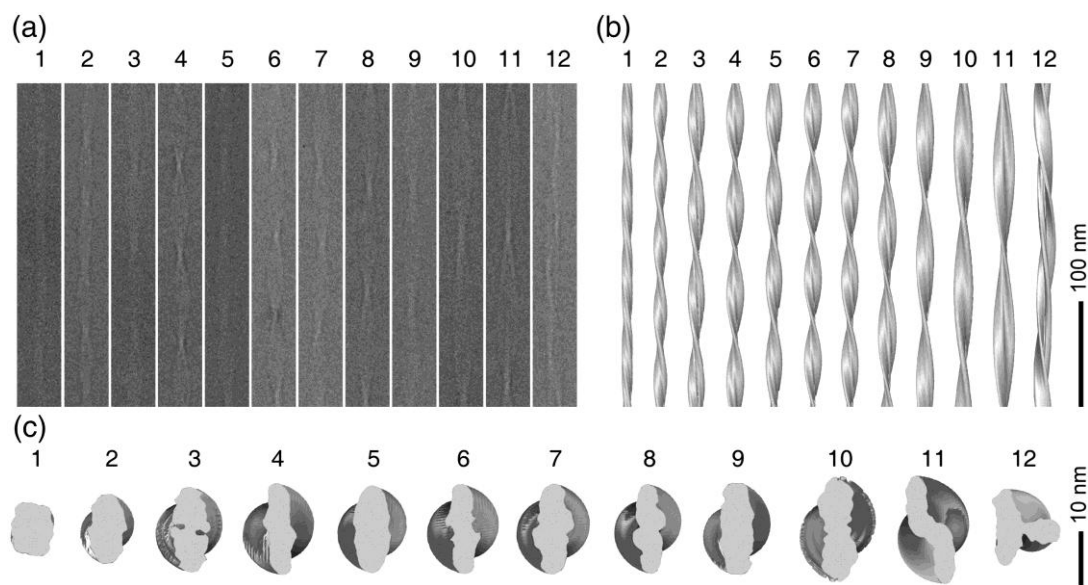


Figure 3.20: an example of α - β polymorphism observed. Cryo-EM reconstructions of 12 individual α - β (1-40) fibrils. (a) Electron micrographs of the 12 individual α - β (1-40) fibrils from the same sample. (b and c) Side (b) and top (c) views of the reconstructed fibrils shown in (a); the image is adapted from (Fandrich et al., 2009, Meinhardt et al., 2009).

Electron microscopic images: Polymorphism among preparations

The TEM is a powerful method to gain structural information about the amyloid fibrils. The EMgraphs were generated by staining with uranyl acetate and placed on carbon grid to observe the morphologies. The samples were diluted 5 to 100 times, depending on the viscosity of the preparation, which increase with the rise of fibril

population. These images display presence of multiple morphologies in same preparation. They include long sheeted assemblies along with other subtype of fibrils. In a number of grids (Figure 3.27), these amyloids appeared to be clustered together, which make it difficult to identify individual characteristics of fibrils. These fibrils show different morphologies for non-agitated and agitated preparations. The short peptide 174-184 forms instantaneously (Figure 3.29) and only one which gave electron diffraction map (Figure 3.30). Non-agitated preparations shows majorly long twisted fibrils, with other thinner fibrils can also be observed (Figure 3.21, 3.22 and 3.23). The samples prepare with agitation, mostly showed cluster of long straight fibrils (Figure 3.24 and 3.25) but often also seen as bundle of thin fibres (Figure 3.26). The fibrils formed in 8 M urea pH 2, shows stability when they are dialyzed against water pH 2 (Figure 3.28), but the morphological appearance is changed.

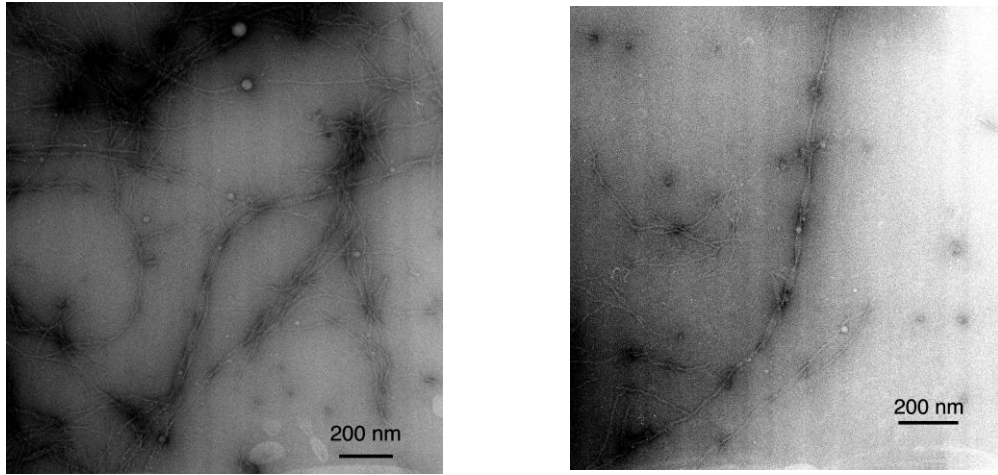


Figure 3.21: EMgraph of recombinant prion protein fibrils, these fibrils formed on long incubation at room temperature, and samples were not agitated. The EMgraphs clearly display a population of long twisted fibrils, which are having twisted about every 80nm and 20 nm in diameter. There are other fibrils presents, which are relatively thinner.

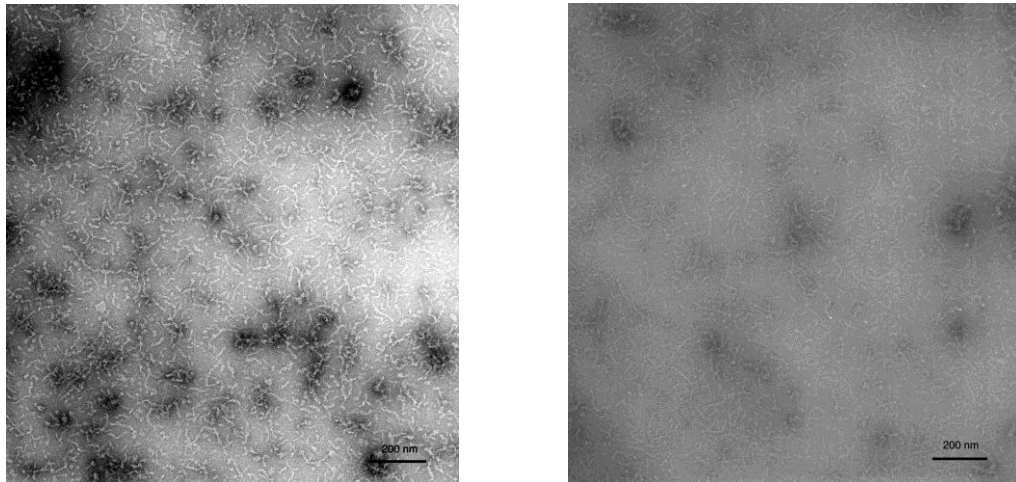


Figure 3.22: The EMgraph of freshly prepared recombinant prion fibrils, samples were non-agitated and clearly display that sample is full of small worm-like fibrils, the length of these fibrils are relatively short and about 100nm.

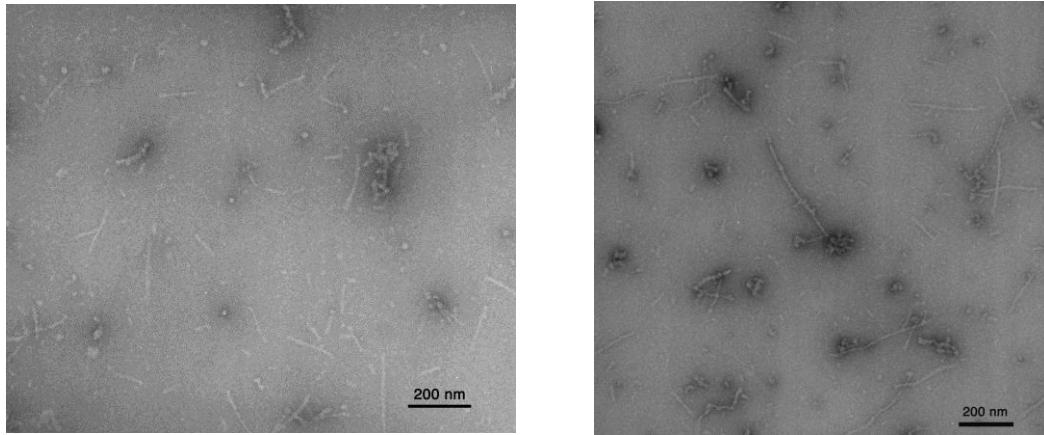


Figure 3.23: The EMgraph of recombinant prion fibrils (non-agitated) display the presence of classic rod-like fibrils along with some twisted fibrils.

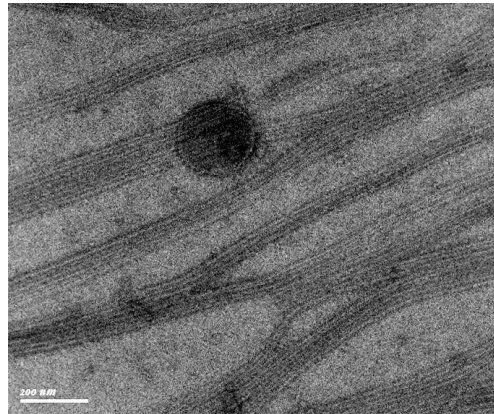


Figure 3.24: The EMgraph of recombinant prion protein fibrils (agitated) displaying long-straight fibrils appearing in bunches for low protein concentration.

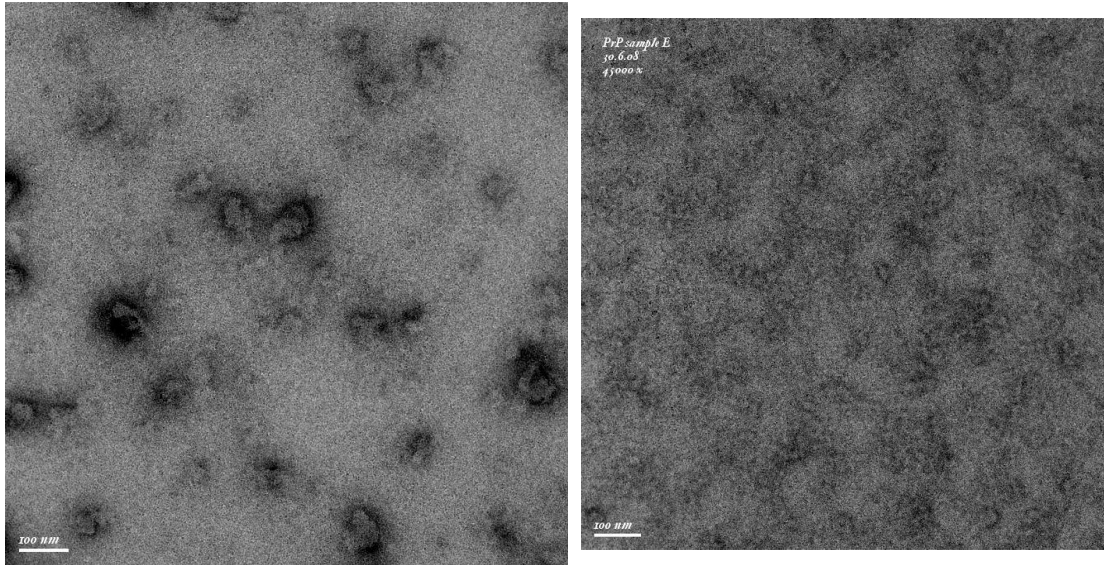


Figure 3.25: The EMgraph is showing a possible presence of high-order oligomers in the sample.

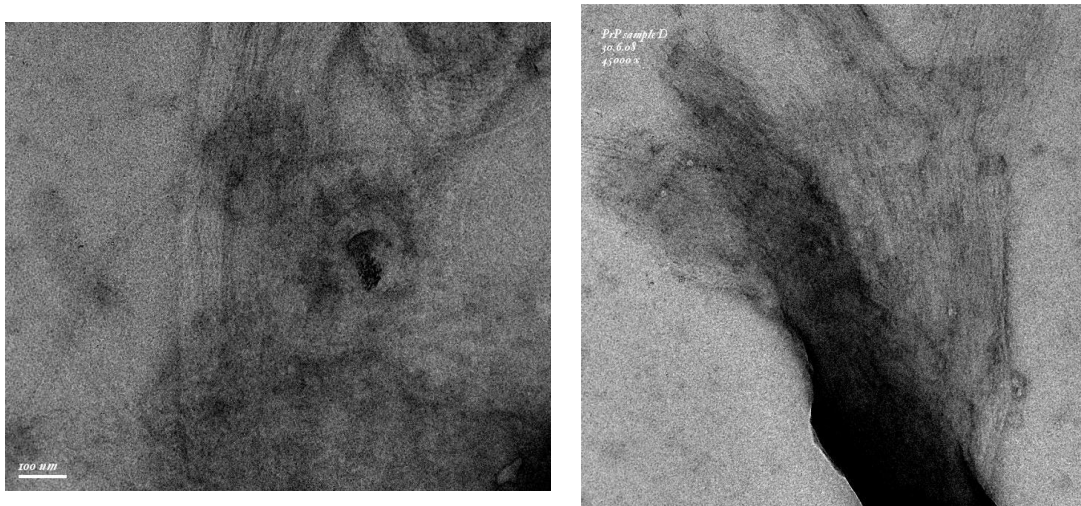


Figure 3.26: These EMgraphs reveal the presence of very-thin fibrils which are bundled together. These images are in accordance with the fibrils morphology observed for unglycosylated mouse prion fibrils (Sim and Caughey, 2009).

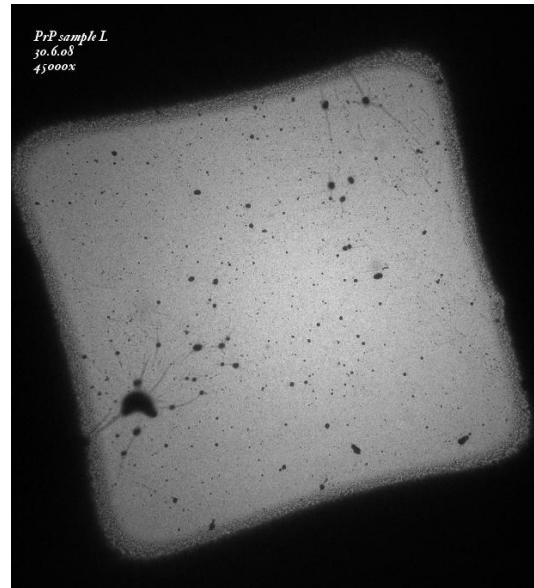


Figure 3.27: The view of EM grid.

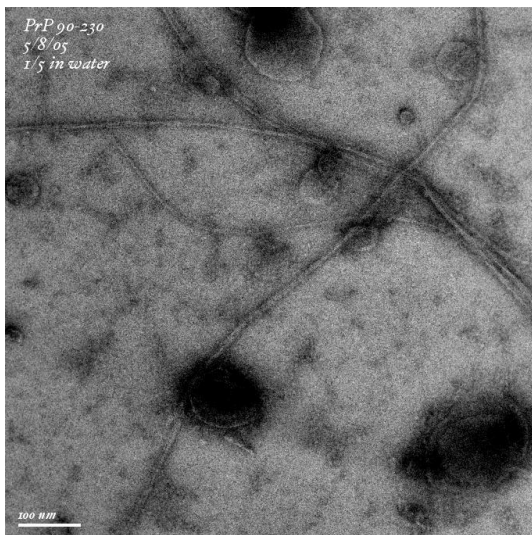


Figure 3.28: The EMgraph for fibrils, which were dialyzed against water, pH2. These are long unbranched straight fibrils

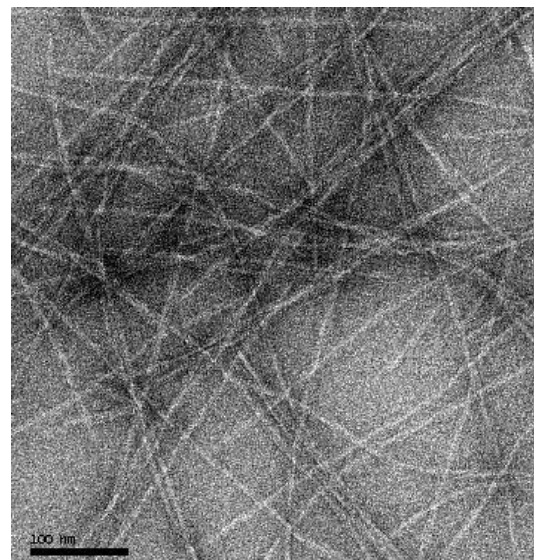


Figure 3.29: The EMgraph for fibrils generated from a synthetic peptide containing residues from 174-184.

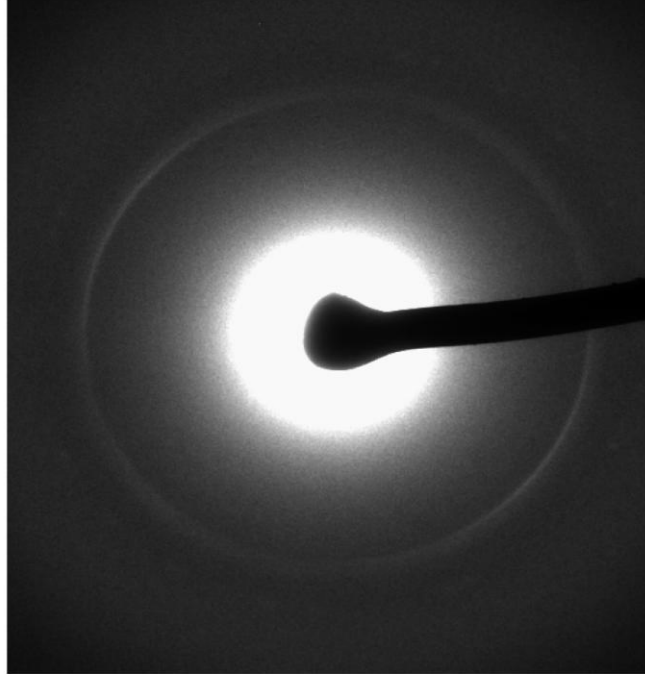


Figure 3.30: The electron diffraction pattern for fibrils formed of hPrP peptide 174-184.

The diffraction data of peptide (174-184) fibril suggest that these fibrils differ from the usual cross- β structure. The β stacks are arranged 4.4 to 4.5 Å apart, which suggest a tilt of 15 to 20 ° in stacking pattern, while regular cross- β sheets are, arranged at 4.7 Å.

Atomic force microscopy: another view of prion polymorphism

The AFM is a powerful technique to provide topological information about the amyloid fibrils. The AFM images usually have height information on left panel and amplitude data on right one. These results help in identifying the existence of multiple morphologies in individual preparations, which explains the complexity of fibril structures, produced from simplistic conditions. The topological studies were done by diluting parent preparations in Tris buffer (40 mM Tris/ Acetic acid pH 7.6, 12.5 mM MgCl₂, 2 mM EDTA) to avoid crowding in AFM images. The images were recorded at the end-point of NMR experiments.

AFM images display broad morphological diversity of fibrils as seen by EM as well; the populations within same preparations vary with respect to their width, height and twisting patterns. The protein seems to cluster and then fibrils are woven out of these clusters. These fibrils are quite long and regular with minor population of small fragmented straight fibrils. A much closer look of these reveals the arrangement of fibrils in bead-like manner, which is an indication of either a base polymerizing unit for fibrils or regular twist in this architecture.

The fibril subtypes included straight or slightly curvy ribbon like fibril, rod-shaped fibrils, and bundles and with beaded nature (Figure 3.31 and 3.32). Most of the time, these amyloids appeared to be clustered together, which make it difficult to identify individual characteristics of fibrils (Figure 3.33). One of the striking facts about

these fibrils was that they were disassembled into smaller oligomers with no or very little fibrils, when urea got crystallized at 4 °C (Figure 3.34). It is most likely urea crystal dissects these fibrils into smaller oligomers as observed with super cooled water, which dissociate mature fibrils (Kim et al., 2008). A few of such preparations also shows dense amorphous aggregate or a low number of fibrils present with oligomers (Figure 3.35).

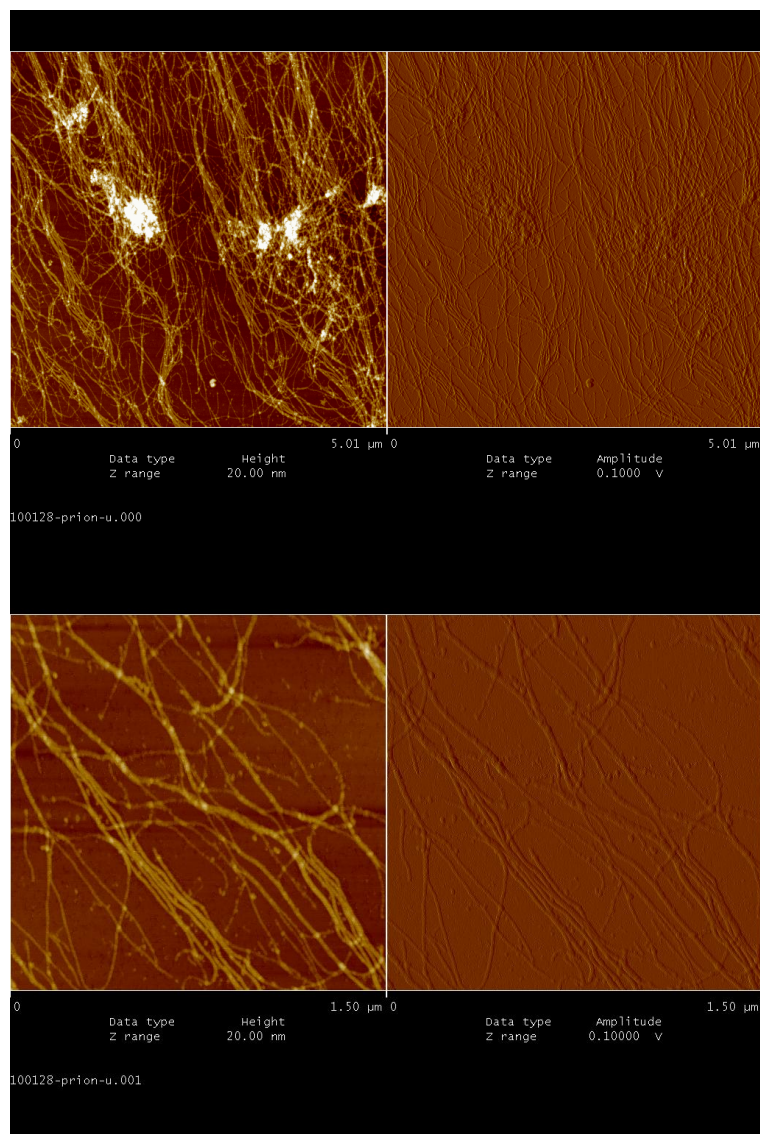


Figure 3.31: The high-resolution AFM images of recombinant human prion

fibrils at two different magnifications (5 μm and 1.5 μm). The left panel shows height data, while amplitude images are shown on right panel. The upper image shows couple of non-fibril aggregates, and fibrils are branching out from there in spun and woven manner. The dense fibrils show variable heights. The detailed view in lower panel shows that most of fibrils are straight but different diameters. A small population of oligomers is also visible.

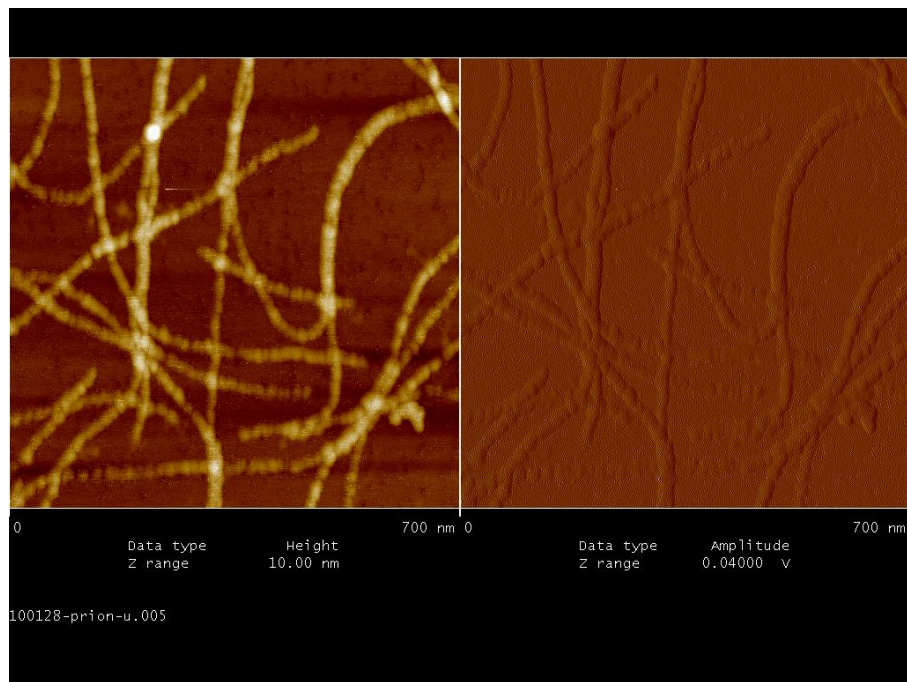


Figure 3.32: The high resolution AFM images of recombinant human prion fibrils at a high magnification (700 nm). The left panel shows height data, while amplitude images are shown on the right panel. The image shows fibrils of variable length but similar height profile. Interestingly, the fibrils are arranged in bead like manner, which probably reflect twist in fibrils.

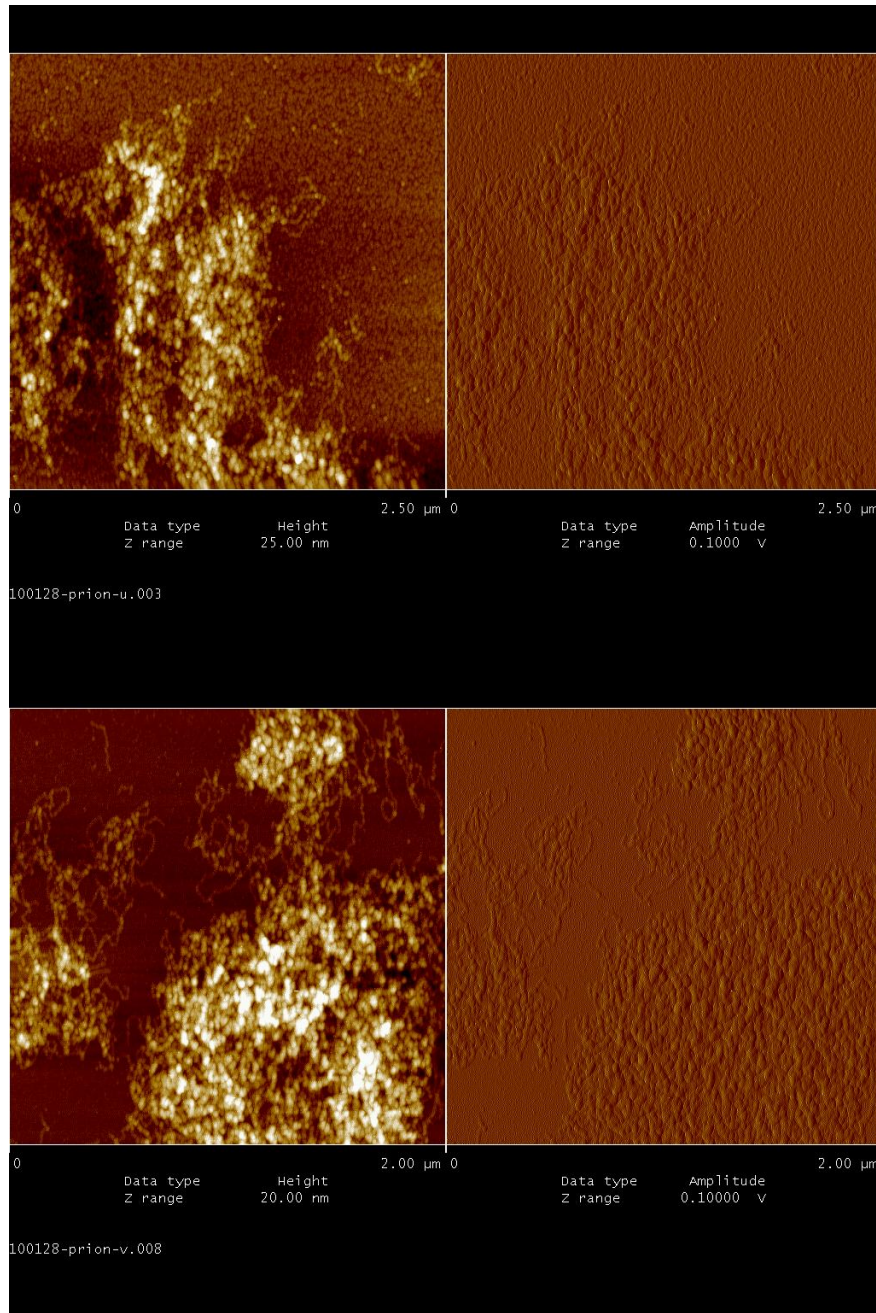


Figure 3.33: The high –resolution AFM images of recombinant human prion aggregates; there are curvy fibril weaving out from those clusters of protein.

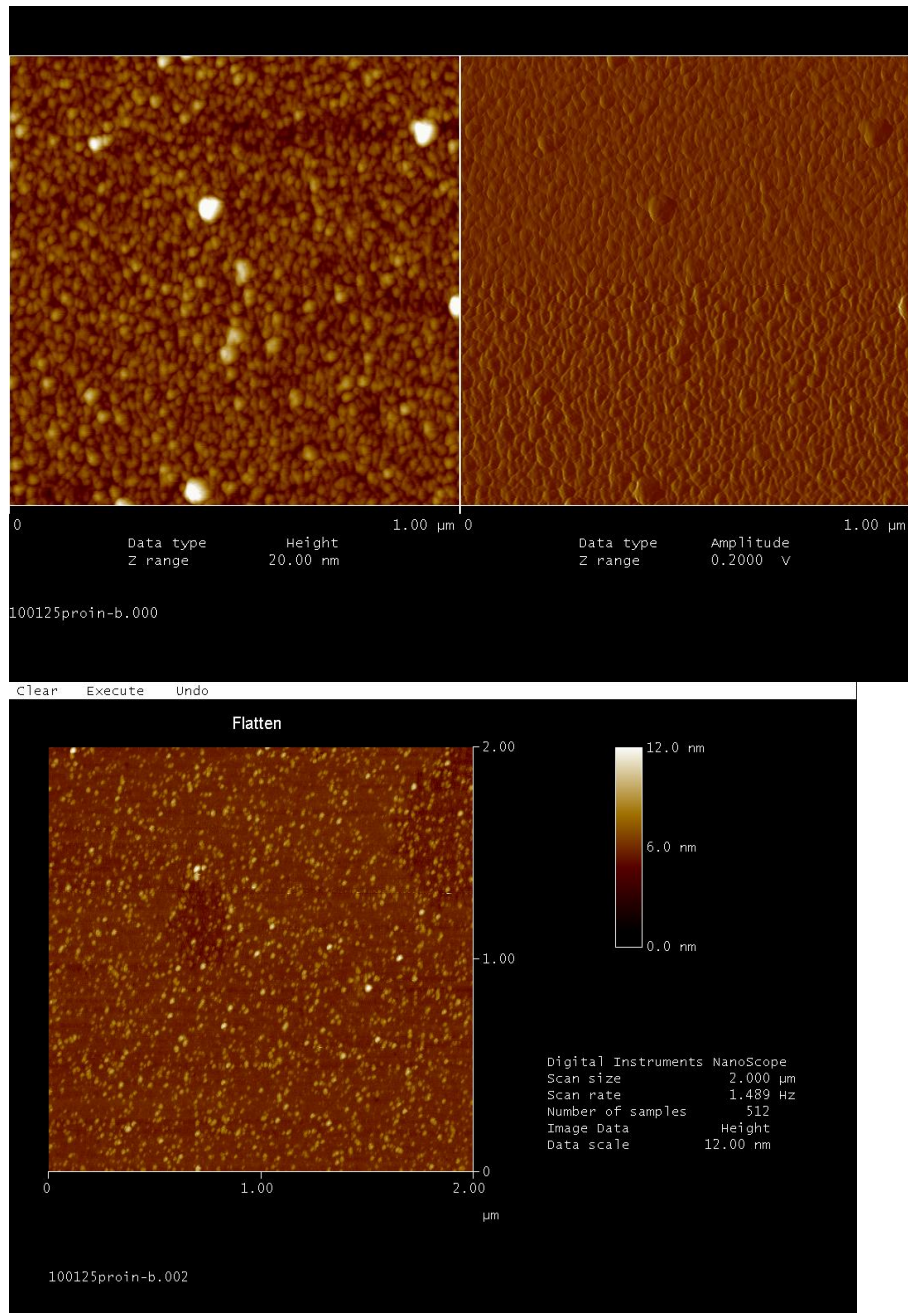


Figure 3.34: The high-resolution AFM images of recombinant human prion aggregates, which were dissected by urea crystal formed at 4 °C, two different dilution of preparations shows presence of large number of oligomeric species.

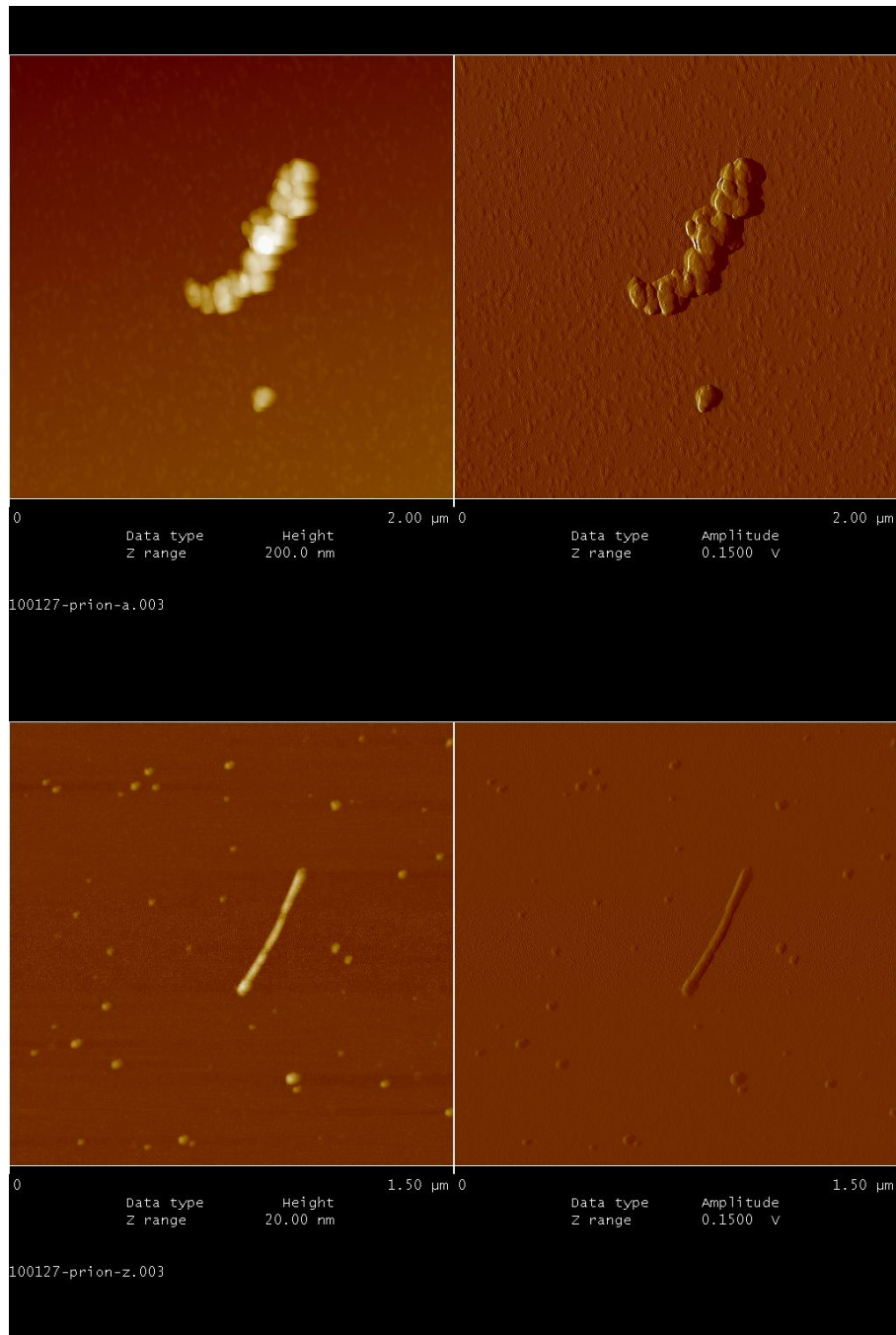


Figure 3.35: The high – resolution AFM images of recombinant human prion aggregates, the upper image shows amorphous aggregate formed, oligomers are visible in high number as well. The lower image shows a single straight fibril with a number of oligomers around.

Solid state NMR of PrP fibrils:

SS-NMR is one of the major techniques available today to understand the structure of solid or semi-solid substances of crystalline/non-crystalline nature. Magic-angle spinning became very relevant to study membrane proteins, macromolecular assemblies and amyloid fibrils (Tycko, 2000, 2003, Siemer et al., 2005, Tycko, 2006b, c, van der Wel et al., 2007, Heise, 2008, Lange et al., 2009, Bayro et al., 2010, Van Melckebeke et al., 2010). The two dimensional solid-state NMR spectroscopy allowing solving structure of these biologically important samples with the very low amount needed. However, there is not much have been achieved on structure of disease-associated fibrils due to inherent nature of amyloid preparations. These preparations are heterogeneous in nature and often irreproducible. A distribution for carbon chemical shifts based on their environment is shown in Figure 3.36.

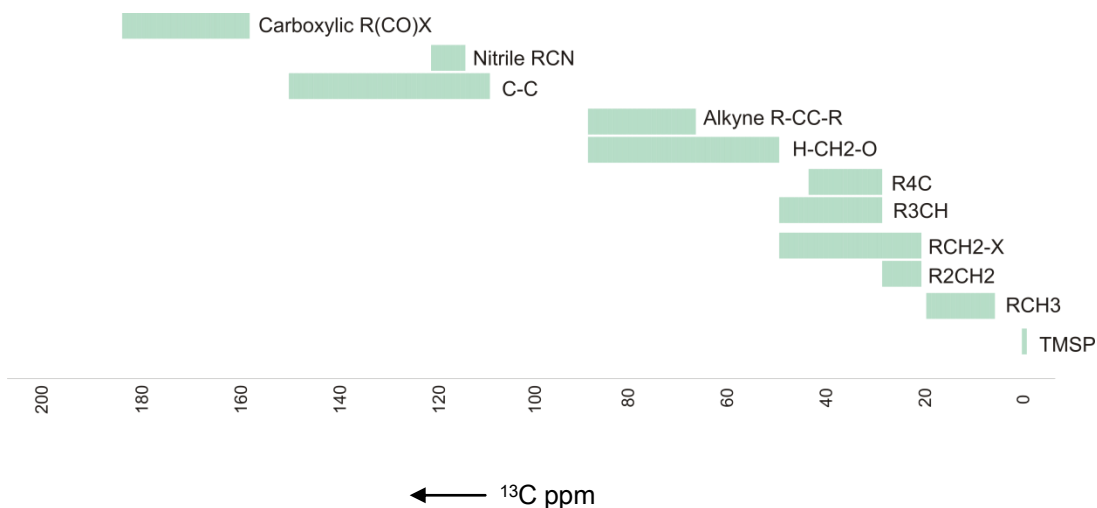


Figure 3.36: The distribution of carbon chemical shift in a typical solid state spectrum.

For our studies, samples were prepared by centrifuging the solution-NMR sample to fit in 4mm MAS-NMR rotor. The solid-state NMR spectra of PrP fibrils show characteristic heterogeneity of prion fibril assemblies. These preparations were not completely rigid and much more appear to have gel-like texture. We have recorded ^{13}C direct polarization and cross-polarization spectra for three of these preparations (Figure 3.37). Cross-polarization spectra shows loss of signals, while direct-polarization spectra display resolved peaks, which indicate that despite gel-like texture, these samples are containing highly mobile regions. Therefore dipole based magnetization transfer is not enough to have cross-polarization in sample.

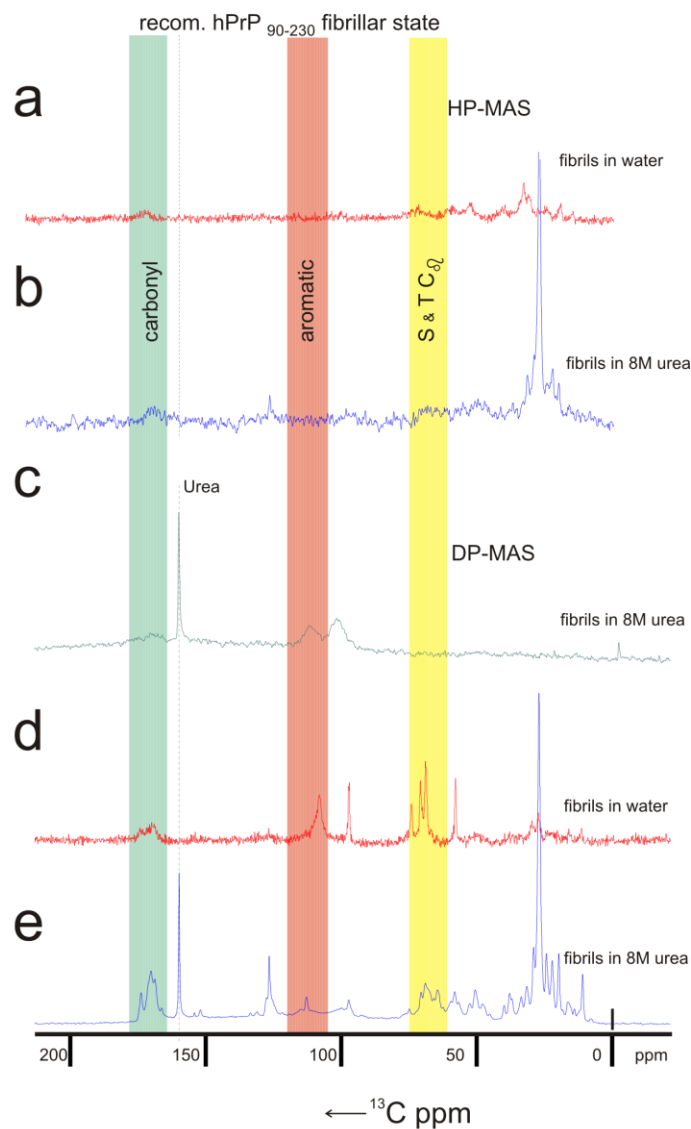


Figure 3.37: The carbon chemical shift for recombinant human prion fibrils, A) and B) HP-MAS spectra of fibrils in water and urea respectively while C) D) and E) are decoupled spectra. The spectra A) and C) are for same sample and display flexible threonine C β and aromatic side chain C atoms, the signals in MAS spectra are weak, indicating flexible nature of fibrils. Spectra A) C) and E) are of fibrils in 8 M urea, displaying highly flexible nature of residues in fibrils.

Hydrogen/Deuterium exchange of fibril core

Due to their size, insolubility, and noncrystalline nature, the structural and dynamic characteristics of amyloid fibrils have been difficult to elucidate using traditional methods such as crystal diffraction. Hydrogen–deuterium exchange (HDX) experiments are based on solvent accessibilities and provide information to characterize the structure and kinetics of proteins. When this method is subjected to amyloids, one can gather information about inaccessible buried residues and relatively more accessible residues, which can be suitable drug targets. The backbone amide protons usually undergo fast exchange with solvent protons, while hydrogen-bonded or buried amide protons show much slower exchange.

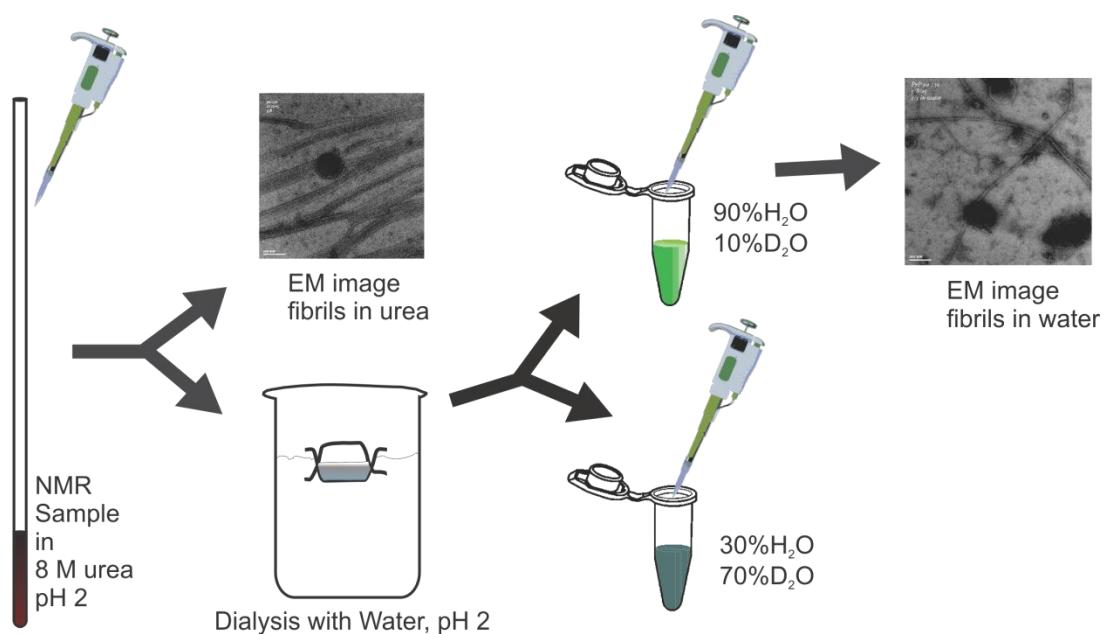


Figure 3.38: The schematic presentation of sample preparation for HDX experiments.

We dialyzed the fibrils, which were formed in 8 M urea, pH 2 against water, pH 2 and then buffer exchanged with 70% D₂O pD 2 (Figure 3.38), to observe deuterium exchange in these already formed fibrils. Presence of fibrils after dialysis and buffer exchange was verified by electron microscopy. In contrast to common understanding of amyloid fibrils being rigid and sterically constraint, recent developments show that these are not completely rigid and continuous reformation of fibrils happens all the time. Therefore, the amyloid fibril assemblies are not static but dynamic structures. The two-dimensional ¹H ¹⁵N HSQCs are used to observe the protection factor of protons. Figure 3.39 shows percentage of protection for fibrils incubated over 6 months in D₂O, bar represents protection for individual residues, while red line shows average over 7 residues. Most of residues show about protection around 40%, while residues 120-123, 144-149, 174-180 and 187-194 shows a low protection and therefore these residues are solvent accessible. The region 187-194 is relatively striking as it shows complete loss of signals. This region is rich in threonine residues HTVTTTTTK and shows high degree of mobility. The relative higher accessibility of these residues was also observed by solid-state spectra, where C_β of threonine residues are seen (Figure 3.37). The fibrils formed from ovine prion protein fragment helix2 and helix3 also display similar behavior for these residues, which makes a rigid helical hairpin structure (Adrover et al., 2010). This piece of information indicates that fibrils undergo structural rearrangement on solvent exchange and the core of amyloid is not entirely rigid and allows residues to adopt conformation according to solvent. These fibrils are made of residues 90-230, which

represents proteinase-K resistant core of naturally occurring prions; therefore the solvent accessibility of residues give relative information about the exposure to solvent, even though they are part of amyloid core.

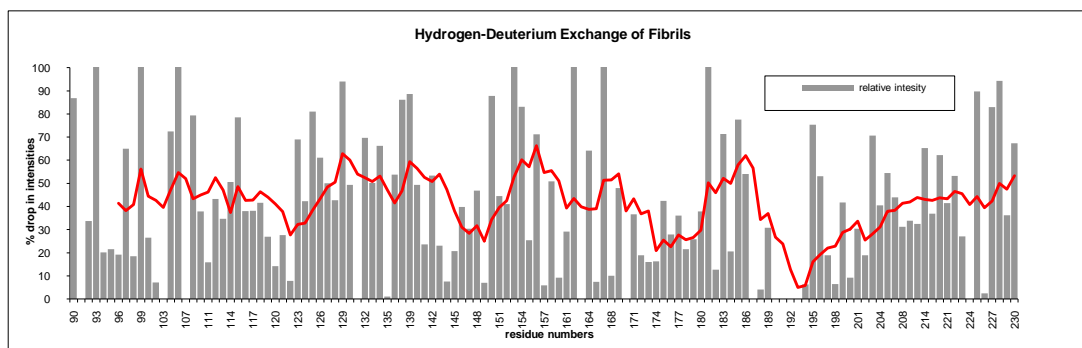


Figure 3.39: Protection plot for deuterium (70%) exchanged fibrils. Most of the residues show about 40% protection. There is a dip around TTTT sequence (189-192) showing that these amide protons are completely exchangeable.

Outlook

		Fibril formation			Finding
		Agitation	Non-agitated		
Recombinant Prion Protein Constructs	Mature Prion Protein	23-230	not studied		
	PK-resistant Core	90-230 90-230 ^{H-tag}	+	+	residues 145-230 form the core, structural polymorphism influence structural determination
	Structured Core	121-230 121-230 ^{H-tag}	not studied	- +	H-tag might influence the fibril formation
	Helix 2 & 3	166-230	amorphous aggregate		sticky rapid aggregation
	Short Peptide	174-184	not studied	++	~20° tilted fibrils ~4.5Å apart

Figure 4.1: outline of various fibrillation studies performed with unfolded recombinant prion protein constructs.

The prion proteins have been studied widely in the last two decades, despite the advancement in our understanding of prion protein, there are a few key questions remain unanswered. One of these crucial questions is *structural characterization of the soluble PrP oligomers and insoluble PrP^{Sc} fibrils*. The complete structural characterization of the soluble oligomeric intermediates is very unlikely and difficult because these intermediate are typically having short lives and display a wide range of conformational landscape and degrees of aggregation. In our studies

we used recombinant prion protein constructs (90-230, 121-230, 174-184 and 166-230) in the highly denaturing environment (Figure 4.1). The longer construct forms fibril in non-agitated and agitated conditions, the core of the amyloid was identified starting from 145 to 223 residues. The 121-230 construct does not form fibrils in non-agitated conditions when purified under oxidized environment while it forms fibril when construct retains 7 x His-tag, and purified in presence of 5mM DTT. The 166-230 construct form aggregates faster under these conditions; these aggregates contain irresolvable mass, when subjected to EM. The short polypeptide segment 174-184 forms fibrils almost instantaneously, the diffraction data shows that these fibrils are different from known fibrils characteristics; they are $\sim 4.5\text{\AA}$ rather than usual 4.7\AA , which indicate that fibrillar β sheets are tilted at the angle of 20° .

The Association prone monomers can lead multiple pathways and therefore end up in formation of either amorphous aggregates, annular or globular oligomers or a number of morphologically different fibrils (Figure 4.2). The complexity of fibril conformations is another interesting and intriguing phenomenon associated with prions; it termed as “prion strains”. These strains were originally characterized by incubation time and the neuropathology observed in the host. The transgenic mice, which are homozygous for the PrP gene (Prnp) allowed to propagated most of the strains indefinitely and provided a laboratory model for studies. The protein-only hypothesis assumes that each strain is associated with different conformer of PrP^{Sc}, which indicate the presence of multiple stable conformations. The mouse model allows propagating about 15 different strains; therefore, we should have approximately 15 different conformations for PrP^{Sc}. The cell-free conversion experiments allowed auto-catalytic replication of PrP to PrP^{Sc}-like conformations. These experiments supported the template assisted model of prion propagation,

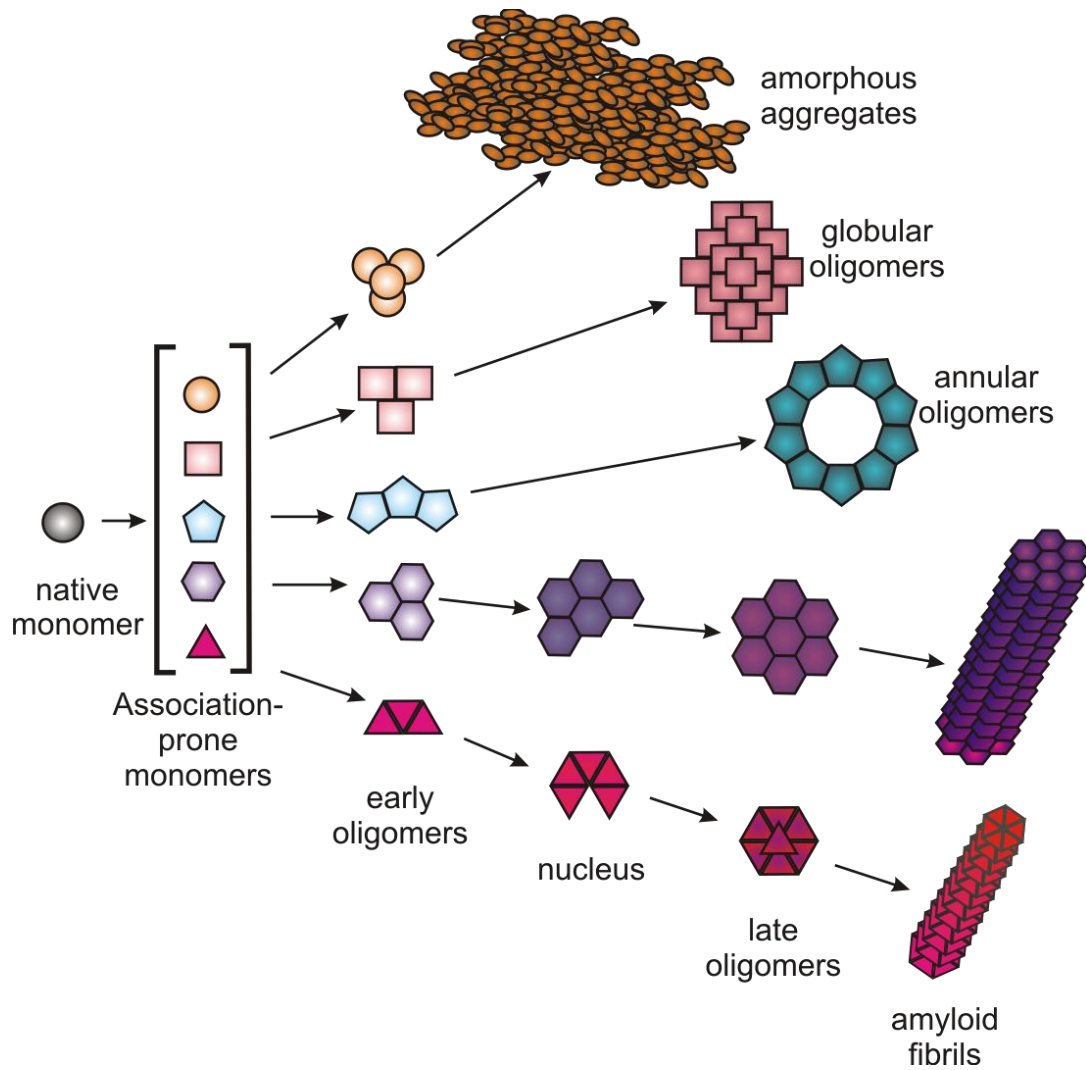


Figure 4.2: Paths of molecular assemblies in a cell, a native monomer adopt to association prone monomer conformations in the suitable environments, these monomers then assemble into early oligomers with variable lag time in the formation of oligomers, and finally lead to end product like amorphous aggregates, globular oligomers, annular oligomers or to amyloids through the formation of nucleus.

which got extended by development of protein misfolding cyclic amplification assay (Soto et al., 2002a). These allowed mimicking PrP^{Sc} like conformations, *in vitro*. The *in-vitro* preparation of fibrils from recombinant prion protein is inherently heterogeneous, which reflects the characteristic nature of prions. However, it makes difficult for routine structural investigations using NMR or crystallography. An isolated single strain would probably allow gaining insight to conformational switching on fibril formation.

The unfolded state of protein represents minimal constrained structure and therefore, our observation of fibril formation in denaturing environment is significantly important. It shows that fibrils can be formed from the extended unfolded state of prion protein. Therefore, our data fill the empty space of information about fibril formation from unfolded state. From initial unfolded extended conformations, these monomers adapt association-prone structures. This lead to oligomerization and the end product of these associations can be amorphous aggregates, globular oligomers, annular oligomers or amyloid fibrils. These amyloid fibrils usually adopt more than one conformation in same preparation, and the observations are done on a pool of strains, than a single isolated amyloid strain. Most of the studies of fibril-kinetics are performed using dyes congo red (Khurana et al., 2001), thioflavin-T (Khurana et al., 2005) or thioflavin-S; however, accuracy of these dyes were always questioned. Recent studies clearly demonstrated that existence of non thioflavin-T binding fibrils for mouse prion strains (Colby et al., 2009), while others have shown significantly different lag time for same recombinant protein in identical conditions (Krebs et al., 2005). These definitely question the use of thioflavin-T as the right candidate to understand the dynamics of fibril formation. Here we present that real time analysis using the NMR

spectroscopy offer the best method for kinetic observations; which does not reflect variability due to different binding mode of dye.

The PrP 27-30 which represents the amyloid core of naturally occurring prions, starts either from 89/90 or 111/112 residue in amino acid sequence and therefore, the residues from 90 to 124 plays a crucial role, although they are unstructured in a native-like environment. PrP^{Sc} models, which were calculated based on electron microscopic images varies in secondary structural details while the experimental data from HDX, MALDI (Cobb et al., 2007, Lu et al., 2007), EPR (Cobb et al., 2008) and our NMR studies agree on the common core region. The solvent inaccessible or rigid core is identified from residue 145 to 223, while last seven residues at C-terminus show the conformational transition on fibril formation.

The new evidence suggested Darwinian evolution of prion strains, suggesting that strains adopt conformations with environment variation and develop drug resistance(Figure 4.3) (Li et al., 2010). The improved energy landscape for prion amyloidal formation will represent the view that sub-strains are distinguishable collectives of prions that can interconvert reproducibly and relatively readily because they are separated by relatively low activation energy barriers. The new scheme also implies that the properties of a strain vary depending on the environment in which it replicates, because the proportions of the component substrains may change to favor the one replicating most rapidly.

Conformational diversity of amyloid fibrils (strains and sub-strains)

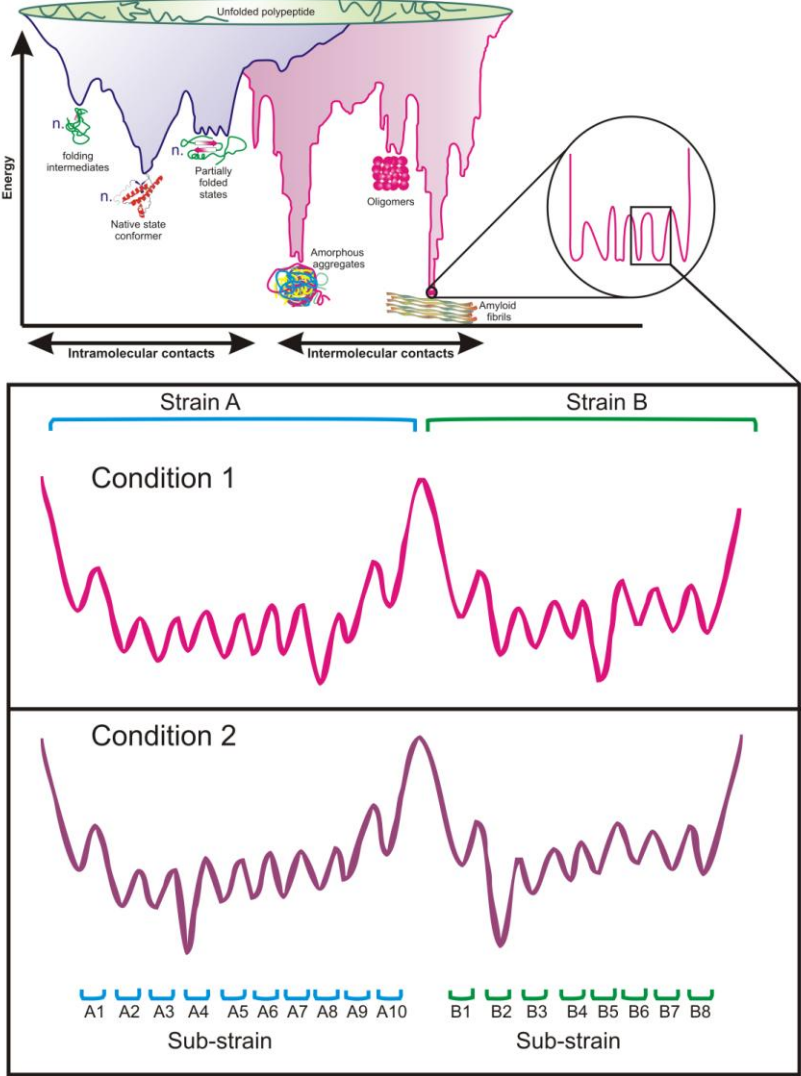


Figure 4.3: With new knowledge about strains and substrains, the energy landscape of amyloid formation should be broadened to include substrain phenomena of amyloid, which is largely depending upon the local environment.

The prion protein has a highly conserved native structure, which may be the central to the abilities of prions to transfer infection across species. Initially, these differences in primary structure have been thought to support the concept of a barrier to cross-species infection, but now it has been demonstrated that the "strain-ness" of a prion is fundamental to its ability to infect a new species. Therefore, two prion strains, which propagate in one species, carry the abilities to cross a transmission barrier. In the context with this knowledge "conformational selection model" (Collinge, 1999) have been proposed, which state that the possible PrP^{Sc} strains that can overcome natural clearance and propagate effectively in mammals, only a subset is compatible with a given host PrP^C structure, and can thereby propagate in that host. With this new piece of information about the prion transmission, the species barriers can be explained by the degree of overlap between strain types that are permissible in the two species concerned. However, it is possible that these prions do not maintain their identity when propagate in a new host but switch structural properties, causing strain "mutation" on crossing between species, or intraspecies transmission due to PrP polymorphism or the effect of genetic background. The pathogenicity of new strain may be different from its progenitor, and may be more toxic. Therefore, these strain mutations has potential public and animal health implications. One of the interesting findings about prions is that shows conformational adaptability (Bartz et al., 2000, Jones and Surewicz, 2005, Surewicz et al., 2006, Meyerett et al., 2008, Cobb and Surewicz, 2009, Colby et al., 2009, Angers et al., 2010), when environment or host is changed. It was astonishing that fibrils formed in 8 M Urea pH 2, could demonstrate this conformational switching when fibrils were transferred from highly viscous urea solution to water, pH 2 by dialysis. The EMgraph confirms the presence of long well ordered fibrils and the ¹H ¹⁵N HSQC spectrum of fibrils in water pH 2 shows

very similar distribution and dispersion of residues. However, HDX experiments show that TTTT sequence (189-192) becomes solvent accessible on this transition demonstrating the strain adaptation and mutation, when the local environment is changed. The high-resolution NMR spectroscopy is the method of choice to investigate the prion kinetics as it can differentiate among different prion strains, as they will exhibit different NMR spectra, due to change in their architecture. The changes can be followed in a time-dependent manner, though may require dedicated NMR time, due to large variability in incubation time.

Appendix

Chemical shift values for recombinant prion protein⁹⁰⁻²³⁰

Residue	Ca	Cb	C'	N	HN	Ha
G 90	44.99		173.99	110.94	8.531	
Q 91	55.89	29.19	176.39	119.74	8.291	
G 92	44.99		174.39	110.14	8.491	
G 93	44.99		174.49	108.64	8.301	
G 94	45.09		174.19	108.74	8.311	
T 95	61.99	69.79	174.49	113.24	8.141	
H 96	54.99	28.49	174.19	120.64	8.611	
S 97	58.49	63.89	174.29	117.34	8.381	
Q 98	56.19	29.09	175.39	122.34	8.511	
W 99	56.99	29.19	175.69	121.94	8.161	
N 100	52.79	38.79	175.89	120.74	8.251	
K 101	52.79	37.99		119.64	8.481	
P 102	62.59	31.79	176.69			
S 103	58.19	63.99	173.99	117.04	8.451	4.461
K 104	54.29	32.59		124.04	8.381	4.341
P 105	62.69	31.59	176.29			
K 106	60.69	37.89	175.79	122.14	8.281	4.331
T 107	61.99	69.59	173.89	118.14	8.151	4.291
N 108	52.89	38.59	174.89	121.44	8.571	4.761
M 109	54.29	32.29	175.89	122.64	8.101	4.481
K 110	56.09	32.79	176.19	122.74	8.391	4.421
H 111	54.99	28.49	174.19	120.34	8.651	4.721
M 112	55.09	32.89	175.49	123.14	8.541	4.521
A 113	52.59	18.99	177.79	126.04	8.481	4.371
G 114	44.79		173.49	108.54	8.361	3.821
A 115	52.49	19.19	177.39	123.74	8.141	4.321
A 116	52.39	18.79	177.39	123.34	8.291	4.321
A 117	52.39	18.79	177.29	123.44	8.201	4.311
A 118	52.49	18.89	177.99	123.34	8.221	4.291
G 119	44.79		173.39	108.04	8.261	3.821
A 120	52.39	19.19	177.49	123.54	8.041	4.361
V 121	62.29	32.39	176.09	120.04	8.161	4.141
V 122	62.29	32.59	176.39	124.94	8.281	4.141
G 123	44.89		174.19	113.04	8.471	
G 124	44.99		173.99	108.44	8.211	
L 125	55.39	42.19	177.79	121.54	8.261	4.381
G 126	45.09		174.29	109.44	8.441	4.201
G 127	44.99		173.59	108.44	8.171	
Y 128	57.69	38.49	175.49	120.14	8.051	4.571

M	129	55.49	32.59	175.69	122.34	8.331	4.381
L	130	55.29	42.19	177.59	123.64	8.221	4.531
G	131	44.99		173.89	109.94	8.411	3.801
S	132	58.09	63.99	174.39	115.44	8.181	4.421
A	133	52.69	18.69	174.69	125.94	8.421	4.361
M	134	55.49	32.79	176.09	118.94	8.251	4.471
S	135	58.19	63.89	173.79	117.14	8.231	4.451
R	136	54.19	30.09		123.64	8.341	4.411
P	137			174.69			
I	138	60.89	38.29	175.79	121.94	8.251	4.411
I	139	60.29	38.49	175.39	126.14	8.201	4.071
H	140	54.59	28.79	173.69	123.44	8.541	4.731
P	141	57.79	39.59	176.79	122.94	8.451	4.661
G	142	44.79		173.89	110.54	8.481	
S	143	58.49	63.89	174.29	115.44	8.261	4.441
D	144	52.89	37.69	174.79	120.74	8.551	4.731
Y	145	58.59	38.19	175.59	120.84	8.091	4.451
E	146	55.79	28.29	175.79	120.94	8.111	4.481
D	147	52.69	37.89	174.89	119.74	8.471	4.671
R	148	56.29	30.29	175.49	121.34	8.161	4.281
Y	149	57.69	38.39	175.29	120.34	8.031	4.741
Y	150	57.79	38.69	175.49	122.14	8.021	4.341
R	151	56.09	30.29	175.19	120.24	8.031	4.481
E	152	55.89	28.49	175.49	121.44	8.291	4.711
N	153	58.29	27.59	174.99	121.34	8.491	4.731
M	154	55.59	32.39	175.49	121.04	8.311	4.311
H	155	52.89	38.29	174.99	120.14	8.511	4.711
R	156	55.89	30.89	175.99	122.84	8.301	4.441
Y	157	55.59	32.59		122.04	8.441	4.341
P	158	63.49	31.79	176.29			
N	159	53.19	38.49	175.59	118.54	8.461	4.701
Q	160	55.99	29.19	175.19	120.64	8.261	4.681
V	161	62.09	32.49	175.19	121.74	8.131	4.031
Y	162	57.49	39.09	174.89	124.24	8.231	4.291
Y	163	57.59	38.99	174.59	123.64	8.181	4.291
R	164	53.59	30.29	175.39	124.94	8.241	4.511
P	165						
M	166			175.39			
D	167	52.89	37.69	175.39	119.54	8.271	4.681
E	168	60.99	38.59	175.59	121.64	8.161	4.241
Y	169	57.59	38.59	175.59	120.44	8.131	4.591
S	170	57.89	63.99	173.99	116.84	8.191	4.411
N	171	52.99	38.19	175.09	121.14	8.461	4.731
Q	172	57.59	28.89	175.29	120.24	8.091	4.531
N	173	53.19	38.59	174.59	119.14	8.391	4.641
N	174	55.29	0	176.09	118.84	8.241	4.471

F	175						
V	176	62.29	32.49	175.59	121.54	8.021	4.481
H	177	54.99	28.59	173.59	122.34	8.581	4.761
D	178	52.89	37.99	174.49	121.14	8.601	4.751
C	179	58.59	27.79	174.09	120.44	8.461	4.731
V	180	61.99	28.29	175.29	122.14	8.201	4.711
N	181	52.89	38.59	175.49	122.84	8.491	4.631
I	182	56.19	38.29	175.99	121.14	8.171	4.261
T	183	61.89	69.59	174.19	119.04	8.301	4.351
I	184	61.99	38.49	175.79	124.44	8.201	4.581
K	185	56.09	32.79	175.59	126.34	8.431	4.331
Q	186	55.89	32.59	173.99	122.34	8.351	4.371
H	187			174.19	120.44	8.741	4.741
T	188			174.09	117.34	8.381	4.381
V	189	62.19	32.79	175.99	123.04	8.401	4.281
T	190	61.89	69.79	174.49	118.74	8.371	4.501
T	191	61.79	69.69	174.39	116.44	8.221	4.351
T	192	61.49	69.89	174.39	116.14	8.261	4.501
T	193	61.59	69.89	174.39	116.74	8.281	4.471
K	194	56.49	32.69	176.69	124.04	8.381	4.341
G	195	44.79		173.69	110.24	8.411	
E	196	55.79	28.59	175.29	119.54	8.171	4.341
N	197	52.89	38.39	174.69	119.94	8.471	4.711
F	198	57.69	39.19	175.69	121.24	8.261	4.701
T	199	61.89	69.89	174.19	115.84	8.151	4.351
E	200	55.89	28.49	176.49	122.64	8.341	4.411
T	201	62.09	69.69	173.89	114.94	8.191	4.331
D	202	52.89	37.99	174.79	121.24	8.461	4.761
V	203	62.49	32.39	175.89	120.84	8.041	4.571
K	204			176.39	124.94	8.321	4.111
M	205			174.89	122.04	8.361	4.341
M	206	55.69	32.69	175.89	121.44	8.371	4.431
E	207	55.89	29.39	175.79	122.24	8.471	
R	208			175.89	125.04	8.291	4.511
V	209	62.09	32.59	170.79	122.74	8.281	
V	210	62.29	32.39	175.89	122.04	8.661	
E	211						
Q	212	55.59	28.49	176.39	124.74	8.451	
M	213	53.29	38.39	174.89	118.44	8.461	4.651
C	214	55.99	28.99	175.49	120.24	8.321	4.371
I	215			176.69	120.64	8.301	4.671
T	216	61.49	69.99	176.59	115.24	8.211	4.381
Q	217	56.29	32.59	175.39	122.34	8.531	4.341
Y	218	55.89	37.89	173.99	122.24	8.411	4.361
E	219						
R	220	55.79	28.29	176.29	121.84	8.201	4.231

E	221	55.69	28.59	175.89	121.24	8.381	4.431
S	222	58.39	63.79	174.39	116.94	8.331	4.431
Q	223	55.89	28.89	175.49	121.84	8.381	4.421
A	224	52.69	18.79	177.19	124.44	8.201	4.301
Y	225	57.99	38.59	175.29	119.44	8.021	4.411
Y	226	57.79	38.59	175.09	121.64	7.941	4.511
Q	227	55.59	29.19	175.59	122.54	8.201	4.321
R	228	55.89	30.59	176.59	123.04	8.431	4.291
G	229	44.79		173.49	110.44	8.451	
S	230	57.59	63.89	176.39	116.14	8.221	4.531

LiteratureLiterature

- Abrahamson M, Jonsdottir S, Olafsson I, Jensson O, Grubb A (Hereditary cystatin C amyloid angiopathy: identification of the disease-causing mutation and specific diagnosis by polymerase chain reaction based analysis. *Hum Genet* 89:377-380.1992).
- Adrover M, Pauwels K, Prigent S, de Chiara C, Xu Z, Chapuis C, Pastore A, Rezaei H (Prion Fibrillization Is Mediated by a Native Structural Element That Comprises Helices H2 and H3. *Journal of Biological Chemistry* 285:21004-21012.2010).
- Aguzzi A (Understanding the diversity of prions. *Nat Cell Biol* 6:290-292.2004).
- Alper T, Cramp WA, Haig DA, Clarke MC (Does the agent of scrapie replicate without nucleic acid? *Nature* 214:764-766.1967).
- Anderson M, Bocharova OV, Makarava N, Breydo L, Salnikov VV, Baskakov IV (Polymorphism and ultrastructural organization of prion protein amyloid fibrils: an insight from high resolution atomic force microscopy. *J Mol Biol* 358:580-596.2006).
- Anfinsen CB (Principles that govern the folding of protein chains. *Science* 181:223-230.1973).
- Angers RC, Kang H-E, Napier D, Browning S, Seward T, Mathiason C, Balachandran A, McKenzie D, Castilla J, Soto C, Jewell J, Graham C, Hoover EA, Telling GC (Prion Strain Mutation Determined by Prion Protein Conformational Compatibility and Primary Structure. *Science* 328:1154-1158.2010).
- Apetri AC, Surewicz K, Surewicz WK (The effect of disease-associated mutations on the folding pathway of human prion protein. *J Biol Chem* 279:18008-18014.2004).
- Apetri AC, Surewicz WK (Kinetic intermediate in the folding of human prion protein. *J Biol Chem* 277:44589-44592.2002).
- Apetri AC, Vanik DL, Surewicz WK (Polymorphism at residue 129 modulates the conformational conversion of the D178N variant of human prion protein 90-231. *Biochemistry* 44:15880-15888.2005).
- Atarashi R, Moore RA, Sim VL, Hughson AG, Dorward DW, Onwubiko HA, Priola SA, Caughey B (Ultrasensitive detection of scrapie prion protein using seeded conversion of recombinant prion protein. *Nat Methods* 4:645-650.2007).

- Baldwin AJ, Anthony-Cahill SJ, Knowles TP, Lippens G, Christodoulou J, Barker PD, Dobson CM (Measurement of amyloid fibril length distributions by inclusion of rotational motion in solution NMR diffusion measurements. *Angew Chem Int Ed Engl* 47:3385-3387.2008).
- Barry RA, Prusiner SB (Monoclonal antibodies to the cellular and scrapie prion proteins. *Journal of Infectious Diseases* 154:518-521.1986).
- Bartz JC, Bessen RA, McKenzie D, Marsh RF, Aiken JM (Adaptation and Selection of Prion Protein Strain Conformations following Interspecies Transmission of Transmissible Mink Encephalopathy. *J Virol* 74:5542-5547.2000).
- Baskakov IV (Autocatalytic conversion of recombinant prion proteins displays a species barrier. *J Biol Chem* 279:7671-7677.2004).
- Baskakov IV, Legname G, Baldwin MA, Prusiner SB, Cohen FE (Pathway complexity of prion protein assembly into amyloid. *J Biol Chem* 277:21140-21148.2002).
- Basler K, Oesch B, Scott M, Westaway D, Walchli M, Groth DF, McKinley MP, Prusiner SB, Weissmann C (Scrapie and cellular PrP isoforms are encoded by the same chromosomal gene. *Cell* 46:417-428.1986).
- Bayro MJ, Maly T, Birkett NR, Macphee CE, Dobson CM, Griffin RG (High-resolution MAS NMR analysis of PI3-SH3 amyloid fibrils: backbone conformation and implications for protofilament assembly and structure. *Biochemistry* 49:7474-7484.2010).
- Becker LE (Slow infections of the central nervous system. *Canadian Journal of Neurological Sciences* 4:81-88.1977).
- Berjanskii MV, Wishart DS (A simple method to predict protein flexibility using secondary chemical shifts. *Journal of the American Chemical Society* 127:14970-14971.2005).
- Bessen RA, Marsh RF (Biochemical and physical properties of the prion protein from two strains of the transmissible mink encephalopathy agent. *J Virol* 66:2096-2101.1992).
- Bessen RA, Marsh RF (Distinct PrP properties suggest the molecular basis of strain variation in transmissible mink encephalopathy. *J Virol* 68:7859-7868.1994).
- Bocharova OV, Breydo L, Parfenov AS, Salnikov VV, Baskakov IV (In vitro conversion of full-length mammalian prion protein produces amyloid form with physical properties of PrP(Sc). *J Mol Biol* 346:645-659.2005).
- Bolton DC, McKinley MP, Prusiner SB (Identification of a protein that purifies with the scrapie prion. *Science* 218:1309-1311.1982).
- Brockwell DJ, Radford SE (Intermediates: ubiquitous species on folding energy landscapes? *Curr Opin Struc Biol* 17:30-37.2007).
- Brown DR, Qin K, Herms JW, Madlung A, Manson J, Strome R, Fraser PE, Kruck T, von Bohlen A, Schulz-Schaeffer W, Giese A, Westaway D, Kretzschmar

- H (The cellular prion protein binds copper in vivo. *Nature* 390:684-687.1997).
- Brown P, Will RG, Bradley R, Asher DM, Detwiler L (Bovine spongiform encephalopathy and variant Creutzfeldt-Jakob disease: Background, evolution, and current concerns. *Emerging Infectious Diseases* 7:6-16.2001).
- Bruce ME, Fraser H (Scrapie strain variation and its implications. *Curr Top Microbiol Immunol* 172:125-138.1991).
- Bruce ME, Will RG, Ironside JW, McConnell I, Drummond D, Suttie A, McCardle L, Chree A, Hope J, Birkett C, Cousens S, Fraser H, Bostock CJ (Transmissions to mice indicate that 'new variant' CJD is caused by the BSE agent. *Nature* 389:498-501.1997).
- Bueler H, Fischer M, Lang Y, Bluethmann H, Lipp HP, DeArmond SJ, Prusiner SB, Aguet M, Weissmann C (Normal development and behaviour of mice lacking the neuronal cell-surface PrP protein. *Nature* 356:577-582.1992).
- Castilla J, Gutierrez Adan A, Brun A, Pintado B, Ramirez MA, Parra B, Doyle D, Rogers M, Salguero FJ, Sanchez C, Sanchez-Vizcaino JM, Torres JM (Early detection of PrPres in BSE-infected bovine PrP transgenic mice. *Arch Virol* 148:677-691.2003).
- Castilla J, Saa P, Hetz C, Soto C (In vitro generation of infectious scrapie prions. *Cell* 121:195-206.2005).
- Caughey B (In vitro expression and biosynthesis of prion protein. *Curr Top Microbiol Immunol* 172:93-107.1991).
- Caughey B, Chesebro B (Transmissible spongiform encephalopathies and prion protein interconversions. *Adv Virus Res* 56:277-311.2001).
- Caughey B, Race RE, Ernst D, Buchmeier MJ, Chesebro B (Prion protein biosynthesis in scrapie-infected and uninfected neuroblastoma cells. *J Virol* 63:175-181.1989).
- Chandler RL (ENCEPHALOPATHY IN MICE PRODUCED BY INOCULATION WITH SCRAPIE BRAIN MATERIAL. *The Lancet* 277:1378-1379.1961).
- Chandler RL (ENCEPHALOPATHY IN MICE. *The Lancet* 279:107-108.1962).
- Chernoff YO, Uptain SM, Lindquist SL (Analysis of prion factors in yeast. *Methods Enzymol* 351:499-538.2002).
- Chesebro B (BSE and prions: uncertainties about the agent. *Science* 279:42-43.1998).
- Chien P, Weissman JS, DePace AH (Emerging principles of conformation-based prion inheritance. *Annu Rev Biochem* 73:617-656.2004).
- Cobb NJ, Apetri AC, Surewicz WK (Prion Protein Amyloid Formation under Native-like Conditions Involves Refolding of the C-terminal {alpha}-Helical Domain. *J Biol Chem* 283:34704-34711.2008).

- Cobb NJ, Sonnichsen FD, McHaourab H, Surewicz WK (Molecular architecture of human prion protein amyloid: a parallel, in-register beta-structure. *Proc Natl Acad Sci U S A* 104:18946-18951.2007).
- Cobb NJ, Surewicz WK (Prion Diseases and Their Biochemical Mechanisms†. *Biochemistry* 48:2574-2585.2009).
- Cohen AS, Calkins E (Electron microscopic observations on a fibrous component in amyloid of diverse origins. *Nature* 183:1202-1203.1959).
- Cohen FE, Pan KM, Huang Z, Baldwin M, Fletterick RJ, Prusiner SB (Structural clues to prion replication. *Science* 264:530-531.1994).
- Colby DW, Giles K, Legname G, Wille H, Baskakov IV, DeArmond SJ, Prusiner SB (Design and construction of diverse mammalian prion strains. *Proc Natl Acad Sci U S A* 106:20417-20422.2009).
- Collinge J (Variant Creutzfeldt-Jakob disease. *Lancet* 354:317-323.1999).
- Collinge J (Prion diseases of humans and animals: their causes and molecular basis. *Annu Rev Neurosci* 24:519-550.2001).
- Couzin J (Biomedicine. An end to the prion debate? Don't count on it. *Science* 305:589.2004).
- Crick F (Central dogma of molecular biology. *Nature* 227:561-563.1970).
- Deleault NR, Harris BT, Rees JR, Supattapone S (Formation of native prions from minimal components in vitro. *Proc Natl Acad Sci U S A* 104:9741-9746.2007).
- DeMarco ML, Daggett V (From conversion to aggregation: protofibril formation of the prion protein. *Proc Natl Acad Sci U S A* 101:2293-2298.2004).
- Detwiler LA (Scrapie. *Rev Sci Tech* 11:491-537.1992).
- Dill KA, Chan HS (From Levinthal to pathways to funnels. *Nat Struct Biol* 4:10-19.1997).
- Dobson CM (Protein folding and its links with human disease. *Biochem Soc Symp* 1-26.2001).
- Dobson CM (Protein folding and misfolding. *Nature* 426:884-890.2003).
- Donne DG, Viles JH, Groth D, Mehlhorn I, James TL, Cohen FE, Prusiner SB, Wright PE, Dyson HJ (Structure of the recombinant full-length hamster prion protein PrP(29-231): the N terminus is highly flexible. *Proc Natl Acad Sci U S A* 94:13452-13457.1997).
- Eanes ED, Glenner GG (X-ray diffraction studies on amyloid filaments. *J Histochem Cytochem* 16:673-677.1968).
- Eggenberger E (Prion disease. *Neurol Clin* 25:833-842, viii.2007).
- Ellis RJ (Macromolecular crowding: an important but neglected aspect of the intracellular environment. *Curr Opin Struct Biol* 11:114-119.2001a).
- Ellis RJ (Macromolecular crowding: obvious but underappreciated. *Trends Biochem Sci* 26:597-604.2001b).

- Engen JR, Smith DL (Investigating protein structure and dynamics by hydrogen exchange MS. *Anal Chem* 73:256A-265A.2001).
- Englander SW (Hydrogen exchange and mass spectrometry: A historical perspective. *J Am Soc Mass Spectrom* 17:1481-1489.2006).
- Fandrich M, Meinhardt J, Grigorieff N (Structural polymorphism of Alzheimer A beta and other amyloid fibrils. *Prion* 3:89-93.2009).
- Field EJ, Farmer F, Caspary EA, Joyce G (Susceptibility of scrapie agent to ionizing radiation. *Nature* 222:90-91.1969).
- Fischer M, Rulicke T, Raeber A, Sailer A, Moser M, Oesch B, Brandner S, Aguzzi A, Weissmann C (Prion protein (PrP) with amino-proximal deletions restoring susceptibility of PrP knockout mice to scrapie. *EMBO J* 15:1255-1264.1996).
- Forloni G, Angeretti N, Chiesa R, Monzani E, Salmona M, Bugiani O, Tagliavini F (Neurotoxicity of a prion protein fragment. *Nature* 362:543-546.1993).
- Gajdusek DC, Gibbs Jr CJ, Alpers M (Experimental transmission of a kuru-like syndrome to chimpanzees. *Nature* 209:794-796.1966).
- Gajdusek DC, Gibbs Jr CJ, Alpers M (Transmission and passage of experimental "kuru" to chimpanzees. *Science* 155:212-214.1967).
- Gasset M, Baldwin MA, Lloyd DH, Gabriel JM, Holtzman DM, Cohen F, Fletterick R, Prusiner SB (Predicted alpha-helical regions of the prion protein when synthesized as peptides form amyloid. *Proc Natl Acad Sci U S A* 89:10940-10944.1992).
- Ghetti B, Piccardo P, Spillantini MG, Ichimiya Y, Porro M, Perini F, Kitamoto T, Tateishi J, Seiler C, Frangione B, Bugiani O, Giaccone G, Prelli F, Goedert M, Dlouhy SR, Tagliavini F (Vascular variant of prion protein cerebral amyloidosis with tau-positive neurofibrillary tangles: the phenotype of the stop codon 145 mutation in PRNP. *Proc Natl Acad Sci U S A* 93:744-748.1996).
- Ghiso J, Jenson O, Frangione B (Amyloid fibrils in hereditary cerebral hemorrhage with amyloidosis of Icelandic type is a variant of gamma-trace basic protein (cystatin C). *Proc Natl Acad Sci U S A* 83:2974-2978.1986).
- Gibbons RA, Hunter GD (Nature of the scrapie agent. *Nature* 215:1041-1043.1967).
- Gibbs CJ, Jr., Gajdusek DC, Latarjet R (Unusual resistance to ionizing radiation of the viruses of kuru, Creutzfeldt-Jakob disease, and scrapie. *Proc Natl Acad Sci U S A* 75:6268-6270.1978).
- Gibbs Jr CJ, Gajdusek DC, Asher DM, Alpers MP, Beck E, Daniel PM, Matthews WB (Creutzfeldt-Jakob disease (spongiform encephalopathy): Transmission to the chimpanzee. *Science* 161:388-389.1968).

- Glover JR, Kowal AS, Schirmer EC, Patino MM, Liu JJ, Lindquist S (Self-seeded fibers formed by Sup35, the protein determinant of [PSI⁺], a heritable prion-like factor of *S. cerevisiae*. *Cell* 89:811-819.1997).
- Gosal WS, Myers SL, Radford SE, Thomson NH (Amyloid under the atomic force microscope. *Protein Pept Lett* 13:261-270.2006).
- Govaerts C, Wille H, Prusiner SB, Cohen FE (Evidence for assembly of prions with left-handed beta-helices into trimers. *Proc Natl Acad Sci U S A* 101:8342-8347.2004).
- Griffith JS (Self-replication and scrapie. *Nature* 215:1043-1044.1967).
- Gu Y, Fujioka H, Mishra RS, Li R, Singh N (Prion peptide 106-126 modulates the aggregation of cellular prion protein and induces the synthesis of potentially neurotoxic transmembrane PrP. *J Biol Chem* 277:2275-2286.2002).
- Hadlow WJ (SCRAPIE AND KURU. *The Lancet* 274:289-290.1959).
- Hadlow WJ (Neuropathology and the Scrapie-Kuru connection. *Brain Pathology* 5:27-31.1995).
- Han S, Hill AF (2008) Analysis of PrP Conformation Using Circular Dichroism. In: *Prion Protein Protocols*, vol. 459 (Hill, A. F., ed), pp 145-159: Humana Press.
- Haraguchi T, Fisher S, Olofsson S, Endo T, Groth D, Tarentino A, Borchelt DR, Teplov D, Hood L, Burlingame A, et al. (Asparagine-linked glycosylation of the scrapie and cellular prion proteins. *Arch Biochem Biophys* 274:1-13.1989).
- Heise H (Solid-state NMR spectroscopy of amyloid proteins. *Chembiochem* 9:179-189.2008).
- Helmus JJ, Surewicz K, Nadaud PS, Surewicz WK, Jaroniec CP (Molecular conformation and dynamics of the Y145Stop variant of human prion protein in amyloid fibrils. *Proc Natl Acad Sci U S A* 105:6284-6289.2008).
- Hermes J, Tings T, Gall S, Madlung A, Giese A, Siebert H, Schurmann P, Windl O, Brose N, Kretzschmar H (Evidence of presynaptic location and function of the prion protein. *J Neurosci* 19:8866-8875.1999).
- Hoofnagle AN, Resing KA, Ahn NG (Protein analysis by hydrogen exchange mass spectrometry. *Annu Rev Biophys Biomol Struct* 32:1-25.2003).
- Hornemann S, Glockshuber R (Autonomous and reversible folding of a soluble amino-terminally truncated segment of the mouse prion protein. *J Mol Biol* 261:614-619.1996).
- Hornshaw MP, McDermott JR, Candy JM (Copper binding to the N-terminal tandem repeat regions of mammalian and avian prion protein. *Biochem Biophys Res Commun* 207:621-629.1995).
- Horwich A (Protein aggregation in disease: a role for folding intermediates forming specific multimeric interactions. *J Clin Invest* 110:1221-1232.2002).

- Hu W, Kieseier B, Frohman E, Eagar TN, Rosenberg RN, Hartung HP, Stuve O (Prion proteins: physiological functions and role in neurological disorders. *J Neurol Sci* 264:1-8.2008).
- Hu W, Rosenberg RN, Stuve O (Prion proteins: a biological role beyond prion diseases. *Acta Neurol Scand* 116:75-82.2007).
- Hunter GD (Scrapie: a prototype slow infection. *J Infect Dis* 125:427-440.1972).
- Hunter GD, Kimberlin RH, Gibbons RA (Scrapie: a modified membrane hypothesis. *J Theor Biol* 20:355-357.1968).
- Hunter N (Prion diseases and the central dogma of molecular biology. *Trends Microbiol* 7:265-266.1999).
- Jackson GS, Murray I, Hosszu LL, Gibbs N, Waltho JP, Clarke AR, Collinge J (Location and properties of metal-binding sites on the human prion protein. *Proc Natl Acad Sci U S A* 98:8531-8535.2001).
- Jahn TR, Radford SE (The Yin and Yang of protein folding. *FEBS J* 272:5962-5970.2005).
- Jarrett JT, Lansbury PT, Jr. (Seeding "one-dimensional crystallization" of amyloid: a pathogenic mechanism in Alzheimer's disease and scrapie? *Cell* 73:1055-1058.1993).
- Jeffrey M, Goodbrand IA, Goodsir CM (Pathology of the transmissible spongiform encephalopathies with special emphasis on ultrastructure. *Micron* 26:277-298.1995).
- Johnson RT, Gibbs CJ, Jr. (Creutzfeldt-Jakob disease and related transmissible spongiform encephalopathies. *N Engl J Med* 339:1994-2004.1998).
- Jones EM, Surewicz WK (Fibril conformation as the basis of species- and strain-dependent seeding specificity of mammalian prion amyloids. *Cell* 121:63-72.2005).
- Keyes ME (The prion challenge to the 'central dogma' of molecular biology, 1965-1991. *Studies in History and Philosophy of Science Part C* 30:181-218.1999a).
- Keyes ME (The prion challenge to the 'central dogma' of molecular biology, 1965-1991. *Studies in History and Philosophy of Science Part C* 30:1-19.1999b).
- Khalili-Shirazi A, Summers L, Linehan J, Mallinson G, Anstee D, Hawke S, Jackson GS, Collinge J (PrP glycoforms are associated in a strain-specific ratio in native PrPSc. *J Gen Virol* 86:2635-2644.2005).
- Kheterpal I, Cook KD, Wetzel R (2006) Hydrogen/Deuterium Exchange Mass Spectrometry Analysis of Protein Aggregates. In: *Methods in Enzymology*, vol. Volume 413 (Indu, K. and Ronald, W., eds), pp 140-166: Academic Press.

- Khurana R, Coleman C, Ionescu-Zanetti C, Carter SA, Krishna V, Grover RK, Roy R, Singh S (Mechanism of thioflavin T binding to amyloid fibrils. *Journal of Structural Biology* 151:229-238.2005).
- Khurana R, Uversky VN, Nielsen L, Fink AL (Is Congo Red an Amyloid-specific Dye? *Journal of Biological Chemistry* 276:22715-22721.2001).
- Kim HY, Cho MK, Riedel D, Fernandez CO, Zweckstetter M (Dissociation of amyloid fibrils of alpha-synuclein in supercooled water. *Angew Chem Int Edit* 47:5046-5048.2008).
- Kim JI, Cali I, Surewicz K, Kong Q, Raymond GJ, Atarashi R, Race B, Qing L, Gambetti P, Caughey B, Surewicz WK (Mammalian prions generated from bacterially expressed prion protein in the absence of any mammalian cofactors. *J Biol Chem* 285:14083-14087.2010).
- Kimberlin RH (Scrapie agent: prions or virinos? *Nature* 297:107-108.1982).
- King CY, Diaz-Avalos R (Protein-only transmission of three yeast prion strains. *Nature* 428:319-323.2004).
- Klein-Seetharaman J, Oikawa M, Grimshaw SB, Wirmer J, Duchardt E, Ueda T, Imoto T, Smith LJ, Dobson CM, Schwalbe H (Long-range interactions within a nonnative protein. *Science* 295:1719-1722.2002).
- Knaus KJ, Morillas M, Swietnicki W, Malone M, Surewicz WK, Yee VC (Crystal structure of the human prion protein reveals a mechanism for oligomerization. *Nat Struct Biol* 8:770-774.2001).
- Kocisko DA, Come JH, Priola SA, Chesebro B, Raymond GJ, Lansbury PT, Caughey B (Cell-free formation of protease-resistant prion protein. *Nature* 370:471-474.1994).
- Kocisko DA, Priola SA, Raymond GJ, Chesebro B, Lansbury PT, Jr., Caughey B (Species specificity in the cell-free conversion of prion protein to protease-resistant forms: a model for the scrapie species barrier. *Proc Natl Acad Sci U S A* 92:3923-3927.1995).
- Koffie RM, Meyer-Luehmann M, Hashimoto T, Adams KW, Mielke ML, Garcia-Alloza M, Micheva KD, Smith SJ, Kim ML, Lee VM, Hyman BT, Spires-Jones TL (Oligomeric amyloid beta associates with postsynaptic densities and correlates with excitatory synapse loss near senile plaques. *Proc Natl Acad Sci U S A* 106:4012-4017.2009).
- Krebs MR, Bromley EH, Donald AM (The binding of thioflavin-T to amyloid fibrils: localisation and implications. *J Struct Biol* 149:30-37.2005).
- Krebs MR, Wilkins DK, Chung EW, Pitkeathly MC, Chamberlain AK, Zurdo J, Robinson CV, Dobson CM (Formation and seeding of amyloid fibrils from wild-type hen lysozyme and a peptide fragment from the beta-domain. *J Mol Biol* 300:541-549.2000).

- Kumar D, Kumar A, Misra JR, Chugh J, Sharma S, Hosur RV (1H, 15N, 13C resonance assignment of folded and 8 M urea-denatured state of SUMO from *Drosophila melanogaster*. *Biomol NMR Assign* 2:13-15.2008).
- Kundu B, Maiti NR, Jones EM, Surewicz KA, Vanik DL, Surewicz WK (Nucleation-dependent conformational conversion of the Y145Stop variant of human prion protein: structural clues for prion propagation. *Proc Natl Acad Sci U S A* 100:12069-12074.2003).
- Kuwata K, Matumoto T, Cheng H, Nagayama K, James TL, Roder H (NMR-detected hydrogen exchange and molecular dynamics simulations provide structural insight into fibril formation of prion protein fragment 106-126. *Proc Natl Acad Sci U S A* 100:14790-14795.2003).
- Lange A, Gattin Z, Van Melckebeke H, Wasmer C, Soragni A, van Gunsteren WF, Meier BH (A combined solid-state NMR and MD characterization of the stability and dynamics of the HET-s(218-289) prion in its amyloid conformation. *ChemBiochem* 10:1657-1665.2009).
- Latarjet R, Muel B, Haig DA, Clarke MC, Alper T (Inactivation of the scrapie agent by near monochromatic ultraviolet light. *Nature* 227:1341-1343.1970).
- Legname G, Baskakov IV, Nguyen HO, Riesner D, Cohen FE, DeArmond SJ, Prusiner SB (Synthetic mammalian prions. *Science* 305:673-676.2004).
- Levinthal.C (Are There Pathways for Protein Folding. *J Chim Phys Pcb* 65:44-&.1968).
- Li J, Browning S, Mahal SP, Oelschlegel AM, Weissmann C (Darwinian evolution of prions in cell culture. *Science* 327:869-872.2010).
- Li L, Guest W, Huang A, Plotkin SS, Cashman NR (Immunological mimicry of PrPC-PrPSc interactions: antibody-induced PrP misfolding. *Protein Eng Des Sel* 22:523-529.2009).
- Liberski PP, Gajdusek DC (Kuru: Forty years later, an historical note. *Brain Pathology* 7:555-560.1997).
- Liu A, Riek R, Wider G, von Schroetter C, Zahn R, Wuthrich K (NMR experiments for resonance assignments of 13C, 15N doubly-labeled flexible polypeptides: application to the human prion protein hPrP(23-230). *J Biomol NMR* 16:127-138.2000).
- Lu X, Wintrode PL, Surewicz WK (Beta-sheet core of human prion protein amyloid fibrils as determined by hydrogen/deuterium exchange. *Proc Natl Acad Sci U S A* 104:1510-1515.2007).
- Makarava N, Kovacs GG, Bocharova O, Savtchenko R, Alexeeva I, Budka H, Rohwer RG, Baskakov IV (Recombinant prion protein induces a new transmissible prion disease in wild-type animals. *Acta Neuropathol* 119:177-187.2010).

- Manuelidis L, Yu ZX, Barquero N, Mullins B (Cells infected with scrapie and Creutzfeldt-Jakob disease agents produce intracellular 25-nm virus-like particles. *Proc Natl Acad Sci U S A* 104:1965-1970.2007).
- Marsh RF, Hadlow WJ (Transmissible mink encephalopathy. *OIE Revue Scientifique et Technique* 11:539-550.1992).
- Masters CL, Gajdusek DC, Gibbs CJ, Jr. (Creutzfeldt-Jakob disease virus isolations from the Gerstmann-Straussler syndrome with an analysis of the various forms of amyloid plaque deposition in the virus-induced spongiform encephalopathies. *Brain* 104:559-588.1981a).
- Masters CL, Gajdusek DC, Gibbs CJ, Jr. (The familial occurrence of Creutzfeldt-Jakob disease and Alzheimer's disease. *Brain* 104:535-558.1981b).
- McKinley MP, Bolton DC, Prusiner SB (A protease-resistant protein is a structural component of the scrapie prion. *Cell* 35:57-62.1983).
- Mead S (Prion disease genetics. *Eur J Hum Genet* 14:273-281.2006).
- Mehlhorn I, Groth D, Stockel J, Moffat B, Reilly D, Yansura D, Willett WS, Baldwin M, Fletterick R, Cohen FE, Vandlen R, Henner D, Prusiner SB (High-level expression and characterization of a purified 142-residue polypeptide of the prion protein. *Biochemistry* 35:5528-5537.1996).
- Meinhardt J, Sachse C, Hortschansky P, Grigorieff N, Fandrich M (A beta(1-40) Fibril Polymorphism Implies Diverse Interaction Patterns in Amyloid Fibrils. *Journal of Molecular Biology* 386:869-877.2009).
- Meyerett C, Michel B, Pulford B, Spraker TR, Nichols TA, Johnson T, Kurt T, Hoover EA, Telling GC, Zabel MD (In vitro strain adaptation of CWD prions by serial protein misfolding cyclic amplification. *Virology* 382:267-276.2008).
- Morales R, Abid K, Soto C (The prion strain phenomenon: molecular basis and unprecedented features. *Biochim Biophys Acta* 1772:681-691.2007).
- Morange M (What history tells us VIII. The progressive construction of a mechanism for prion diseases. *Journal of Biosciences* 32:223-227.2007).
- Naito A, Kawamura I (Solid-state NMR as a method to reveal structure and membrane-interaction of amyloidogenic proteins and peptides. *Biochimica et Biophysica Acta (BBA) - Biomembranes* 1768:1900-1912.2007).
- Nazabal A, Hornemann S, Aguzzi A, Zenobi R (Hydrogen/deuterium exchange mass spectrometry identifies two highly protected regions in recombinant full-length prion protein amyloid fibrils. *J Mass Spectrom* 44:965-977.2009).
- Nelson R, Eisenberg D (Structural models of amyloid-like fibrils. *Adv Protein Chem* 73:235-282.2006).
- Nelson R, Sawaya MR, Balbirnie M, Madsen AO, Riek C, Grothe R, Eisenberg D (Structure of the cross-beta spine of amyloid-like fibrils. *Nature* 435:773-778.2005).

- Oesch B, Westaway D, Walchli M, McKinley MP, Kent SB, Aebersold R, Barry RA, Tempst P, Teplow DB, Hood LE, et al. (A cellular gene encodes scrapie PrP 27-30 protein. *Cell* 40:735-746.1985).
- Paci E, Vendruscolo M, Karplus M (Validity of Go models: comparison with a solvent-shielded empirical energy decomposition. *Biophys J* 83:3032-3038.2002).
- Palsson PA (Dr. Bjorn Sigurdsson (1913-1959). A memorial tribute. *Ann N Y Acad Sci* 724:1-5.1994).
- Pan KM, Baldwin M, Nguyen J, Gasset M, Serban A, Groth D, Mehlhorn I, Huang Z, Fletterick RJ, Cohen FE, et al. (Conversion of alpha-helices into beta-sheets features in the formation of the scrapie prion proteins. *Proc Natl Acad Sci U S A* 90:10962-10966.1993).
- Panchal SC, Bhavesh NS, Hosur RV (Improved 3D triple resonance experiments, HNN and HN(C)N, for HN and ¹⁵N sequential correlations in (¹³C, ¹⁵N) labeled proteins: application to unfolded proteins. *J Biomol NMR* 20:135-147.2001).
- Paramithiotis E, Pinard M, Lawton T, LaBoissiere S, Leathers VL, Zou WQ, Estey LA, Lamontagne J, Lehto MT, Kondejewski LH, Francoeur GP, Papadopoulos M, Haghghat A, Spatz SJ, Head M, Will R, Ironside J, O'Rourke K, Tonelli Q, Ledebur HC, Chakrabarty A, Cashman NR (A prion protein epitope selective for the pathologically misfolded conformation. *Nat Med* 9:893-899.2003).
- Pattison IH, Jones KM (The possible nature of the transmissible agent of scrapie. *Vet Rec* 80:2-9.1967).
- Pattison IH, Millson GC (Scrapie produced experimentally in goats with special reference to the clinical syndrome. *J Comp Pathol* 71:101-109.1961).
- Platt GW, Xue WF, Homans SW, Radford SE (Probing dynamics within amyloid fibrils using a novel capping method. *Angew Chem Int Ed Engl* 48:5705-5707.2009).
- Polymenidou M, Heppner FL, Pelliccioli EC, Urich E, Miele G, Braun N, Wopfner F, Schatzl HM, Becher B, Aguzzi A (Humoral immune response to native eukaryotic prion protein correlates with anti-prion protection. *Proc Natl Acad Sci U S A* 101 Suppl 2:14670-14676.2004).
- Priola SA, Vorberg I (Molecular aspects of disease pathogenesis in the transmissible spongiform encephalopathies. *Methods Mol Biol* 268:517-540.2004).
- Prusiner SB (Novel proteinaceous infectious particles cause scrapie. *Science* 216:136-144.1982).
- Prusiner SB (Prions. *Proc Natl Acad Sci U S A* 95:13363-13383.1998).

- Prusiner SB, Bolton DC, Groth DF, Bowman KA, Cochran SP, McKinley MP (Further purification and characterization of scrapie prions. *Biochemistry* 21:6942-6950.1982a).
- Prusiner SB, Cochran SP, Groth DF (Measurement of the scrapie agent using an incubation time interval assay. *Annals of neurology* 11:353-358.1982b).
- Prusiner SB, Garfin DE, Cochran SP, McKinley MP, Groth DF, Hadlow WJ, Race RE, Eklund CM (Experimental scrapie in the mouse: electrophoretic and sedimentation properties of the partially purified agent. *J Neurochem* 35:574-582.1980a).
- Prusiner SB, Groth D, Serban A, Koehler R, Foster D, Torchia M, Burton D, Yang SL, DeArmond SJ (Ablation of the prion protein (PrP) gene in mice prevents scrapie and facilitates production of anti-PrP antibodies. *Proc Natl Acad Sci U S A* 90:10608-10612.1993).
- Prusiner SB, Groth DF, Bildstein C, Masiarz FR, McKinley MP, Cochran SP (Electrophoretic properties of the scrapie agent in agarose gels. *Proc Natl Acad Sci U S A* 77:2984-2988.1980b).
- Prusiner SB, Groth DF, Cochran SP, Masiarz FR, McKinley MP, Martinez HM (Molecular properties, partial purification, and assay by incubation period measurements of the hamster scrapie agent. *Biochemistry* 19:4883-4891.1980c).
- Prusiner SB, Groth DF, Cochran SP, McKinley MP, Masiarz FR (Gel electrophoresis and glass permeation chromatography of the hamster scrapie agent after enzymatic digestion and detergent extraction. *Biochemistry* 19:4892-4898.1980d).
- Prusiner SB, McKinley MP, Bowman KA (Scrapie prions aggregate to form amyloid-like birefringent rods. *Cell* 35:349-358.1983).
- Prusiner SB, Scott M, Foster D, Pan KM, Groth D, Mirenda C, Torchia M, Yang SL, Serban D, Carlson GA, et al. (Transgenic studies implicate interactions between homologous PrP isoforms in scrapie prion replication. *Cell* 63:673-686.1990).
- Puchtler H, Sweat F (A review of early concepts of amyloid in context with contemporary chemical literature from 1839 to 1859. *J Histochem Cytochem* 14:123-134.1966).
- Riek R, Hornemann S, Wider G, Billeter M, Glockshuber R, Wuthrich K (NMR structure of the mouse prion protein domain PrP(121-321). *Nature* 382:180-182.1996).
- Salman MD (Chronic wasting disease in deer and elk: Scientific facts and findings. *Journal of Veterinary Medical Science* 65:761-768.2003).
- Sattler M, Schleucher J, Griesinger C (Heteronuclear multidimensional NMR experiments for the structure determination of proteins in solution

- employing pulsed field gradients. *Progress in Nuclear Magnetic Resonance Spectroscopy* 34:93-158.1999).
- Schubert M, Oschkinat H, Schmieder P (MUSIC and aromatic residues: amino acid type-selective (1)H-(15)N correlations, III. *J Magn Reson* 153:186-192.2001a).
- Schubert M, Oschkinat H, Schmieder P (MUSIC, selective pulses, and tuned delays: amino acid type-selective (1)H-(15)N correlations, II. *J Magn Reson* 148:61-72.2001b).
- Schubert M, Smalla M, Schmieder P, Oschkinat H (MUSIC in triple-resonance experiments: amino acid type-selective (1)H-(15)N correlations. *J Magn Reson* 141:34-43.1999).
- Scott M, Foster D, Miranda C, Serban D, Coufal F, Walchli M, Torchia M, Groth D, Carlson G, DeArmond SJ, Westaway D, Prusiner SB (Transgenic mice expressing hamster prion protein produce species-specific scrapie infectivity and amyloid plaques. *Cell* 59:847-857.1989).
- Shen Y, Delaglio F, Cornilescu G, Bax A (TALOS plus : a hybrid method for predicting protein backbone torsion angles from NMR chemical shifts. *Journal of Biomolecular Nmr* 44:213-223.2009).
- Shirahama T, Cohen AS (HIGH-RESOLUTION ELECTRON MICROSCOPIC ANALYSIS OF THE AMYLOID FIBRIL. *The Journal of Cell Biology* 33:679-708.1967).
- Shortle D, Ackerman MS (Persistence of native-like topology in a denatured protein in 8 M urea. *Science* 293:487-489.2001).
- Siemer AB, Ritter C, Ernst M, Riek R, Meier BH (High-resolution solid-state NMR spectroscopy of the prion protein HET-s in its amyloid conformation. *Angew Chem Int Ed Engl* 44:2441-2444.2005).
- Silveira JR, Raymond GJ, Hughson AG, Race RE, Sim VL, Hayes SF, Caughey B (The most infectious prion protein particles. *Nature* 437:257-261.2005).
- Sim VL, Caughey B (Ultrastructures and strain comparison of under-glycosylated scrapie prion fibrils. *Neurobiol Aging* 30:2031-2042.2009).
- Singh N, Gu Y, Bose S, Kalepu S, Mishra RS, Verghese S (Prion peptide 106-126 as a model for prion replication and neurotoxicity. *Front Biosci* 7:a60-71.2002).
- Sipe JD, Cohen AS (Review: history of the amyloid fibril. *J Struct Biol* 130:88-98.2000).
- Smith DL, Deng Y, Zhang Z (Probing the non-covalent structure of proteins by amide hydrogen exchange and mass spectrometry. *J Mass Spectrom* 32:135-146.1997).
- Soto C, Saborio GP, Anderes L (Cyclic amplification of protein misfolding: application to prion-related disorders and beyond. *Trends in Neurosciences* 25:390-394.2002a).

- Soto C, Saborio GP, Anderes L (Cyclic amplification of protein misfolding: application to prion-related disorders and beyond. *Trends Neurosci* 25:390-394.2002b).
- Sparkes RS, Simon M, Cohn VH, Fournier RE, Lem J, Klisak I, Heinzmann C, Blatt C, Lucero M, Mohandas T, et al. (Assignment of the human and mouse prion protein genes to homologous chromosomes. *Proc Natl Acad Sci U S A* 83:7358-7362.1986).
- Stahl N, Baldwin MA, Teplow DB, Hood L, Gibson BW, Burlingame AL, Prusiner SB (Structural studies of the scrapie prion protein using mass spectrometry and amino acid sequencing. *Biochemistry* 32:1991-2002.1993).
- Stahl N, Prusiner SB (Prions and prion proteins. *FASEB Journal* 5:2799-2807.1991).
- Supattapone S (Biochemistry. What makes a prion infectious? *Science* 327:1091-1092.2010).
- Surewicz WK, Jones EM, Apetri AC (The Emerging Principles of Mammalian Prion Propagation and Transmissibility Barriers: Insight from Studies in Vitro. *Accounts of Chemical Research* 39:654-662.2006).
- Swietnicki W, Morillas M, Chen SG, Gambetti P, Surewicz WK (Aggregation and fibrillization of the recombinant human prion protein huPrP90-231. *Biochemistry* 39:424-431.2000).
- Sy MS, Gambetti P, Wong BS (Human prion diseases. *Med Clin North Am* 86:551-571, vi-vii.2002).
- Tagliavini F, Prelli F, Verga L, Giaccone G, Sarma R, Gorevic P, Ghetti B, Passerini F, Ghibaudi E, Forloni G, et al. (Synthetic peptides homologous to prion protein residues 106-147 form amyloid-like fibrils in vitro. *Proc Natl Acad Sci U S A* 90:9678-9682.1993).
- Tanaka M, Chien P, Naber N, Cooke R, Weissman JS (Conformational variations in an infectious protein determine prion strain differences. *Nature* 428:323-328.2004).
- Telling GC (Prion protein genes and prion diseases: studies in transgenic mice. *Neuropathol Appl Neurobiol* 26:209-220.2000).
- Thukral L, Smith JC, Daidone I (Common folding mechanism of a beta-hairpin peptide via non-native turn formation revealed by unbiased molecular dynamics simulations. *J Am Chem Soc* 131:18147-18152.2009).
- Turk E, Teplow DB, Hood LE, Prusiner SB (Purification and properties of the cellular and scrapie hamster prion proteins. *Eur J Biochem* 176:21-30.1988).
- Tycko R (Solid-state NMR as a probe of amyloid fibril structure. *Curr Opin Chem Biol* 4:500-506.2000).
- Tycko R (Insights into the amyloid folding problem from solid-state NMR. *Biochemistry* 42:3151-3159.2003).

- Tycko R (Progress towards a molecular-level structural understanding of amyloid fibrils. *Curr Opin Struct Biol* 14:96-103.2004).
- Tycko R (Molecular structure of amyloid fibrils: insights from solid-state NMR. *Quarterly Reviews of Biophysics* 39:1-55.2006a).
- Tycko R (Molecular structure of amyloid fibrils: insights from solid-state NMR. *Q Rev Biophys* 39:1-55.2006b).
- Tycko R (Solid-state NMR as a probe of amyloid structure. *Protein Pept Lett* 13:229-234.2006c).
- Uptain SM, Lindquist S (Prions as protein-based genetic elements. *Annu Rev Microbiol* 56:703-741.2002).
- van der Kamp MW, Daggett V (The consequences of pathogenic mutations to the human prion protein. *Protein Eng Des Sel* 22:461-468.2009).
- van der Wel PC, Lewandowski JR, Griffin RG (Solid-state NMR study of amyloid nanocrystals and fibrils formed by the peptide GNNQQNY from yeast prion protein Sup35p. *J Am Chem Soc* 129:5117-5130.2007).
- Van Melckebeke H, Wasmer C, Lange A, Ab E, Loquet A, Bockmann A, Meier BH (Atomic-Resolution Three-Dimensional Structure of HET-s(218-289) Amyloid Fibrils by Solid-State NMR Spectroscopy. *J Am Chem Soc*.2010).
- Vanik DL, Surewicz KA, Surewicz WK (Molecular basis of barriers for interspecies transmissibility of mammalian prions. *Mol Cell* 14:139-145.2004).
- Vassallo N, Herms J (Cellular prion protein function in copper homeostasis and redox signalling at the synapse. *J Neurochem* 86:538-544.2003).
- Viles JH, Cohen FE, Prusiner SB, Goodin DB, Wright PE, Dyson HJ (Copper binding to the prion protein: structural implications of four identical cooperative binding sites. *Proc Natl Acad Sci U S A* 96:2042-2047.1999).
- Waggoner DJ, Drisaldi B, Bartnikas TB, Casareno RL, Prohaska JR, Gitlin JD, Harris DA (Brain copper content and cuproenzyme activity do not vary with prion protein expression level. *J Biol Chem* 275:7455-7458.2000).
- Wagner G, Stassinopoulou CI, Wuthrich K (Amide-proton exchange studies by two-dimensional correlated ¹H NMR in two chemically modified analogs of the basic pancreatic trypsin inhibitor. *Eur J Biochem* 145:431-436.1984).
- Wand AJ, Roder H, Englander SW (Two-dimensional ¹H NMR studies of cytochrome c: hydrogen exchange in the N-terminal helix. *Biochemistry* 25:1107-1114.1986).
- Wang F, Wang X, Yuan CG, Ma J (Generating a prion with bacterially expressed recombinant prion protein. *Science* 327:1132-1135.2010).
- Watzlawik J, Skora L, Frense D, Griesinger C, Zweckstetter M, Schulz-Schaeffer WJ, Kramer ML (Prion protein helix1 promotes aggregation but is not converted into beta-sheet. *J Biol Chem* 281:30242-30250.2006).

- Weber P, Giese A, Piening N, Mitteregger G, Thomzig A, Beekes M, Kretzschmar HA (Cell-free formation of misfolded prion protein with authentic prion infectivity. *Proc Natl Acad Sci U S A* 103:15818-15823.2006).
- Weissmann C (A 'unified theory' of prion propagation. *Nature* 352:679-683.1991).
- Weissmann C (The state of the prion. *Nat Rev Microbiol* 2:861-871.2004).
- Weissmann C (Birth of a prion: spontaneous generation revisited. *Cell* 122:165-168.2005).
- Weissmann C, Flechsig E (PrP knock-out and PrP transgenic mice in prion research. *Br Med Bull* 66:43-60.2003).
- Westergard L, Christensen HM, Harris DA (The cellular prion protein (PrP(C)): its physiological function and role in disease. *Biochim Biophys Acta* 1772:629-644.2007).
- Westermarck P (ed.) (2006) *Amyloidosis and Amyloid Proteins: Brief History and Definitions*.
- Westermarck P, Benson MD, Buxbaum JN, Cohen AS, Frangione B, Ikeda S, Masters CL, Merlini G, Saraiva MJ, Sipe JD (Amyloid: toward terminology clarification. Report from the Nomenclature Committee of the International Society of Amyloidosis. *Amyloid* 12:1-4.2005).
- Wickner RB ([URE3] as an altered URE2 protein: evidence for a prion analog in *Saccharomyces cerevisiae*. *Science* 264:566-569.1994).
- Wickner RB, Edskes HK, Shewmaker F, Nakayashiki T, Engel A, McCann L, Kryndushkin D (Yeast prions: evolution of the prion concept. *Prion* 1:94-100.2007).
- Wille H, Bian W, McDonald M, Kendall A, Colby DW, Bloch L, Ollesch J, Borovinskiy AL, Cohen FE, Prusiner SB, Stubbs G (Natural and synthetic prion structure from X-ray fiber diffraction. *Proc Natl Acad Sci U S A* 106:16990-16995.2009).
- Wille H, Michelitsch MD, Guenebaut V, Supattapone S, Serban A, Cohen FE, Agard DA, Prusiner SB (Structural studies of the scrapie prion protein by electron crystallography. *Proc Natl Acad Sci U S A* 99:3563-3568.2002).
- Wirmer J, Schlorb C, Klein-Seetharaman J, Hirano R, Ueda T, Imoto T, Schwalbe H (Modulation of compactness and long-range interactions of unfolded lysozyme by single point mutations. *Angew Chem Int Ed Engl* 43:5780-5785.2004).
- Wolynes PG, Onuchic JN, Thirumalai D (Navigating the folding routes. *Science* 267:1619-1620.1995).
- Woolhouse ME, Coen P, Matthews L, Foster JD, Elsen JM, Lewis RM, Haydon DT, Hunter N (A centuries-long epidemic of scrapie in British sheep? *Trends Microbiol* 9:67-70.2001).

- Wopfner F, Weidenhofer G, Schneider R, von Brunn A, Gilch S, Schwarz TF, Werner T, Schatzl HM (Analysis of 27 mammalian and 9 avian PrPs reveals high conservation of flexible regions of the prion protein. *J Mol Biol* 289:1163-1178.1999).
- Xu M, Ermolenkov VV, He W, Uversky VN, Fredriksen L, Lednev IK (Lysozyme fibrillation: deep UV Raman spectroscopic characterization of protein structural transformation. *Biopolymers* 79:58-61.2005).
- Zahn R, Liu A, Luhrs T, Riek R, von Schroetter C, Lopez Garcia F, Billeter M, Calzolari L, Wider G, Wuthrich K (NMR solution structure of the human prion protein. *Proc Natl Acad Sci U S A* 97:145-150.2000).
- Zahn R, von Schroetter C, Wuthrich K (Human prion proteins expressed in *Escherichia coli* and purified by high-affinity column refolding. *FEBS Lett* 417:400-404.1997).

Ausführliche Deutschsprachige Zusammenfassung

Einleitung

Neurodegenerative Krankheiten, die im Zusammenhang mit dem humanen Prionprotein stehen, sind durch die strukturelle Umordnung von Domänen des monomeren zellulären Prionproteins (PrP^C) in eine oligomere β -Struktur-reiche fibrilläre Form charakterisiert. Natives PrP^C besitzt einen unstrukturierten N-Terminus und eine strukturell wohl definierte C-terminale Domäne, die aus drei α -Helices und einem zweisträngigen kurzen antiparallelen β -Faltblatt besteht. Die Strukturen rekombinanter Prionproteine aus Säugern, Vögeln, Reptilien und Amphibien zeigen ähnliche globuläre Faltungen. Weil die nativen Strukturen der Prionproteine sehr ähnlich sind, erklären sie basierend auf dem aktuellen Wissenstand die beobachteten sequenzspezifischen Speziesbarrieren sowie Unterschiede im Zeitpunkt des Ausbruchs der Krankheit(en) nicht.

Der Mechanismus, der der strukturellen Umwandlung eines weitestgehend α -helikalen Proteins in die 'cross- β '-Struktur des fibrillären Zustands zu Grunde liegt, ist unbekannt. Modelle für den Mechanismus sind auf der Basis von elektronenmikroskopischen Daten sowie MD-Simulationen vorgeschlagen worden. Jedoch sind hoch auflösende strukturelle Daten für den fibrillären Zustand des Prionenproteins nicht verfügbar, was möglicherweise auf die konformationelle Heterogenität der amyloiden Fibrillen zurück zu führen ist. Diese Fibrillen werden typischerweise unter denaturierenden Bedingungen generiert (1M GdnCl, 3M Harnstoff, 20mM Natriumacetat pH 5,0 bei 37°C). Unlängst wurde gezeigt, dass Fibrillen, die aus rekombinantem PrP gewonnen werden, für Hamster toxisch sind.

Obwohl sie posttranslational nicht modifiziert waren, erwiesen sie sich in Hamstern im Zuge serieller Übertragung als infektiös.

Werden Fibrillen unter denaturierenden Bedingungen generiert, vollzieht das Prionprotein eine konformationelle Umwandlung. So entsteht ein Ensemble entfalteter Konformationen, aus dem sich bei einem kontinuierlichen Schüttelvorgang Fibrillen oder amorphe Aggregate bilden. Amyloide Fibrillen, besonders die des humanen Prionproteins, sind konformationell heterogen. Die Heterogenität der Fibrillen könnte auch für die Vielfältigkeit der Prionenstämme verantwortlich sein. Im Licht der oben diskutierten Experimente, bei denen Fibrillen aus rekombinantem PrP in Hamster eingebracht wurden, kann die Hypothese aufgestellt werden, dass Prionenstämme durch verschiedene Konformationen in ihren protofibrillären und fibrillären Zuständen gekennzeichnet sind und dass die Konformation *in vivo* durch Lipidverankerung oder Interaktion mit polyanionischen Spezies wie RNA beeinflusst wird. Die konformationelle Heterogenität könnte außerdem mit verschiedenen Pfaden der Fibrillenbildung in Verbindung stehen. Allen Pfaden, die zur Fibrillenbildung führen, wird es jedoch gemeinsam sein, dass sich die Polypeptidkette des nativen Proteins während der Fibrillenbildung lokal oder aber global entfaltet. Bisher ist nur wenig bekannt über die Fibrillenbildung unter hoch denaturierenden Bedingungen.

Ziel der Arbeit

Maßgebliche Fortschritte wurden im Bereich der Prionenbiologie in den letzten zwanzig Jahren erzielt. So gab es bedeutende Fortschritte auf dem Weg zum endgültigen Beweis der 'Protein-only'-Hypothese. Trotz dieser Fortschritte bleiben essentielle Fragen unbeantwortet. Einige Untersuchungen haben die

Bildung von Fibrillen ausgehend von nativ-ähnlichen und partiell gefalteten Zuständen des rekombinanten Prionproteins gezeigt. Über die Fibrillenbildung aus dem entfalteten Zustand ist hingegen nur begrenzte Information verfügbar, wobei postuliert wurde, dass sich PrP partiell oder gar vollständig entfalten muss, damit das konformationelle „Umschalten“ stattfinden kann. Harnstoff wurde in der Vergangenheit zur Entfaltung von Proteinen benutzt und hat umfangreiche Informationen über entfaltete Zustände von Proteinen geliefert. Das wesentliche Ziel meiner Arbeit war, die Fibrillenbildung des Prionenproteins aus seinem chemisch denaturierten Zustand (8M Harnstoff pH 2,0 bei 25°C) zu etablieren und zu charakterisieren sowie die strukturelle Umwandlung einzelner Polypeptidsegmente vom entfalteten Zustand in den fibrillären Zustand abzubilden. Dies hat uns erlaubt, ein atomares Bild der Dynamik und der Missfaltungseignisse des Prionproteins zu zeichnen.

Ergebnisse

Zuordnung

Ein umfassendes Verständnis des Missfaltungs- und Aggregationprozesses des Prionproteins erfordert die Charakterisierung aller Spezies, die auf dem Weg durch den – thermodynamisch gesprochen – Aggregationstrichter populiert werden. Diese beinhalten den entfalteten Zustand, partiell gefaltete Intermediate, präfibrilläre Oligomere, Protofibrillen und ausgereifte amyloide Fibrillen. Das Ensemble des entfalteten Zustands ist von besonderer Wichtigkeit, weil gemeinhin angenommen wird, dass das Prionprotein bzw. jedes andere Protein sich im Verlauf der Missfaltung partiell oder vollständig entfalten muss. Die strukturelle Charakterisierung des entfalteten Zustands des rekombinanten Prionproteins mittels NMR ist auf Grund der komplexen Natur des Proteins außerordentlich

herausfordernd gewesen. Grundsätzlich ist die NMR-spektroskopische Untersuchung wegen der geringen Dispersion der Amid- und Kohlenstoffresonanzen in entfalteten oder partiell gefalteten Proteinen schwierig. Der Aggregationsprozess des Prionproteins erschwerte die Zuordnung des Proteinrückgrats beträchtlich. Ein dreidimensionales NMR-Experiment erfordert üblicherweise drei bis vier Tage Messzeit; Zeit, in der sich das Verhältnis von Monomer zu Oligomer in der NMR-Probe verändert. Mit Hilfe von HNN- und MUSIC-basierten HSQC-Experimenten konnten die Amidrückgratresonanzen eindeutig identifiziert und zugeordnet werden. Die anfängliche Zuordnung der Amidrückgratresonanzen wurde mittels herkömmlicher Tripelresonanzexperimente (HNCACB, CBCA(CO)NH, HNCA, HN(CO)CA, HNCO, HCCCONH) vorgenommen. In einer bedeutenden Anzahl von Fällen wurde Resonanzüberlapp festgestellt, der durch die Kombination von zwei oder mehr Experimenten behoben werden konnte. Die nahezu vollständige Zuordnung der ^1H und ^{15}N Proteinrückgratresonanzen der rekombinanten PrP-Fragmente 90-230, 121-230 und 166-230 in 8M Harnstoff pH 2,0 bei 25°C konnte erzielt werden.

Aminosäuren des Fibrillenkerns

Das rekombinante Prionprotein bildet Amyloid-ähnliche Fibrillen in einer hoch denaturierenden Umgebung, was durch EM und AFM bestätigt werden konnte. Wir haben die Veränderungen während der Fibrillenbildung mit NMR-Spektroskopie verfolgt und können die Resonanzen basierend auf ihrem Verhalten grob in drei Kategorien einteilen: (I) Resonanzen mit einer langsamen Abnahme der Signalintensität (90-144), (II) Resonanzen mit einer schnellen Abnahme der Intensität, die zum Schluss vollständig verschwinden (145-223), wobei einige Aminosäuren (149, 150, 151 und 177) bis zum vierten Tag in dieser Region eine langsamere Abnahme zeigen und die Aminosäuren 180 und 208 am siebten Tag

noch beobachtbar sind, und (III) Resonanzen, die während des Aggregationsprozesses eine Veränderung in ihrer chemischen Verschiebung erfahren. Der Verlust an Signalintensität kommt auf Grund langsamer durch Molekülrotation bedingter Reorientierung zustande, ausgelöst durch die rigiden Bereiche der Fibrillen. Auf der anderen Seite stammen die Signale, die beobachtbar bleiben, von beweglichen Bereichen der Fibrillen. Das Vorhandensein rigider und beweglicher Fibrillenbereiche wird außerdem durch Festkörper-NMR-Experimente unterstützt. Somit bildet das Segment zwischen den Aminosäuren 145 und 223 den rigiden Kern der Fibrille, was β -Strang 2, Helix 2 und dem wesentlichen Teil von Helix 3 der nativen monomeren Struktur entspricht. Die C-terminalen Aminosäuren von 224 bis 230 weisen Signalverschiebungen auf und deuten deshalb die Anpassung an eine spezifische Fibrillenkonformation an. Der hauptsächliche Teil des N-terminalen Segments 90-144 verbleibt dynamisch, was durch seine Zugänglichkeit für Amyloid-spezifische Antikörper verstanden werden kann. Dies liefert neuartigen strukturellen Einblick in die Amyloid-Bildung ausgehend vom entfalteten Zustand des Fragmentes 90-230, welches den Proteinase K-resistenten Teil natürlich vorkommender Prionen darstellt. Frühere Untersuchungen auf der Basis von H/D-Austausch-MS- sowie EPR-spektroskopischen Experimenten hatten für den Fibrillenkern den Aminosäureabschnitt 160-220 etabliert. In diesen Studien erfolgte die Fibrillenbildung ausgehend von entweder nativ-ähnlichen oder partiell entfalteten Zuständen des rekombinanten Prionproteins. Deshalb ist es durchaus bemerkenswert, dass Fibrillen, die ausgehend vom monomeren entfalteten Zustand gebildet werden, den gleichen Amyloid-Kern aufweisen.

Polymorphismus

Die auf der molekularen sowie auf der Quartärstrukturebene zu findende strukturelle Heterogenität amyloider Fibrillen zu verstehen, ist eine große

Herausforderung an die Wissenschaft von heute. Es ist allgemein bekannt, dass die Kernbildung als Vorstufe und die Kinetik der Bildung von amyloiden Fibrillen nicht nur von inhärenten Eigenschaften wie Aminosäurezusammensetzung bzw. -sequenz oder Polypeptidkettenlänge, sondern auch von experimentellen Bedingungen wie Temperatur, Konzentration(en) an Ionen und/oder Denaturantien, pH, der Anwendung von Schüttelbewegungen und dem Vorhandensein von Aggregationskeimen abhängt. Trotz der Kenntnis über diese Faktoren ist der Mechanismus der Selbstassemblierung, der zur Bildung geordneter Fibrillen führt, nicht gut verstanden. Die Kombination dieser Faktoren trägt zu einer der schwierigsten Fragestellungen im Bereich der Proteinaggregation bei, welche das Auftreten des 'Aggregat- bzw. Fibrillenpolymorphismus' behandelt. Aggregate können verschiedene Vorzugsarchitekturen aufweisen, was teilweise von nur geringfügigen Änderungen in der Aminosäuresequenz oder den experimentellen Bedingungen abhängt. In unseren Studien waren wir in der Lage, die Fibrillenbildung in einer hoch denaturierenden Umgebung (8M Harnstoff pH 2,0) zu beobachten. Die so gebildeten Fibrillen zeigen strukturellen Polymorphismus, was mittels EM, AFM und NMR festgestellt wurde, und sind unterglykosylierten Scrapie-Fibrillen ähnlich. Die verschiedenen Morphologien der Fibrillen sollen in verschiedenen molekularen Strukturen begründet sein und könnten zur Entstehung verschiedener Prionenstämme führen. Deshalb ist es notwendig, Einblick in das Phänomen der Prionenstämme zu gewinnen, wo ein und dasselbe Prionprotein eine Auswahl infektiöser Konformationen annehmen kann, die sich hinsichtlich ihrer Spezifität und Übertragungsbarriere unterscheiden.

Adaptierung

Fibrillen wurden gegen Wasser pH 2,0 dialysiert und anschließend ein Pufferaustausch mit 70% D₂O pD 2,0 vorgenommen, um Deuteriumaustausch zu

beobachten. Fibrillen wurden nach Dialyse und Pufferaustausch mittels EM verifiziert. Im Gegensatz zum allgemeinen Verständnis, dass amyloide Fibrillen rigide sind, zeigen neue Studien, dass diese nicht vollständig rigide sind, sondern kontinuierlich umgebildet werden. Aus diesem Grund sind amyloide Fibrillen nicht statische, sondern dynamische Strukturen. Die meisten Aminosäuren zeigen Schutz vor Austausch von gut 40%, wohingegen die Sequenzabschnitte 120-123, 144-149, 174-180 und 187-194 geringen Austauschschutz aufweisen und somit lösungsmittelzugänglich sind. Die Region 187-194 ist relativ bemerkenswert, weil die zugehörigen Signale vollständig verschwinden. Sie ist reich an Threoninseitenketten (HTVTTT'TTK) und zeigt ein hohes Maß an Beweglichkeit. Die Fibrillen, die mit einem Fragment des Prionproteins aus Schaf (Helices 2 und 3) gebildet wurden, weisen für diese Aminosäuren ein ähnliches Verhalten auf. Dies deutet darauf hin, dass sich Fibrillen als Reaktion auf veränderte Lösungsbedingungen strukturell umordnen und dass der Amyloid-Kern nicht vollständig rigide ist und bestimmten Aminosäuren erlaubt, eine den Lösungsbedingungen entsprechende Konformation anzunehmen.

Ausblick

Eine der ausschlaggebenden Fragestellungen im Bereich der Prionenbiologie ist die strukturelle Charakterisierung löslicher PrP-Oligomere sowie unlöslicher Fibrillen (PrP^{Sc}). Die vollständige strukturelle Charakterisierung löslicher oligomerer Intermediate ist schwierig auf Grund ihrer kurzen Lebensdauern und weil sie eine große Anzahl an Konformationen und Aggregationsgraden aufweisen. Aggregationsanfällige Monomere können verschiedene Pfade einschlagen und deshalb zur Bildung von amorphen Aggregaten, ringförmigen oder globulären Oligomeren oder einer Anzahl morphologisch unterschiedlicher Fibrillen führen.

Der entfaltete Zustand stellt die am wenigsten eingeschränkte Struktur dar, weshalb unsere Beobachtung der Fibrillenbildung in einer hoch denaturierenden Umgebung bedeutsam und wichtig ist. Dies zeigt, dass Fibrillen ausgehend vom entfalteten Zustand des Prionproteins gebildet werden können. Unsere Daten füllen deshalb den bisher kahlen Informationsraum über die Fibrillenbildung aus dem entfalteten Zustand. Der lösungsmittelunzugängliche und rigide Kern erstreckt sich über den Sequenzbereich 145-223, während die letzten sieben C-terminalen Aminosäuren eine konformationelle Umwandlung im Zuge der Fibrillenbildung durchlaufen. Hochauflösende NMR-Spektroskopie ist die Methode der Wahl zur Untersuchung der Prionenbildungskinetik, weil sie zwischen verschiedenen Prionenstämmen unterscheiden kann, die auf Grund von Änderungen in ihrer Architektur unterschiedliche NMR-Spektren aufweisen werden. Diese Änderungen können zeitabhängig verfolgt werden, wenngleich wegen großer Variabilität in der Inkubationszeit dezidierte Messzeit erforderlich sein wird.

Acknowledgements

It is my pleasure to extend my sincere gratitude and appreciation to all the people who made this dissertation possible.

First and foremost, I would like to express my deep sense of gratitude to my supervisor, Prof. Dr. Harald Schwalbe, who has an attitude and substance of a genius, for his persistent help, encouragement and valuable guidance. He continuously and convincingly conveyed a spirit of adventure in research. He has supported me throughout my thesis with his patience and knowledge whilst allowing me to grow as an independent researcher. I shall always remain indebted to him. I am also thankful to him for providing unrestricted access to the laboratory facilities.

Words are not enough to convey my sincerest thanks to my “zwietgutachter” Prof. Dr. Clemens Glaubitz for his encouragement, support, suggestions and continuing interaction, which provided me with a deeper insight into my research area. I am also thankful to Dr. Ines Lehner, Nicole Pflieger, Dr. Jakob Lopez and Dr. Jun Yang; who spent many hours to get the worthy spectrum from flexible fibrils.

I would like to thank Dr. Janet Vonck for helping me out with electron microscopy by capturing beautiful images of fibrils. Deep appreciation should be made to Dr. Khashti Ballabh Joshi, Dr. Thorsten-Lars Schmidt and Prof. Dr. Alexander Heckel for their contribution on capturing and analyzing the atomic force microscopic images of fibrils. I would like to thank Prof. Dr. Bernd Brutschy and Mihaela Cazacu for trying out the LILBID measurements and wonderful discussions on amyloids.

I express my sincere thanks to Prof. Dr. Walter Volkmandt, Dr. Monika Schneider, and Dr. Krishna Saxena, who kept me aware of biosafety during this research.

My warm thanks are due to Dr. Christian Richter and Dr. Johannes Gottfried Zimmermann, for all the help at the spectrometers and rescuing at difficult times.

My heartiest thank goes to Dr. Karin Abarca-Heidemann for giving me aspirations and courage, when I needed it most. Her cheerful and lively nature was an instrumental and driving force many a times.

I wish to express my warm and sincere thanks to Dr. Henry Jonker, who shared the bench next to me in biolab, for his friendship and stimulating interactions during the long hours in the lab.

Dr. Stephan Rehm, my special thanks goes to him; he has been a helping hand, whenever I look for one, whether it is moving in to new apartment or in office.

Huge, huge thanks to Anna Paulus and Elena Hartmann for making life easier. It would have been impossible for things to work out properly without being them around. I express my heartfelt and deep sense of gratitude to you.

I would like to thank Dr. Christian Gerum, Dr. Kai Schalepow, and Dr. Sridahr Sreeramulu for proof reading of my thesis.

I extend my thanks to Dr. Karin Abarca-Heidemann, Janina Buck and Dr. Kai Schalepow for German translations.

Best regards to all the past and present members of our lab for providing a very good atmosphere: Dr. Karin Abarca Heidemann, Dr. Nuria Aboitiz, Dr. Katrin Ackermann, Dr. Aphrodite Anastasiadis-Pool, Marie Anders-Maurer, Tomislav Argirevic, Neda Bakhtiari, Katja Barthelmes, Dr. Holger Berk, Anna Bischoff, Dr. Janina Buck, Florian Buhr, Dr. Aleksejs Cerepanov, Dr. Emily Collins, Dr. Elke Duchardt-Ferner, Dr. Jan-Peter Ferner, Dr. Boris Fürtig, Dr. Christian Gerum, Dr. Artur Gieldon, Dr. Jürgen Graf, Dr. Steffen Grimm, Martin Hähnke, Friederike Heinicke, Fabian Hiller, Dr. Serge Ilin, Dr. Henry Jonker, Deep Chatterjee, Dr. Mirko Cevc, Hannah Steinert, Irene Bessi, Ajit Paul Kaur, Melanie Koschinat, Anna Lena Lieblein, Tanja Machnik, Dr. Vijayalaxmi Manoharan, Daniel Mathieu, Sarah Mensch, Hillary Moberly, Dr. Muruga Poopathi Raja, Dr. Hamid Nasiri, Gerd Nielsen, Dr. Jonas Noeske, Senada Nozinovic, Anke Reining, Dr. Christian Richter, Jörg Rinnenthal, Dr. Sridhar Sreeramulu, Dr. Santosh Lakshmi Gande, Dr. Kai Schlepckow, Dr. Christian Schlörb, Dr. Nicole Schmut, Robert Silvers, Dr. Stephan Rehm, Max Stadler, Jochen Stehle, Elke Stirnal, Anna Wacker, Dominic Wagner, Dr. Karla Werner, Dr. Julia Wirmer-Bartoschek, Prof. Jens Wöhnert, Dr. Johannes Gottfried Zimmermann.

I am also grateful to Dr. Markus Fandrich, Dr. Ritu Khurana, Dr. Ashutosh Kumar, Dr. Neel Sarovar Bhavesh, Dr. Navaratna Vajpayee and Prof. Dr. Raja Roy for fruitful discussions during conferences.

I thank my younger brother Mr. Arun Kumar Singh, for helping with complex mathematical problems using MATLAB.

There are many others who have encouraged me and supported my work. I would like to thank them all. I thank Dr. Neeraj Tiwari, my dear old friend, for being there for me in my happy and sad moments. Thanks to Dr. Khalid Siddiqui and Dr. Sridhar Sreeramulu for their deep and sincere friendship, modest support, and motivation. I thank Dr. Radhan Ramadass and Dr. Muruga Poopathi Raja for their honesty and for their ways to share science and for their sense of humor. I thank Indian students in the campus for making it homely. A special gratitude goes to Jagdeep Kaur, Dr. Sarika Shastri, Dr. Santosh Kumar Mishra, Dr. Taslimarif Saiyed and Dr. Sanjeev Baniwal for being an extremely diverse crowd of people and at the same time being helpful and exciting friends.

My special thanks to Dr. Pankaj Singh, who is always there, whenever I have problem with eyes. I thank his wife Sapna Singh and little wonder “Shaurya”, who included me as part of their family. I also like to thank to Indian community in Frankfurt, especially to Bhatnagar and Srivastava families. Mr. Gagan Srivastava and Mrs. Renu Srivastava were like uncle and aunt, during my whole stay in Frankfurt. I found the sweetest cousin in Avanti and Udit. I also like to thank “meine deutschen Schwiegereltern Gudrun und Christian” and “Oma Gisela”.

My deepest gratitude goes to my family for their unflagging love and support throughout my life. This work has come to completion with the blessings of my parents and my in-laws. I cannot express my feelings in words for my wife “Jagriti” who has always been a constant source of encouragement and help throughout. I would like to acknowledge my elder brother Shri Sanjeev Kumar Singh, who had been a role model for me to follow unconsciously when I was a teenager and has always been one of my best counselors, and sister-in-law Nilay Singh’s constant support and encouragement. I owe my loving thanks to my nephew Aalind; he has been a constant source of love.

I gratefully acknowledge International Max Planck research school on structure and function of biological membranes and EU for the finance support.

Last but not the least; I thank God for being so generous and kind to me.

Curriculum vitae

Jitendra Kumar

Am Brückengarten 9a
60431, Frankfurt am Main



Personal Data

Date of Birth: 01 June 1976
Place of Birth: Aligarh
Nationality: Indian
Family Status: Married to Jagriti Kumar

School Education:

07/80 – 06/86 Primary Education at Jugaldevi Saraswati Shishu Mandir, Kanpur
07/86 – 06/91 High School at Ramkrishna Mission Higher Secondary School, Kanpur
07/91 – 06/93 Intermediate at Bishambhar Nath Sanatan Dharm Inter College, Kanpur

University Education:

07/93 – 06/96 B.Sc. in Physics, Chemistry and Mathematics at Vikramajit Singh Sanatan Dharam College, Kanpur
08/96 – 05/99 M.Sc. in Biotechnology at University of Calicut
Dissertation on “Overexpression, Purification and Characterization of Yeast Hexokinase P1” under the guidance of Prof. Dr. Gotam K Jarori, Department of Biological Sciences, Tata Institute of Fundamental Research, Mumbai

Doctoral Study:

02/03 – Under the supervision of Prof. Dr. Harald Schwalbe at Goethe University, Frankfurt

Achievements:

2003: International Max Planck Research School Fellowship

- 2001: Council of Scientific and Industrial Research (CSIR) India – Junior Research Fellow
- 2000: Council of Scientific and Industrial Research (CSIR) India – National Eligibility Test for Lectureship in Life Sciences
- 1996: Department of Biotechnology (DBT), Govt. of India, Fellowship for M. Sc. Biotechnology
- 1986-93: Junior High School Scholarship & Ekikrat Scholarship Gov. of Uttar Pradesh, India

Experiences:

- 2001 – 2003: CSIR – Junior Research Fellow, Division of Molecular and Structural Biology, Central Drug Research Institute, Lucknow, India working on project associated with Structural Genomics of Mycobacterium Tuberculosis, Advisor: Dr. H. S. Subramanya
- 1999 – 2000: Lecturer, Dr. Virendra Swarup Center of Advance Science and Technology, D.A.V. College, Kanpur, India

Academic Teachers:

Prof. Dr. V.J. Phillip, Prof. Dr. M.V. Joseph, Prof. Dr. P. N. Ravindran, Prof. Dr. Gotam K Jarori, Prof. Dr. K.S. Krishanan, Prof. Dr. N. P. Singh, Prof. Dr. Vinod Bhakuni, Prof. Dr. C.M. Gupta, Prof. Dr. P. R. Maulik, Prof. Dr. Saman Habib, Prof. Dr. Ritu Khurana, Prof. Dr. H. S. Subramanya, Prof. Dr. Raja Roy, Prof. Dr. Clemens Glaubitz and Prof. Dr. Harald Schwalbe.